February 2023
Version 1.0

Global Food Security-support Analysis Data (GFSAD) Project

Landsat-derived Global Rainfed and Irrigated-Cropland Product @ 30-m (LGRIP30) of the World (GFSADLGRIP30WORLD)

Algorithm Theoretical Basis Document (ATBD)

USGS EROS
Sioux Falls, South Dakota

Document History

Document Version	Publication Date	Description
1.0	May 2022	Original
1.1	October 2022	Modification made according to USGS reviewer comments
1.2	February 2023	Modifications made according to LPDACC reviewer comments

Contents

I. Members of the team

This Global Food Security-support Analysis Data (GFSAD) Landsat-derived Global Rainfed and Irrigated-Cropland Product @ 30-m (LGRIP30) of the World (GFSADLGRIP30WORLD) was produced by the following team members. Their specific role is mentioned below:

Dr. Pardhasaradhi Teluguntla, Research Scientist, Bay Area Environmental Research Institute (BAERI) co-led (with Prasad) the GFSADLGRIP30WORLD product generation effort. Dr. Teluguntla was instrumental in the designing, coding, computing, analyzing, and synthesis of the Landsat-derived Global Rainfed and Irrigated-Cropland Product @ 30-m (LGRIP30) for the nominal year 2015. He was also instrumental in writing the manuscripts, ATBDs, and user documentations.

Dr. Prasad S. Thenkabail, Senior Scientist (ST), United States Geological Survey, is the Principal Investigator (PI) of the GFSAD project. Dr. Thenkabail was instrumental in developing the conceptual framework of the GFSAD project and co-led the (with Pardha) design and development of the Landsat-derived Global Rainfed and Irrigated-Cropland Product @ 30-m (LGRIP30) for the nominal year 2015. He was also instrumental in writing the manuscripts, ATBDs, and user documentations.

Mr. Adam Oliphant, Geographer**,** United States Geological Survey (USGS), shared his expertise in cloud computing and Machine Learning Algorithm implementation in Google Earth Engine (GEE) for LGRIP30 product generation.

Dr. Murali Krishna Gumma, Principal Scientist at the International Crops Research Institute for the Semi-Arid Tropics (ICRISAT), helped collect reference data used in the machine learning algorithms and in validation of the LGRIP30 products.

Dr. Itiya Aneece, Research Geographer, United States Geological Survey (USGS), provided valuable insights through discussions on the cloud computing aspects and methodological aspects of the LGRIP30 products.

Mr. Daniel Foley, Geographer, United States Geological Survey (USGS), provided valuable insights during product development and its validations.

Mr. Richard McCormick, Student developer, helped in development of the croplands.org website and in tiling LGRIP30 products for LP DAAC.

Summary

This algorithm theoretical basis document (ATBD) presents and discusses the Landsat-derived Global Rainfed and Irrigated-area Product @ 30m (LGRIP30) for the nominal year 2015. The LGRIP30 product was evaluated for accuracies, errors, and uncertainties. The resulting error matrix showed an overall accuracy of 86.5%. The irrigated class has a producer's accuracy of 86.7% and user's accuracy of 84.3%. The rainfed class has a producer's accuracy of 86.3% and user's accuracy of 88.4%.

Abstract

Climate variability and ballooning populations are putting unprecedented pressure on agricultural croplands and their water use, which are vital for ensuring global food and water security in the twenty-first century. In addition, the COVID-19 pandemic, military conflicts, and changing diets have added to looming global food insecurity. Therefore, there is a critical need to produce consistent and accurate global cropland products at fine spatial resolution (e.g., farm-scale, 30m or better), which are generated consistently, accurately, and routinely (e.g., every year). In this regard, earlier we produced the world's first Landsat-derived global cropland extent product @ 30m (GCEP30) (Thenkabail et al., 2021; download @ LP DAAC) funded by NASA MEaSUREs and USGS. *The high impact of our previously-funded NASA GFSAD products such as Landsat-derived global cropland extent product @30m or GCEP30, 1km cropland dominance, and 1km irrigated versus rainfed is demonstrated by the use of these data by 126 countries during 2018-2021 (97 countries in 2021 alone, 72 countries in 2022 alone), continued average downloads every month by about 20 countries, publication of 12 key peer-reviewed articles which already have about 1500 citations in a short time-period (2017-present), and use for a wide range of applications.* Therefore, the **overarching goal** of this continuity global food security-support analysis data (GFSAD) project is to develop comprehensive data and products in support global food and water security in the twenty-first Century. This is achieved by developing cropland models, maps, and monitoring tools leading to a wide array of products using machine learning algorithms (MLAs), satellite sensor based big-data analytics, and cloud-computing. We focus on producing three distinct Landsat-derived global cropland products in this new GFSAD project:

1. Global Rainfed and Irrigated Product @ 30m (LGRIP30).
2. Global Cropping Intensity Product @ 30m (LGCIP30) &
3. Global Crop Type Products @ 30m (LGCTY30)

This algorithm theoretical basis document (ATBD) presents and discussed Landsat-derived Global Rainfed and Irrigated-area Product @ 30m (LGRIP30) for the nominal year 2015. The LGRIP30 cropland product was generated using Landsat-8 time-series data, multiple supervised and unsupervised Machine learning algorithms (MLAs) such as random forest, support vector machines, decision trees, ISOCLASS clustering, and spectral matching techniques (e.g., Thenkabail et al., 2021, Oliphant et al., 2019, Teluguntla et al., 2018, 2015, Xiong et al., 2017a, Thenkabail et al., 2012, 2009, 2007, 2005) as outlined in the methods section, utilizing the Google Earth Engine (GEE) and\or other cloud platforms.

All crop products were evaluated for accuracies, errors, and uncertainties using independent dataset. The resulting error matrix showed an overall accuracy of 86.5%. The irrigated class has a producer's accuracy of 86.7% (errors of omissions of = 13.3%) and user's accuracy of 84.3% (errors of commissions = 15.7%). The rainfed class has a producer's accuracy of 86.3% (errors of omissions of = 13.7%) and user's accuracy of 88.4% (errors of commissions = 11.6%). The LGRIP30 determined total global net irrigated area (TGNIA) of 1,802,929,008 hectares (or 1.80 billion hectares or Bha) of croplands of which 1,087,185,109 hectares (1.09 Bha) was rainfed and the rest 715,743,899 hectares (0.71 Bha) was irrigated. The data is released through NASA's Land Processes Distributed Active Archive Center (LP DAAC):
DOI: https://doi.org/10.5067/Community/LGRIP/LGRIP30.00
The LGRIP30 product can be browsed at full resolution @:
https://croplandsdev.users.earthengine.app/view/croplands-dev-internal

II. Historical Context and Background Information

The global food and water security scenario in the twenty-first century will be an extraordinarily complex one. The population of the world will continue to balloon and reach 9.7 billion by 2050 and nearly 11-12 billion by 2100 (UN DESA, 2021). In addition, global daily average calorie consumption is expected to rise from 2789 kcal/person/day in the year 2000 to 3130 kcal/person/day by the year 2050 (World Bank, 2022, Bodirsky et al., 2015, FAO 2012b). These consumption figures may rise even higher if traditionally low meat consuming nations start increasing meat consumption enabled by economic growth. Food habits of people are diversifying considerably (e.g., rice, wheat, or maize only to a mix of rice, wheat, maize, pulses, fruits, and vegetables). At the same time, about 30 to 50% of the food produced globally is wasted (UNEP, 2021, IME, 2013). Added to all these already daunting needs are the food security challenges from the COVID-19 pandemic, the Russia-Ukraine conflict, and related supply-chain disruptions. COVID-19 lockdowns and wars are heavily impacting food production and trade mechanisms for all leading cropland countries. For example, the 10 largest countries in terms of cropland area as a percentage of the total global net cropland area or GNCA (1.873 Bha), in order of ranking, were: India (179.8 Mha, 9.6%); United States (167.8 Mha, 8.95%); China (165.2 Mha, 8.82%); Russia (155.8 Mha, 8.32%); Brazil (64 Mha, 3.42%); Ukraine (43.4 Mha, 2.32%); Canada (42.9 Mha, 2.29%); Argentina (38.4 Mha, 2.05%); Indonesia (37.4 Mha, 2.0%); and Nigeria (35.7 Mha, 1.91%) (Thenkabail et al., 2021). These 10 countries have 50% (937 Mha) of the GNCA; four of them (India, United States, China, and Russia) alone encompass 670 Mha (36% of the GNCA) (Thenkabail et al., 2021). Given that twenty-first century food consumption is heavily dependent on the global supply-chain and all these leading global cropland countries are affected by these disruptions, many experts have already warned of the grave consequences of these distressing events and the associated disruptions to food productions and supply-chains (Glauber and Laborde, 2022). The United Nation's Food and Agriculture Organization has noted the potential grave danger to global food supply because of war and pandemic related supply-chain issues. Ukraine and Russia together produce nearly 30 percent of the world's traded wheat with 26 countries getting more than half of their wheat from these two countries (Bourne, 2022). Most of the world depends significantly on nitrogen and potassium fertilizers from Russia, Ukraine, and Belarus (Glauber and Laborde, 2022). So, the recent war in the region creates a dire situation for global food security and for sustainable food prices throughout the world. Further, abandonment and conversion of fertile agricultural lands (UN DESA, 2021), migration of rural to less productive urban/peri-urban agriculture (UN DESA, 2021), climate change related droughts (Teluguntla et al., 2017, Thenkabail and Wu, 2012), the need to decrease agri-food system related greenhouse gas emissions (Tubiello et al., 2021, Boden et al., 2017, Vermeulen et al., 2012), and the ballooning global population are all exacerbating food insecurity.

Additionally, global food and water security challenges are tightly intertwined. In a changing climate, the quantity and quality of surface and ground water are decreasing. Demands for agricultural and alternative uses (e.g., industrial, ecological) of water are simultaneously increasing. Adding to this complexity, urban migration and climate change related precipitation extremes necessitate new infrastructure to maintain water availability for new cropland. Thus, 30m (field scale where 1 pixel = 0.09 hectares) cropland products, including their intensity and irrigation status, are needed to monitor change and aid decision-making for issues of global food and water security.

GFSAD will make significant contributions to the Earth System Data Records (**ESDRs**), the Group on Earth Observations (**GEO**) Agriculture and Water Societal Beneficial Areas (**GEO Ag. SBAs**), and the GEO Global Agricultural Monitoring (**GEOGLAM**). All data will be released through LP DAAC, such as, for example, our recent releases

1. Global cropland extent product @ 30m (GCEP30)

https://lpdaac.usgs.gov/news/release-of-gfsad-30-meter-cropland-extent-products/

2. Global crop dominance product @ 1 km:

https://lpdaac.usgs.gov/products/gfsad1kcdv001/

3. Global cropland mask product at 1 km:

https://lpdaac.usgs.gov/products/gfsad1kcmv001/

All the above studies and products indicate global agricultural land and water in the 21st century will be in a constant state of flux (You and Sun, 2022) requiring us to understand, model, map, and monitor these changes over space and time rapidly, routinely, and accurately year after year. This challenge invariably calls for very comprehensive global food security-support analysis data (GFSAD) products at fine spatial resolution representing field-scale (30m or better) routinely and accurately covering the entire Earth. Hence, the **overarching goal** of this project is to produce GFSAD models, maps, and monitoring tools using machine learning algorithms (MLAs) on cloud computing platforms with the ability to handle multi-satellite, multi-sensor remotely sensed big-data, leading to a comprehensive set of global cropland products. In this regard, we have developed and released the world's highest resolution Landsat derived global cropland extent product @ 30m (GCEP30). This data was released on NASA's The Land Processes Distributed Active Archive Center (LP DAAC) and comprehensive methods, approaches, and results are published in the USGS professional paper (Thenkabail et al., 2021) as well as series of journal papers (Gumma et al., 2022, Zhang et al., 2022, Xing et al., 2022, Nagaraj et al., 2021, Zohaib et al., 2019, Gumma et al., 2019, Oliphant et al., 2019, Teluguntla et al., 2018, 2017, Xiong et al., 2017a, 2017b, Massey et al., 2017, 2018, Phalke et al., 2020, Congalton et al., 2017, and Yadav and Congalton, 2018).

However, a comprehensive assessment, modeling, mapping, and monitoring of global food security scenario requires multiple cropland products and not limited to cropland extents. As a result, we are expanding GFSAD project by adding additional cropland products that include:

1. Landsat-derived Global rainfed & irrigated product @ 30m (LGRIP30).
2. Landsat-derived Global cropping intensity product @ 30m (LGCIP30).
3. Landsat-derived Global crop type product @ 30m (LGCTY30).

This Algorithm Theoretical Basis Document (ATBD) is focused on Landsat-derived Global rainfed & irrigated product @ 30m (LGRIP30) (Table 1). In this ATBD document we will provide detailed description of the data, methods, approaches, and results of the LPRIP product for the year 2015 (LGRIP30-2015).

Table 1. **LGRIP30.** Global Food Security-support Analysis Data (GFSAD) Project Landsat-derived Global Rainfed and Irrigated-Cropland Product @ 30-m (LGRIP30) of the World (GFSAD-LGRIP30WORLD) for the nominal year 2015.

Product Name	Short Name	Spatial resolution	Temporal coverage
Landsat-derived Global Rainfed and Irrigated-Cropland Product @ 30-m (LGRIP30)	GFSADLGRIP30WORLD	30-m	Nominal 2015

Note: Nominal here means that the Landsat-8 16-day data used to produce the product is for two to three years (2014-2016), but the product is reported as nominal year 2015.

III. Rationale for Development of the Algorithms

During the green revolution era (~1950-2010) the world's population rose from 2.5 billion to about 7 billion because global food security was mainly ensured through a combination of factors: (a) cropland expansion from ~300 million hectares to ~1.8 billion hectares (Potapov et al., 2022, Thenkabail et al., 2021), (b) irrigation expansion from ~50 million hectares to ~400 million hectares (Siebert et al., 2015), (c) genetic engineering through high yield, fast growing, short-duration crops (Lenaerts et al., 2019), (d) cropland intensification from single to double or triple cropping, in some irrigated croplands (Hu et al., 2020, Wu et al., 2018), (e) heavy inputs such as fertilizer and nitrogen application (He et al., 2021), and (f) improvements in land management (e.g., leveling, drainage) (Viana et al., 2022).

Ensuring food security for ~9.7 billion people by the year 2050 and ~11 billion people by the year 2100 sustainably will require a paradigm shift on how our land and water are used for food production, referred to as the evergreen revolution, where food security is sustained and assured in the years ahead without significant disruption (FAO, 2021a, b; UN DESA, 2021). Measures to achieve this include: **(1)** increased crop water productivity (more crop per drop; kg/m^3) (Foley et al., 2019, Rijsberman 2014), **(2)** improved cropland productivity (more crop per unit of land; kg/m^2) (Hefferon, 2016), and **(3)** adaptation to the changing climate (Mekonnen et al., 2021, Tripathi et al., 2016, Gartland and Gartland, 2016). Climate change adaptations include: (i) Climate Smart Agriculture (FAO, 2021a, Campbell et al., 2014), (ii) extreme weather agriculture (Wheeler and Lobley, 2021, Gbegbelegbe et al., 2014), (iii) drought tolerant agriculture (Enenkel et al., 2015), **(4)** advancing urban and peri-urban agriculture (Badami and Ramankutty 2015, Thebo, et al., 2014), **(5)** avoiding allocation of fertile cropland areas to biofuels or urbanization (van Vliet et al., 2017, Tripathi et al., 2016), **(6)** balancing food crops with dairy, meat, and fish (Forster and Radulovich 2015), **(7)** exploring new sources of food (Forster and Radulovich 2015), **(8)** reducing food waste (FAO, 2021a, Girotto et al, 2015), **(9)** creating food banks during good years (Fuss et al., 2015, Fanzo 2015, Wilkinson 2015), **(10)** maintaining rich biodiversity (Sukara 2014), **(11)** planning virtual croplands (Würtenberger et al., 2006) and virtual water use (Hanasaki et al., 2010), **(12)** precision farming, **(13)** accurate and cropland mapping for better crop management (Thenkabail et al., 2021, Teluguntla et al., 2017, 2015; Xiong et al., 2017b), **(14)** using geospatial technologies for improved planning (Potapov et al., 2022, Platonov et al., 2008, Biradar et al., 2009), **(15)** increasing global cropland use intensity through better allocation of nitrogen (N), other fertilizers, and irrigation (Hu et al., 2020, Niedertscheider et al., 2016, Odegard and van der Voet 2014), **(16)** increasing cropland use intensity (Gumma et al., 2016), and **(17)** adapting to low or zero carbon agriculture by measures such as increasing no-till cropland areas (Puigdueta et al., 2021).

IV. Importance of mapping global irrigated and rainfed areas

Importance of mapping irrigated and rainfed croplands cannot be overemphasized. First, both irrigated and rainfed areas are water guzzlers since about 80-90% of all human water use goes towards producing food. Irrigated areas consume blue water. That is the water delivered to farms through irrigation systems either from surface water (e.g., lakes, reservoirs, tanks, river diversions) or ground water resources (e.g., tube wells, open wells). Rainfed areas consume green water. That is water coming from direct precipitation (e.g., rainfall, snowfall, soil moisture). Of the 1.873 billion hectares of global croplands (Thenkabail et al., 2021), roughly 75% is rainfed and 25% is irrigated (Siebert et al., 2013, Thenkabail et al., 2012, 2011, 2009a, Biradar et al., 2009, Teluguntla et al., 2015, Portmann et al.,2010). Second, accurate estimates of irrigated and rainfed areas are lacking because of lack of finer resolution mapping at global level. Given that croplands consume overwhelming proportion of human water use, an accurate estimate of crop water use will require accurate estimates of irrigated and rainfed croplands. Third, the productivity of irrigated areas is anywhere between 2-5 times higher than rainfed croplands. As a result, 25% global irrigated areas produce nearly 40% of the food and the rest 75% of the rainfed croplands produces the rest 60% of the food. So, increasing irrigated areas is one solution to increasing global food production for the ballooning populations. Nevertheless, it is a complex issue of balancing crop water use, food production, and sustainable production systems. Fourth, understanding, mapping, modeling, and monitoring irrigated and rainfed areas separately is of great importance to assessing crop water productivity, crop productivity, crop water use, and in strategizing food and water security in the twenty first century. Rainfed croplands meet about 60% of the food and nutritional needs of the World's population and are backbone of the marginal or subsistence farmers. They are increasingly seen as better alternative to irrigated agriculture because of its environmental friendliness and sustainability over long periods of time (Biradar et al., 2009). Given that there is large swatch of equipped areas of rainfed croplands that have crop low productivity, opportunities to increase food production in these croplands by utilizing modern technologies of genetic engineering, low water consuming crops, and shorter crop growing seasons even by a small margin will lead to large quantities of food.

In post-second World War era and subsequent de-colonization, there was great thrust is irrigation infrastructure development throughout the world, but specifically in Asia. Globally, the irrigated landscape remains very dynamic. Although the annual rate of increase of irrigated areas has slowed to about 1 %, this still represents an increase of between 2 and 3 million hectares each year. There is a smaller corresponding annual loss of irrigated area to salinity and water logging as well as abandonment of uneconomic projects. Countries such as China and India continue to build large multi-purpose dam projects that also supply water for irrigation. In sub-Saharan Africa irrigation is perennially seen as having unfulfilled potential. Elsewhere in the world there are moratoria on dam building and even the decommissioning of dams in the western USA. In mapping rainfed and irrigated areas, we ask some key questions, that include:

1. How much irrigation or rainfed cropland areas do we have now?
2. How much do we need in the future to meet food and nutritional security of growing populations?
3. How do we achieve the above through sustainable development and by preserving environment and climate balance?
4. How much blue water and green water does it require, and will this be available, especially in a scenario of alternative water demands?

5. How does the scenario change in demographic changes where much of the world will be urbanized and massive numbers of rural population will move out of agriculture?

1. Producing a coarse-resolution nominal 1-km irrigated and rainfed cropland product of the world as a mask for the higher resolution products

Currently, the highest resolution irrigated and rainfed cropland products derived from remote sensing are at nominal 1-km spatial resolution (Figure 1) derived by fusing several existing products and discussed in detail by (Teluguntla et al., 2016, 2015; Table 2). Many existing products (Table 2) were carefully analyzed (Teluguntla et al., 2016, 2015) and a synthesis map was produced (Figure 1). This led to a disaggregated five class global cropland extent map derived at nominal 1-km (Figure 1, Table 2) derived primarily based on four major studies: Thenkabail et al. (2009a, 2011), Pittman et al. (2010), Yu et al. (2013), and Friedl et al. (2010). These products use SPOT Vegetation, AVHRR, and several other ancillary data as described in those publications. Class 1 to Class 5 (Figure 1) are cropland classes, that are dominated by irrigated and rainfed agriculture. However, class 4 and Class 5 have ONLY minor or very minor fractions of croplands. Refer to Table 3 for cropland statistics of this map. The class 1 "Irrigation major" (Figure 1, Table 3) are irrigated by large reservoirs created by large and medium dams, barrages, and even large ground water pumping. The class 2 "Irrigation minor" (Figure 1, Table 3) are areas irrigated by small reservoirs, irrigation tanks, open wells, and other minor irrigation. However, it is very hard to draw a strict boundary between major and minor irrigation and in places there can be significant mixing. So, when major irrigated areas such as the Ganges basin, California's central valley, Nile basin etc. are clearly distinguishable as major irrigation, in other areas major and minor irrigation may intermix. Table 3 provides the proportion of areas (counted as 1-km pixels) occupied by each of these classes. A detailed description on how this fusion product of irrigated and rainfed at nominal 1 km resolution (e.g., Figure 1) was produced is presented in Teluguntla et al. (2016) and hence won't be repeated here. This cropland mask product was also released on NASA's LP DAAC: https://lpdaac.usgs.gov/products/gfsad1kcmv001/

The 5-class Figure 1 is finally aggregated into 2-class irrigated and rainfed map (Figure 2). Figure 2 provides the global rainfed and irrigated-area product @ 1000m (GRIP1000) derived using SPOT-vegetation, AVHRR, and ancillary data (Teluguntla et al., 2016, Thenkabail et al., 2012, 2011). GRIP1000 forms a preliminary mask-layer for production of finer resolution irrigated and rainfed cropland products. This we do by:

First, starting with GRIP1000 (Figure 1, 2; Teluguntla 2016, 2015) to produce MODIS 250m time-series data derived global irrigated and rainfed cropland product of the world (MGRIP250; Figure 3, 4, 5, 6, 7).

Second, starting with MGRIP250 (Figure 3, 5, 7) to produce Landsat 30m time-series data derived global irrigated and rainfed cropland product of the world (LGRIP30). The LGRIP30 is the product that will be produced during this work.

Coarse-resolution products GRIP1000 (Figure 1, 2) and MGRIP250 (Figure 3, 5, 7) are invaluable baseline starting point products in ultimately deriving LGRIP30. To re-iterate, the final goal is to produce LGRIP30. But we do that by first starting with GRIP1000, followed by producing an interim MGRIP250 and finally producing LGRIP30.

Table 2. State-of-the art global cropland mapping using satellite remote sensing

Sno	Name*	Institution**	Sensors***	Resolution, Nominal (meters)	Time, Nominal (year)	Classes	Reference
A. Global cropland products							
1	GCEP30	USGS	Landsat 7 & 8	30	2021	Croplands	Thenkabail et al. (2021)
2	UCL	UCDL	Multiple	250	2010	Croplands, irrigated, rainfed	Waldner et al. (2016)
3	MODIS Cropland	SDSU & UMD	MODIS	250	2000	Croplands	Pitman et al. (2010)
4	GRIPC	BU	MODIS	500	2005	Croplands, irrigated, rainfed	Salmon et al. (2015)
5	GFSADCD1KM	USGS	AVHRR	1000	2010	Crop dominance, irrigated, rainfed	Thenkabail et al. (2012)
6	GFSADCM1KM	USGS	AVHRR, MODIS, Landsat	1000	2010	Croplands, irrigated, rainfed	Teluguntla et al. (2015)
7	GIAM	IWMI	AVHRR, SPOT VEG	1000-10,000	2000	Croplands, irrigated	Thenkabail et al. (2009)
8	GMRCA	IWMI	AVHRR, SPOT VEG	1000-10,000	2000	Croplands, rainfed	Biradar et al. (2009)
9	MIRCA2000	UB		10,000	2000	Croplands. irrigated	Portman, Seibert & Doll (2009)
10	SAGE-Crop	UW		100,000	2000	Croplands, crop dominance	Monfreda, Ramankutty & Foley (2008)
11	SAGE-Agri	UW		100,000	2000	Croplands, crop dominance	Ramankutty et al.(2008)
B. Global LULC products in which cropland classes exist							
12	WorldCover10V2	ESA	Sentnel-2	10	2021	LULC	Zanaga et al. (2022)
13	WorldCover10V1	ESA	Sentnel-2	10	2020	LULC	Zanaga et al. (2021), Karra et al. (2021)
14	Globeland30	NGCC	Landsat 7	30	2010	LULC	Chen et al. (2015)
15	FROM-GLC	CAS	Landsat 7	30	2000	Croplands	Yu et al. (2013)
16	FROMGC	CESS	Landsat 7	30	Circa 2010	LULC	Gong et al. (2013)
17	CGLS-LC100	Copernicus	PROBA-V	100	2015	LULC	Buchhorn et al.(2020)
18	MODIS-JRC	JRC/MARS	MODIS, Landsat	250	2009	LULC	Vancutsem et al. (2012)
19	Globcover	ESA	MERIS	300	2005, 2009	LULC	Defourny et al. (2009)
20	MCD12Q1	NASA	MODIS	500	2004 - now	LULC	Leroux et al. (2014)
21	GLC	BU	MODIS	500		LULC	Friedal et al. (2010)
22	DISCover	USGS	AVHRR	1000	1992-93	LULC	Loveland et al.(2000)
23	LULC 2000	USGS	AVHRR	2000	2000	LULC	Soulard et al. (2014)
24	GLC 2000	JRC	SPOT	1/112°	2000	LULC	Fritz et al. (2010)

Note:

*** =** GCEP30= Global cropland extent product@30m; UCL = Unified Cropland Layer; GFSADCM1KM= Global Food Security-Support Analysis Data Cropland Mask @ 1-km; GRIPC= Global Rainfed, Irrigated, and Paddy Croplands;GFSADCD1KM= Global Food Security-Support Analysis Data Crop Dominance @ 1-km; MIRCA2000= Global monthly irrigated and rainfed crop areas around the year 2000; GIAM- Global Irrigated Area Map; GMRCA= Global Map of Rainfed Cropland Areas; SAGE= Center for Sustainability and the Global Environment;LULC = land use and land cover: MCD12Q1= MODIS Land Cover Type product; FROM-GLC = Fine Resolution Observation and Monitoring of Global Land Cover;FROMGC = Finer Resolution Observation and Monitoring of Global Land Cover CGLS= Copernicus Global Land Cover Layers; MODIS-JRC = MODIS Joint Research center; GLC = Global Land Cover.

**** =** UCDL = Université Catholique de Louvain, Belgium; USGS = United States Geological Survey; BU = Boston University SDSU = South Dakota State University. UMD = University of Maryland; UB = University of Bonn; IWMI= International Water Management Institute; UW = University of Wisconsin. NGCC = National Geomatics Center of China; NASA = National Aeronautics and Space Administration; CAS = Chinese Academy of Sciences. MARS = Monitoring Agricultural Resources; ESA = The European Space Agency.

***** =** AVHRR = Advanced Very High Resolution radiometer; MODIS = Moderate Resolution Imaging Spectroradiometer; SPOT = Satellite Pour l'Observation de la Terre MERIS = Medium-Spectral Resolution, Imaging Spectrometer; Proba-V sensor is a European follow-on to the SPOT VGT mission

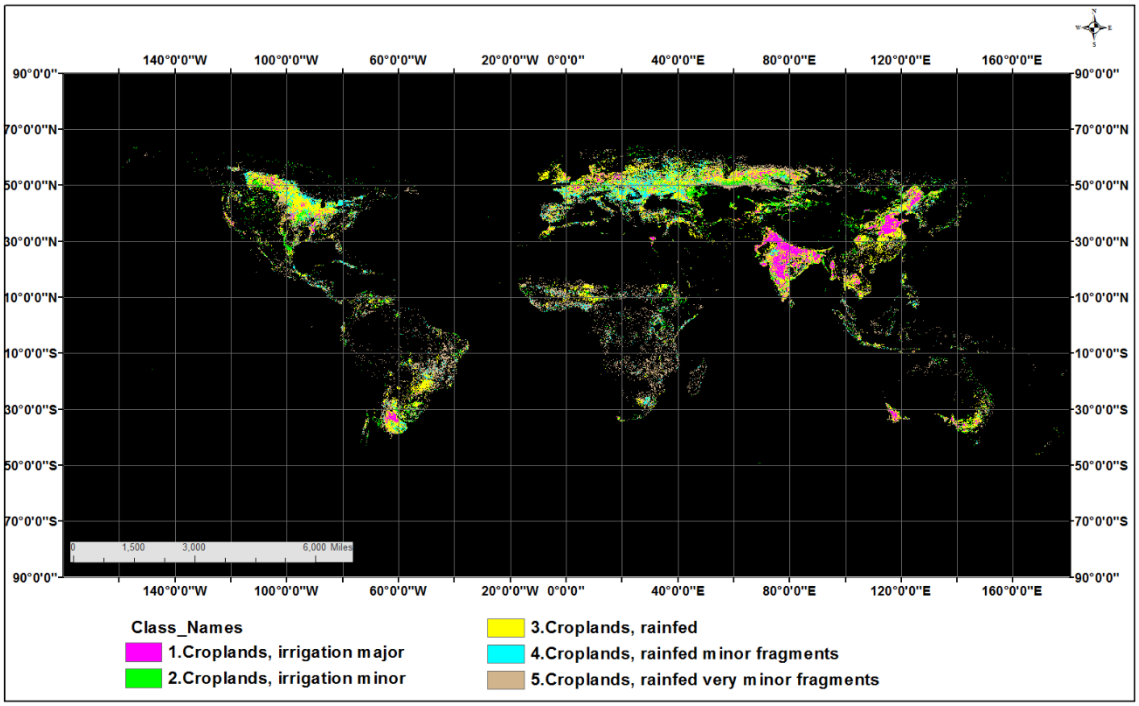

Figure 1. GRIP1000-5class map. A 5-class SPOT-Vegetation, AVHRR, and other ancillary data derived global rainfed and irrigated-area product @ 1000m (GRIP1000) developed using multiple-satellite sensor time-series data and ancillary data as reported in Teluguntla et al. (2016, 2015). The proportion of pixels distributed for each class in Shown in Table 3.

Table 3. GRIP1000-5classes and areas. Cropland area distribution of 5-class global rainfed and irrigated-area product @ 1000m (GRIP1000) (Teluguntla et al., 2016, 2015) shown in Figure 1.

Class#	Class Description	Pixels	Percent
#	Names	1 km	%
1	1.Croplands, irrigation major	3091988	13
2	2.Croplands, irrigation minor	4810869	21
3	3.Croplands, rainfed	11733044	50
4	4.Croplands, rainfed minor fragments	3858035	16
5	5.Croplands, rainfed very minor fragments	13700176	
	Class 1 to 4 total	23493936	100.0%

[1]= approximately 2.3 billion hectares (class 1 to 4) of cropland is estimated. But this is full pixel area. Actual area is = sub-pixel area (SPA). The SPA is not estimated here. See Thenkabail et al. (2007b) for the methods for calculating SPAs.
[2] = % calculated based on Class 1 to 4.
[3]= Class 5 is very minor cropland fragments

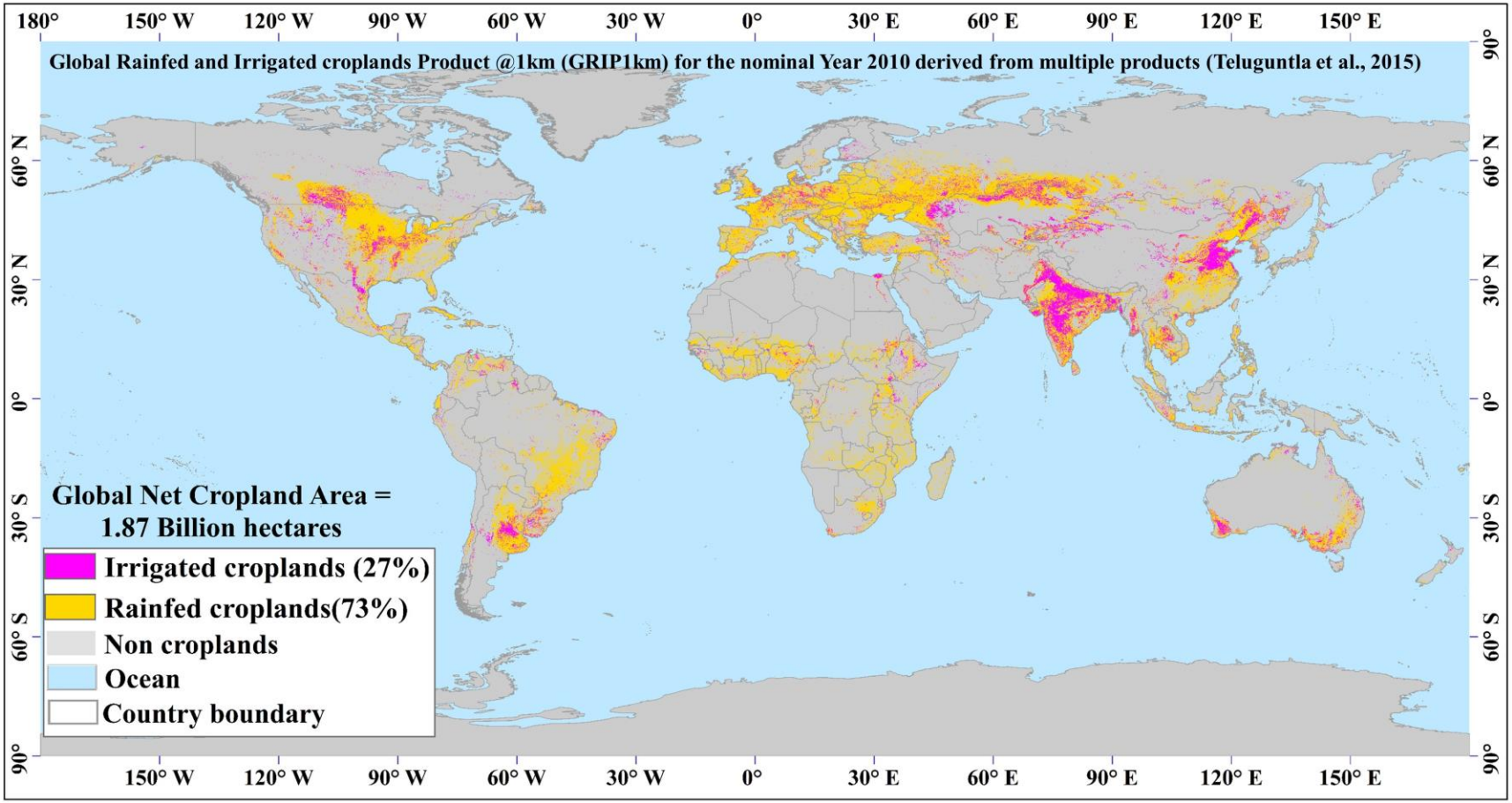

Figure 2. GRIP1000-2class map. An aggregated 2-class SPOT-Vegetation, AVHRR and other ancillary data derived global rainfed and irrigated-area product @ 1000m (GRIP1000) developed using multiple-satellite sensor time-series data and ancillary data as reported in Teluguntla et al. (2016, 2015). This map is derived by aggregating the 5-class map shown in Figure 1. Based on the pixel proportion, 27% of the pixels are under irrigated areas and the rest 73% are under rainfed areas.

2. Producing a coarse-resolution nominal 250-m irrigated and rainfed cropland product of the world as a mask for the higher resolution products

Using the 1-km (1 pixel = 100 hectares) global rainfed and irrigated-area product (GRIP1000; Figure 1, 2; Teluguntla et al., 2016, 2015; Thenkabail et al., 2012, 2011, Biradar et al., 2009), we developed the next higher-level product. This next higher-level product is called the Moderate Resolution Imaging Spectroradiometer (MODIS) time-series data derived global rainfed and irrigated-area product at 250m (1 pixel = 6.25 hectares) or MGRIP250. These two interim products that further led to a Landsat satellite-derived 30 m (1 pixel = 0.09 hectares) global rainfed and irrigated-area product at 30m (LGRIP30). We will fist discuss the MGRIP250 that will lead to LGRIP30.

At 250m two global cropland products were produced using methods and approaches discussed in Teluguntla et al. (2016, 2015), and Thenkabail et al. (2012, 2011, 2010, 2009a, 2007, 2005). These products are:

1. MODIS-derived 11-class global irrigated-area product @ 250m (MGIP250-11 class; Figure 3) developed using MODIS 250m time-series data for the nominal year 2015. The signature of these 11 classes are shown in Figure 4.
2. MODIS-derived 13-class global rainfed-area product @ 250m (MGRP250-13 class; Figure 5) developed using MODIS 250m time-series data for the nominal year 201. The signatures of these 13 classes are shown in Figure 6. and
3. The above two products were merged to produce an aggregated 2-class MODIS-derived 250m global rainfed and irrigated-area product (MGRIP250-2 class) (Figure 7).

The MGIP250-11 class irrigated area product (Figure 3, 4) has:

1. Four irrigated single cropland classes of different types.
2. Four irrigated double cropland classes of different types.
3. Two continuous irrigated cropland classes of different types; and
4. One fallow irrigated cropland class.

The MGRP250-13 class rainfed area product (Figure 5, 6) has:

1. Eight rainfed single cropland classes of different types.
2. Three rainfed double cropland classes of different types.
3. One continuous rainfed cropland class; and
4. One fallow rainfed cropland class.

Each of these classes show where geographically they occur (Figure 3, 5) and what their phenological signatures during a calendar year (Figure 4, 6).

The MGIP250-11 class irrigated product and the MGRP250-13 rainfed class product were aggregated to produce a simplified 2-calss composite MGRIP250-2 class rainfed and irrigated of the world (Figure 7). This MGRIP250 (Figure 7) will form stepping-stone baseline product for higher level Landsat-derived Global Rainfed and Irrigated-Cropland Product @ 30-m (LGRIP30) of the World (GFSADLGRIP30WORLD). We will discuss this LRIP30 product of the world (GFSADLGRIP30WORLD) thoroughly in this publication.

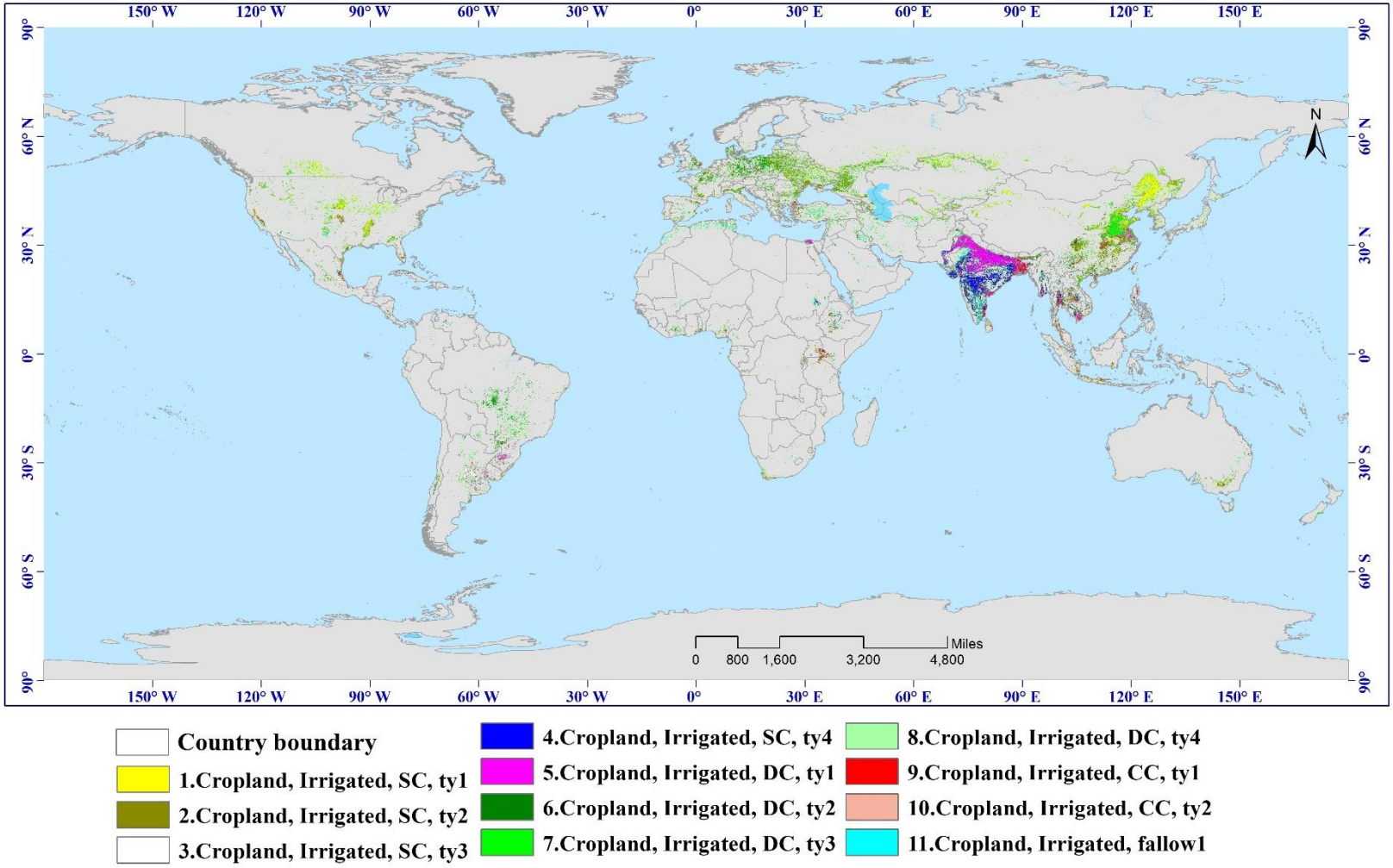

Figure 3. MGIP250-11 class irrigated area product (see signatures of these classes in Figure 4). A MODIS-derived Global irrigated-area product @ 250m with 11 classes (MGIP250-11class) developed using MODIS 250m time-series data for the nominal year 2015. The Moderate Resolution Imaging Spectroradiometer (MODIS) normalized difference vegetation index (NDVI) signatures of these 11-classes are shown in Figure 4.

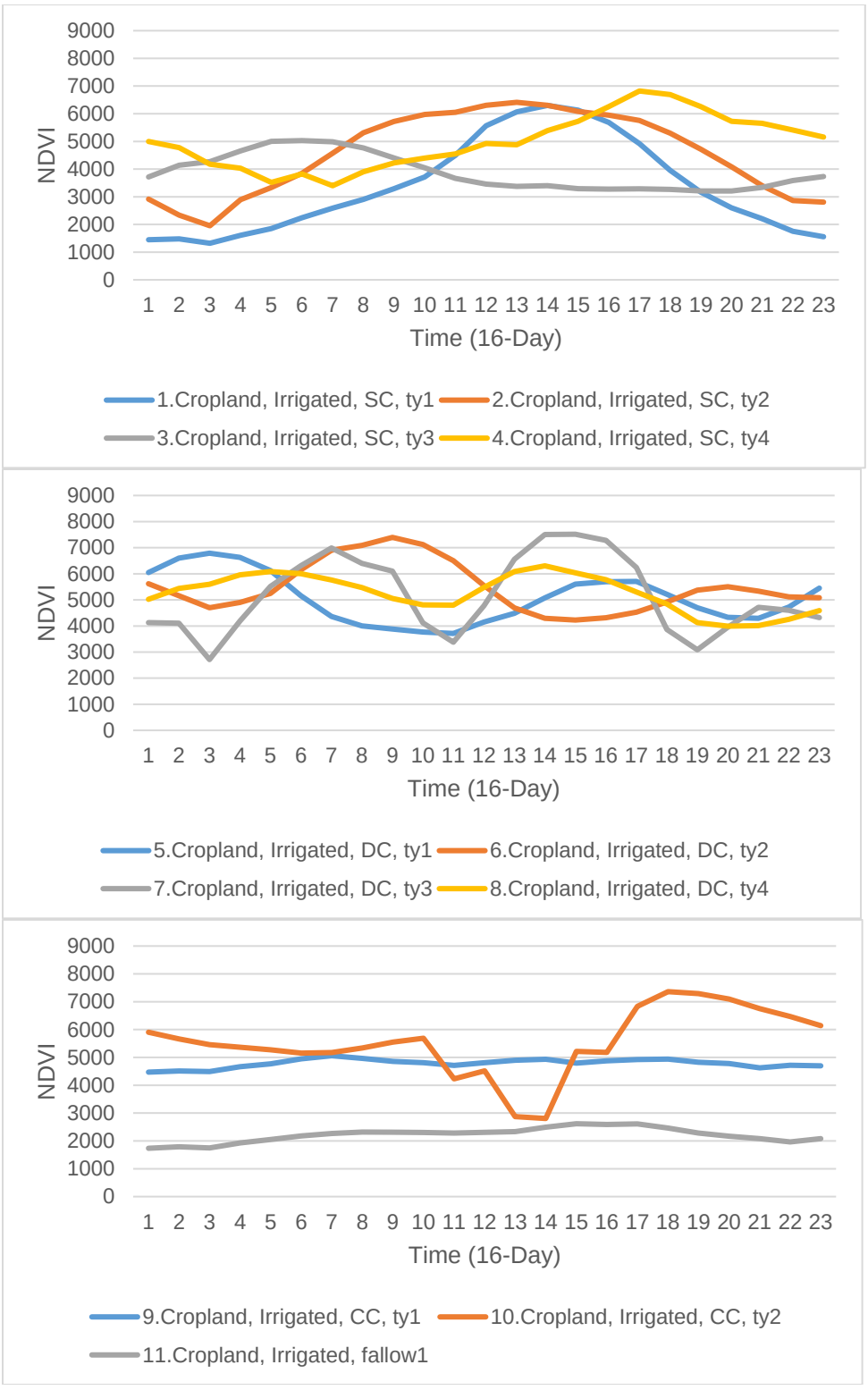

Figure 4. MGIP250-11 class irrigated area product signatures (for map of these 11 classes see Figure 3). Mean time-series Moderate Resolution Imaging Spectroradiometer (MODIS) normalized difference vegetation index (NDVI) signatures of the 11-classes of global irrigated-area product @ 250m (MGIP250-11 class) map shown in Figure 3.

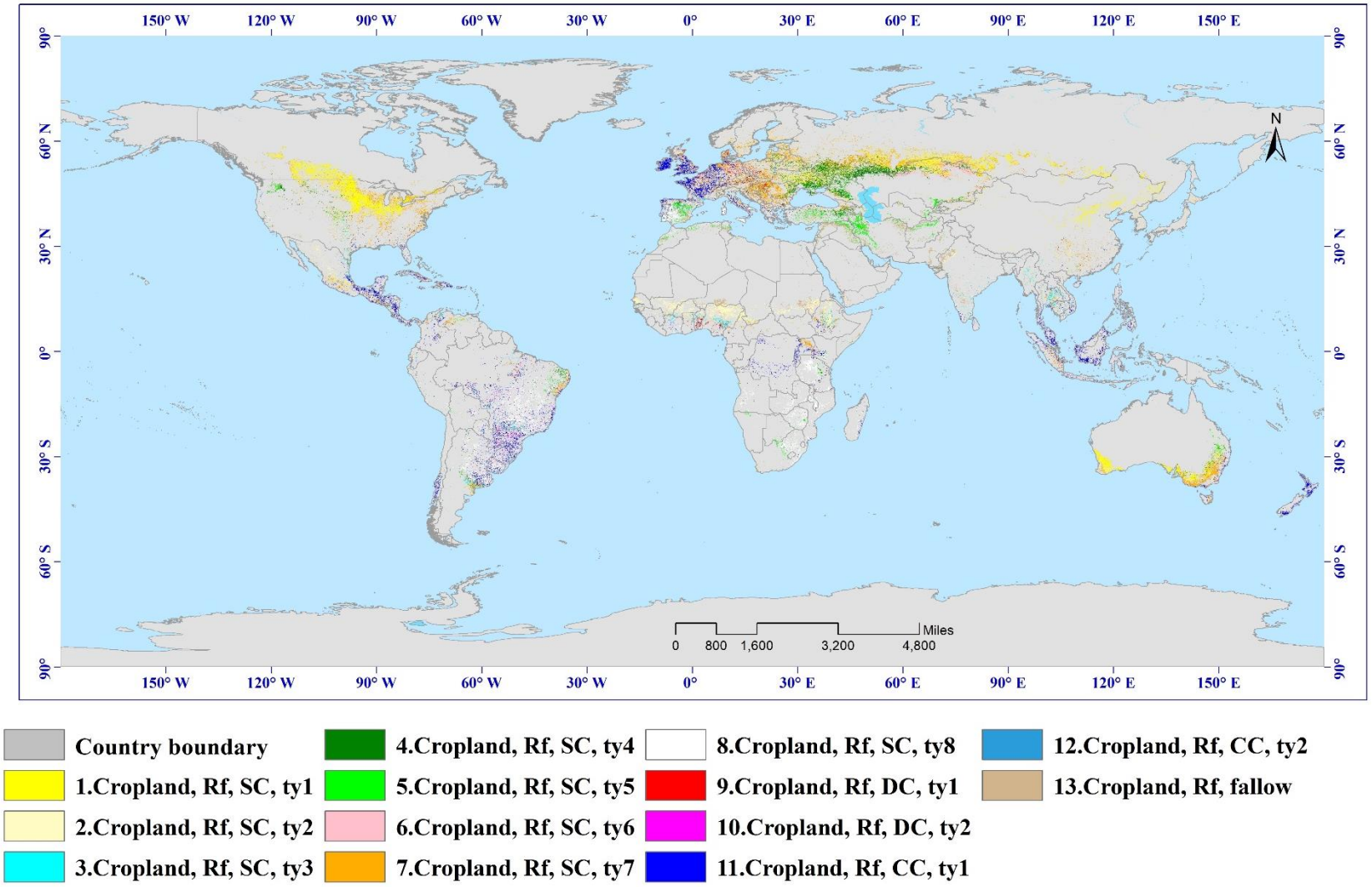

Figure 5. MGRP250-13 class rainfed area product (for signatures of these 13 classes see Figure 6). A MODIS-derived 13-class Global rainfed-area product @ 250m (MGRP250) developed using MODIS 250m time-series data for the nominal year 2015. The Moderate Resolution Imaging Spectroradiometer (MODIS) normalized difference vegetation index (NDVI) signatures of these 13-classes are shown in Figure 6.

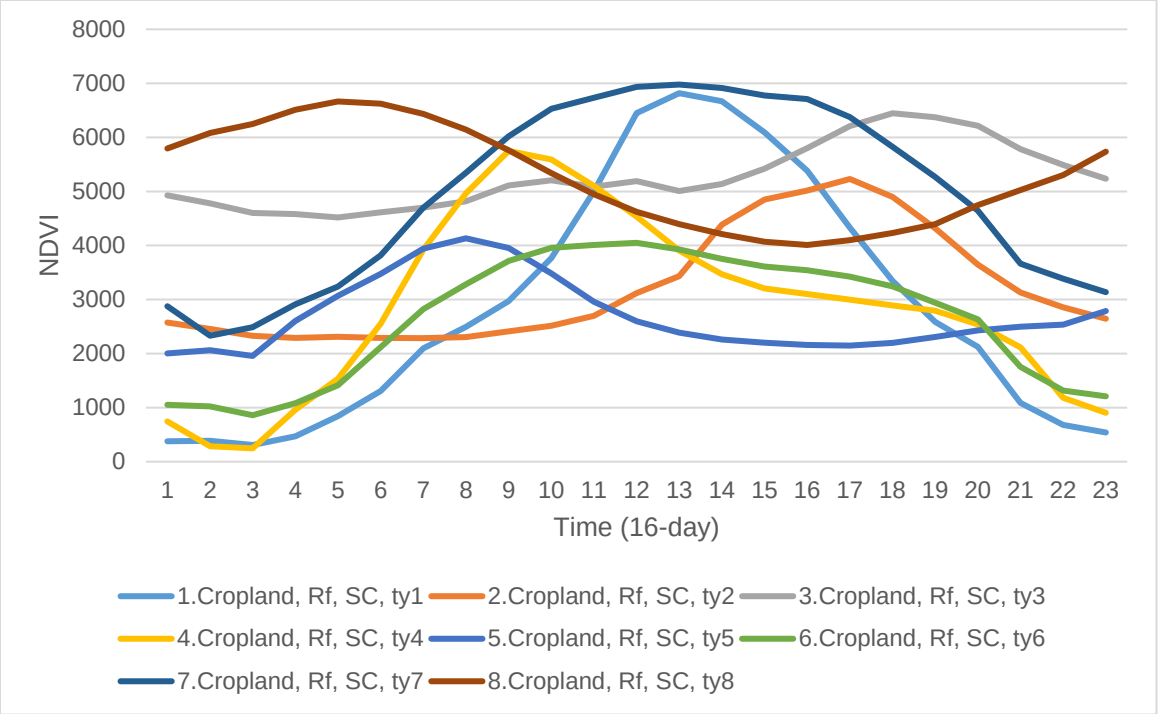

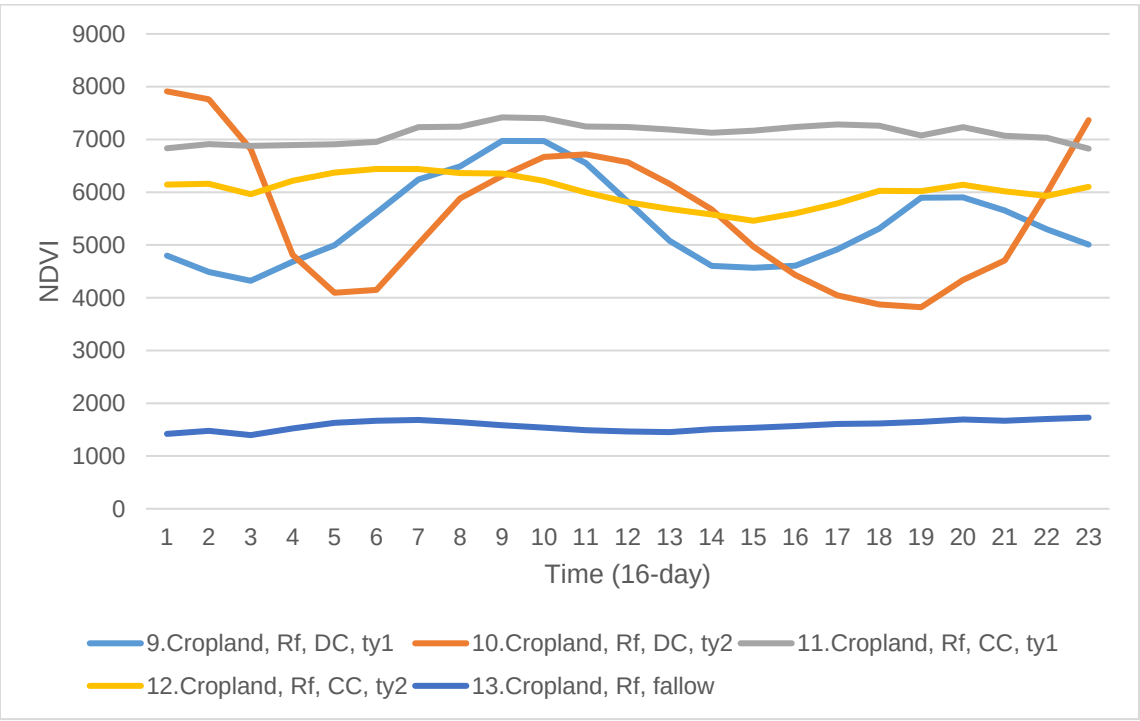

Figure 6. MGRP250-13 class rainfed area product signatures (for map of these 13 classes see Figure 5). Mean time-series Moderate Resolution Imaging Spectroradiometer (MODIS) normalized difference vegetation index (NDVI) signatures of the 13-classes of global rainfed-area product @ 250m (MGRP250) map shown in Figure 5.

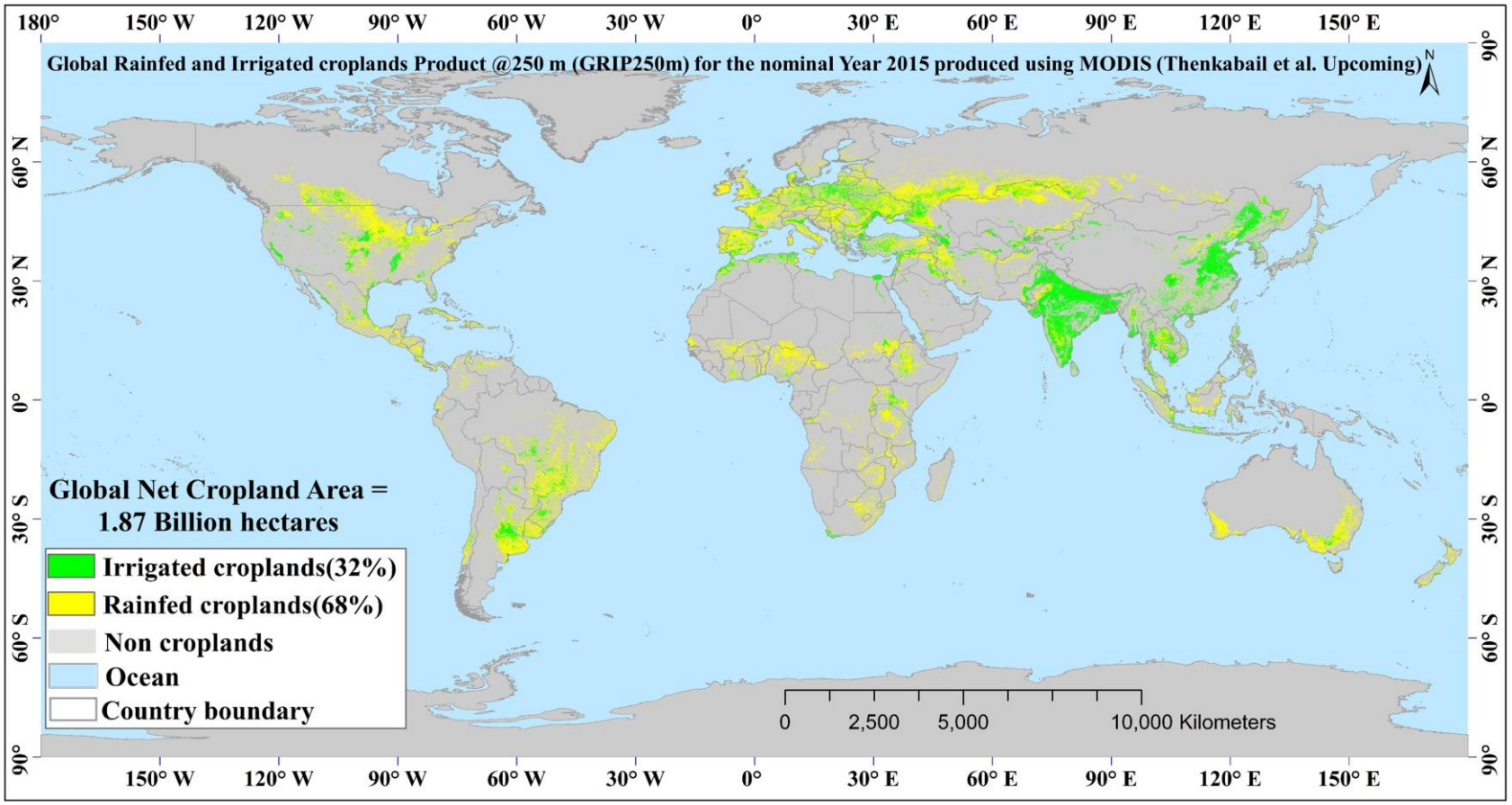

Figure 7. MGRIP250-2 class rainfed and irrigated area product. An Aggregated 2-class MODIS-derived Global rainfed and irrigated-area product @ 250m (MGRIP250) developed using MODIS 250m time-series data for the nominal year 2015. This map is produced by aggregating the MODIS-derived global irrigated-area product, MGIP250-11 class product (Figure 3), and MODIS-derived global rainfed-area product, MGRP250-13 class product (Figure 5) into MGRIP250-2class simplified rainfed and irrigated area product of the world that forms as a baseline starting point for producing the Landsat-derived global rainfed and irrigated area product @ 30 m (LGRIP30).

3. Lack of irrigated and rainfed cropland maps at high resolution (30m or better) product

There remains considerable uncertainty about the precise extent, area and cropping intensity of irrigated and rainfed areas assessments in different parts of the world, due to the dynamics referred to above and systematic problems of under and over-reporting in country statistics and\or uncertainties in coarse resolution remote sensing data derived products.

Teluguntla et al. (2015) reviewed various global irrigated and rainfed cropland products that are available in the public domain. Thenkabail et al., (2012, 2011, 2009a) and Biradar et al., (2009) reported the first remote sensing based global irrigated and rainfed cropland maps and statistics through multi-sensor remote sensing data fusion along with secondary data, and in-situ data. This led to coarse resolution (1-10 km) global irrigated and rainfed cropland products such as the one illustrated in Figure 1. Siebert et al., (2005) produced the first global irrigated area based on country statistics and GIS techniques. This is known as UN FAO global map of irrigated area (FAO-GMIA). These products are certainly advance in terms of using remote sensing, national statistics, and GIS techniques for mapping irrigated and rainfed cropland mapping at the global scale at 1-10 km spatial resolution. Nevertheless, these products lacked the field scale high resolution detail in mapping irrigated and rainfed croplands that lead to uncertainties on precise location of irrigated and rainfed croplands, especially when field sizes were small, or farms were fragmented. It also led to cascading errors in higher level products such as crop type mapping, crop water uses assessments, and crop water productivity mapping and modeling.

The main motivation to develop the Landsat-derived Global Rainfed and Irrigated-Cropland Product @ 30-m (LGRIP30) of the World (GFSADLGRIP30WORLD) was to:

1. Produce the global highest known resolution (1 pixel = 30 m or 0.09 hectares per pixel) global irrigated and rainfed cropland maps using Landsat time-series data.
2. Develop methods and techniques of mapping LGRIP30 that involve twenty-first century remote sensing involving big data analytics, machine learning, cloud computing, and artificial intelligence.
3. Enable the use of LGRIP30 for accurate assessment of crop water use, crop productivity, and crop water productivity.
4. Facilitate production of cropland products that are of great importance for food and water security assessments, modelling, mapping, and monitoring.

V. Algorithm Description

1. Preparing the area for the study

First step in global irrigated and rainfed cropland mapping is to establish global cropland areas. We have described in great details methods and approaches to Landsat derived global cropland extent product (GCEP30; Thenkabail et al., 2021) and published this data on NASA's LP DAAC (https://lpdaac.usgs.gov/news/release-of-gfsad-30-meter-cropland-extent-products/).
The GCEP30 product established that there is 1.8 billion hectares of global croplands, the spatial distribution of it is shown in Figure 8. Once the GCEP30 is produced (Figure 8), we need to identify which of these croplands are irrigated and which are rainfed. The process of doing this is described in detail in series of sub-sections below.

2. Definitions

Cropland mapping definitions using remote sensing were based on discussions in several global food security support analysis data (GFSAD) project workshops captured (Thenkabail et al., 2021). Key to effective mapping is a precise and clear definition of what will be mapped. It is the first and primary step, with different definitions leading to different products.

For example, irrigated areas are defined and understood differently in different applications and contexts. One can define them as areas which receive irrigation at least once during their crop growing period. Alternatively, they can be defined as areas which receive irrigation to meet at least half of their crop water requirements during the growing season.

One other definition can be that these are areas that are irrigated throughout the growing season. In each of these cases, the irrigated area extent mapped will vary. Similarly, croplands can be defined as all agricultural areas irrespective of type of crops grown or they may be limited to food crops (and not the fodder crops or plantation crops). So, it is obvious that having a clear understanding of the definitions of what we map is extremely important for the integrity of the products developed.

We defined cropland products as follows:

- **Minimum mapping unit**

The minimum mapping unit of a particular crop is an area of 3 by 3 (0.81 hectares) Landsat pixels identified as having the same crop type (Congalton (2015)).

- **Cropland extent**

All cultivated plants harvested for food, feed, and fiber, including plantations (e.g., orchards, vineyards, coffee, tea, rubber).

- **What is a cropland pixel? What is an irrigated pixel?**

In a 30mx30m pixel area (0.09 hectares), croplands are either cropped or left fallow. The croplands are either equipped for irrigation (e.g., within a command area of surface water irrigation system or has assess to extracted ground water) or not equipped for irrigation (left for rainfed).

- **Irrigated areas**:

Irrigated areas are cropland areas that are irrigated during the crop growing season through artificial application of water to meet the crop water demand requirements, partially or fully. Irrigated areas are those areas which are irrigated one or more times during crop growing season. Some irrigated areas are watered throughout the growing season and others only when there is deficit water for optimal crop growth.

Irrigation sources can be varied and includes water drawn from surface and ground water reservoirs. Surface irrigation sources include major-medium-small reservoirs created by dams or barriers diverting water from the river systems. Ground water sources include open wells and tube-wells drawing water from deep acquirers.

- **Rainfed areas**:

Rainfed areas are the cropland areas with no artificial irrigation whatsoever and are completely precipitation dependent.

Precipitation includes moisture retained in soils prior to cropping season from snowfall\rainfall and direct rainfall on the croplands during the crop growing season.

- **Cropping intensity**

Number of cropping cycles on a piece of croplands within a 12-month period. Cropping intensity can be single, double, triple, or continuous (e.g., plantations).

- **Crop types**

All crops grown in irrigated and rainfed croplands are considered. Major world crops, that occupy about 70% of the cropland areas globally, include Wheat, Corn, Rice, Barley, Soybeans, Pulses, Cotton, Potatoes, sorghum, and sugarcane.

Specific to this ATBD, irrigated and rainfed cropland mapped are defined above and approach to mapping them using Landsat 30m remote sensing data is discussed below.

3. Reference training and validation data

First, we used an excellent distribution of ~112,000 global irrigated and rainfed cropland field-data samples (Figure 9) available with us to train, test, and validate the products. These data are from multiple sources (Figure 9) such as: (a) sub-meter to 5 m very high-resolution imagery (VHRI), (b) other map sources obtained from our partners or from literature, and (c) through numerous field visits to many countries by various people during 2003-2017 timeframe.

Further, during this project, we established 16,435 samples (Figure 10, 11; Table 4) for training and testing and 10,477 for validation (Figure 12; Table 4). Of the 16,435 samples for training and testing, there were 7,544 irrigated samples (Figure 10; Table 4) and 8,891 rainfed samples (Figure 11; Table 4). Of the 10,477 samples for validation, there were 4,810 irrigated samples and 5,667 rainfed samples (Figure 12; Table 4).

These samples are distinctly distributed around the world: (a) Figure 10 shows distribution of irrigated area samples, (b) Figure 11 shows distribution of rainfed area samples, and (c) Figure

12 shows validation samples for irrigated and rainfed croplands. Table 4 provides the number of samples distributed in each of the 13 agro-ecological zones (AEZs) (Figure 13). The initial 74 AEZs (Thenkabail et al., 2021) were simplified to 13 AEZs.

These extensive sample data (Figure 9-12, Table 4) were sourced from many state-of-the-art datasets such as the USDA CDL, AAFC, European Monitoring agricultural resources, CGIAR through their Consortium for Spatial Information, and numerous other sources. When these data were gathered from sub-meter to 5-m very high-resolution data, they have information on croplands versus non-croplands. The ground data samples had information such as croplands, non-croplands, crop watering methods (irrigated or rainfed), and crop types.

Figures 10 and 11 illustrate the samples collected in this study from ground surveys, sub-meter to 5-m very high spatial resolution imagery (VHRI) providing irrigated and rainfed cropland locations. These samples (Figure 10 and 11) were used only for training and testing machine learning algorithms (MLAs) when producing the Landsat-derived Global Rainfed and Irrigated-Cropland Product @ 30-m (LGRIP30). Figure 12 shows samples used only for validation the LGRIP30.

Table 4 shows the sample distribution in each of the 13 AEZs for irrigated and rainfed crops. The nature of the samples distributed in Figure 9 through 11 are illustrated taking some ground data for (a) rainfed areas (top half of Figure 14), (b) irrigated areas (bottom half of Figure 14). The nature of the samples distributed in Figure 9 through 11 were also illustrated taking some sub-meter to 5-m very high-resolution imagery for: (c) irrigated areas (Figure 15), and (d) rainfed areas (Figure 16).

4. Image Stratification

The world was segmented into 13 zones (Figure 13b) from original 74 AEZs (Figure 13a) or a combination of some of the zones together to process the data and produce Landsat-derived global rainfed & irrigated product @ 30m (LGRIP30). The 74 AEZs are well described in Thenkabail et al., 2021. The 13 zones were derived from 74 zones inorder to simplify processing mechanism.

5. Data Fusion, Data Integration, and Analysis Ready Data Cube (ARD-Cubes)

Landsat 8 time-series surface reflectance product that is already available on the Google Earth Engine (GEE) (Gorelick et., 2017) was the primary data used in the study. Data for every 16 days from January 1, 2014, through December 31, 2016, was used in processing. In total 10 bands (blue, green, red, NIR, SWIR1, SWIR2, TIR, EVI, NDWI, NDVI) of data were processed. All Landsat-8 images were cloud masked using CFMask in GEE (Foga et al. 2017). Other 30m resolution bands such as the Shuttle Radar Topography Mission (SRTM) elevation and slope, soils (SoilGrids250m WRB; Poggio et al. 2021), and local information were added to data cubes for each AEZ as needed to best help separate classes. These Landsat analysis ready data cubes (ARD-cubes, e.g., Figure 17) were composed on a cloud platform like GEE (Thenkabail et al., 2021, Oliphant, 2019, Phalke et al., 2020, Xiong et al., 2017a) to help seamlessly code and compute using MLAs.

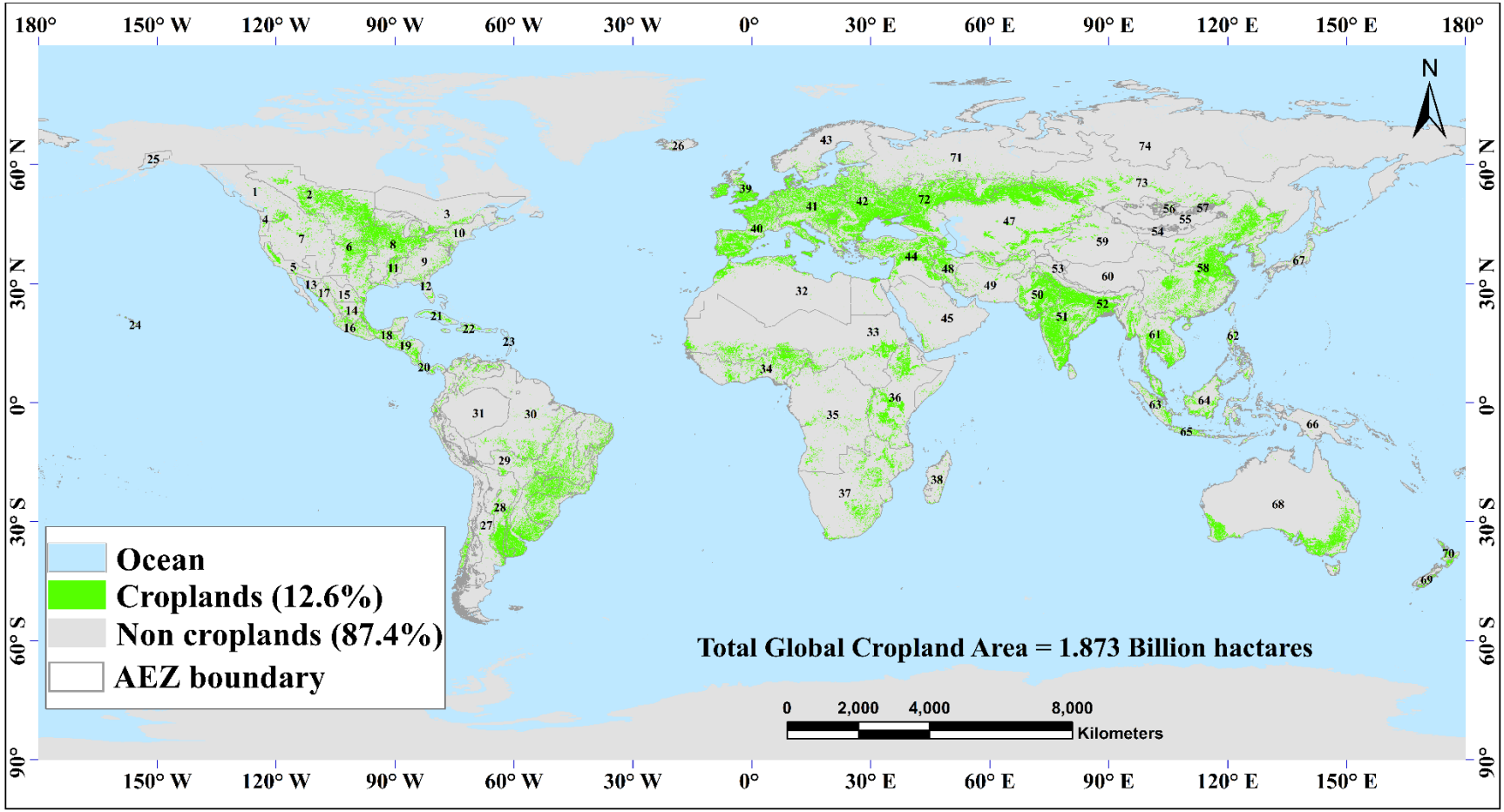

Figure 8. GCEP30. The Landsat-derived Global cropland extent product @ 30m (GCEP30) (Thenkabail et al., 2021).

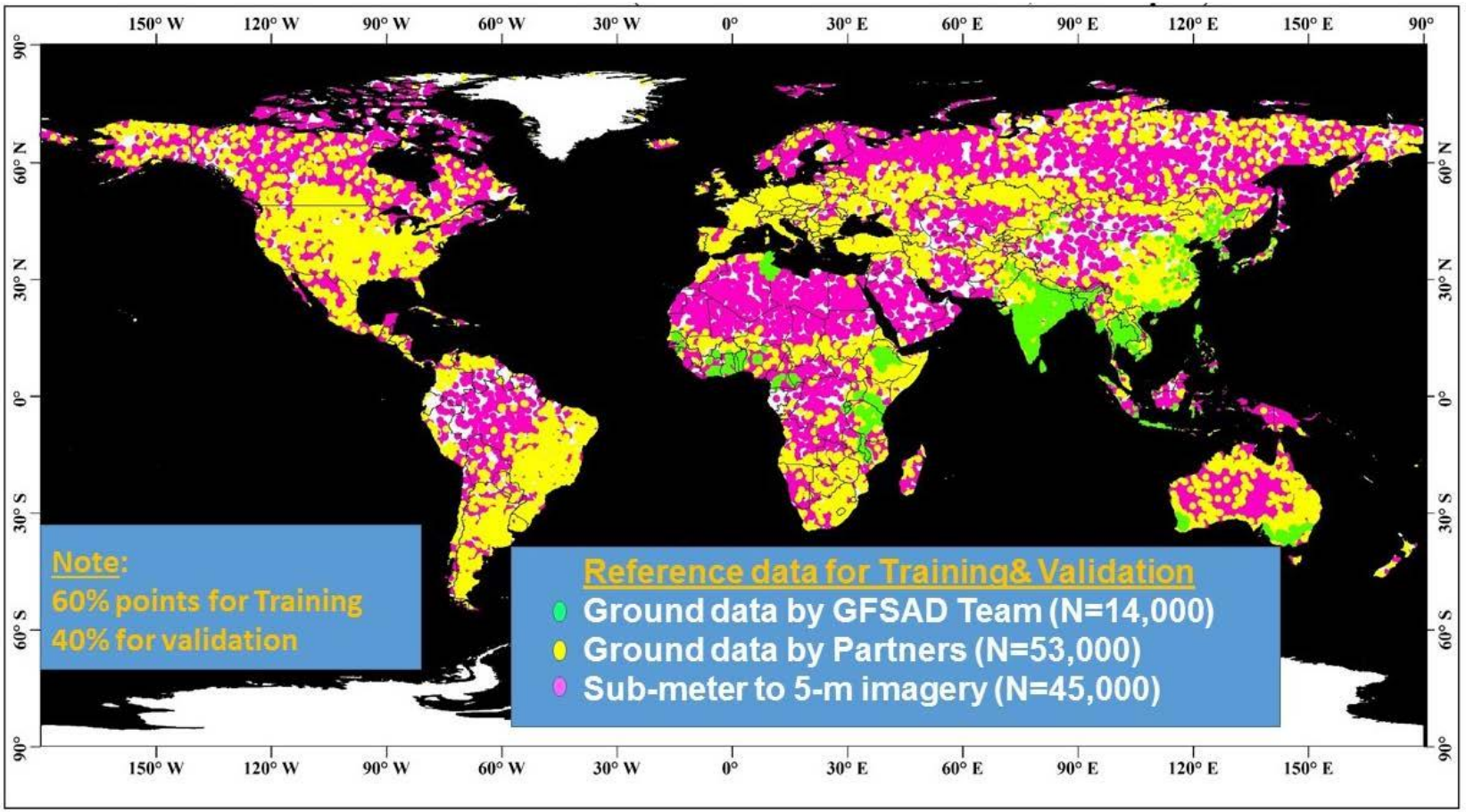

Figure 9. Ground data on croplands including irrigation and rainfed. Distribution of Reference data gathered from multiple sources either through ground data or through sub-meter to 5-m very high-resolution imagery data (Thenkabail et al., 2021, Congalton et al., 2017). These data have both croplands **versus** non-croplands as well as rainfed croplands **versus** irrigated croplands. Detailed description of these data is provided in Thenkabail et al., 2021. Of these data 19,171 samples, well spread-out throughout the world were used in validating the Landsat 30m derived on global cropland extent product (GCEP30) and the process is described by Thenkabail et al. (2021) and Congalton et al., 2017. The validation data are also made available through NASA's LP DAAC (Congalton et al., 2017).

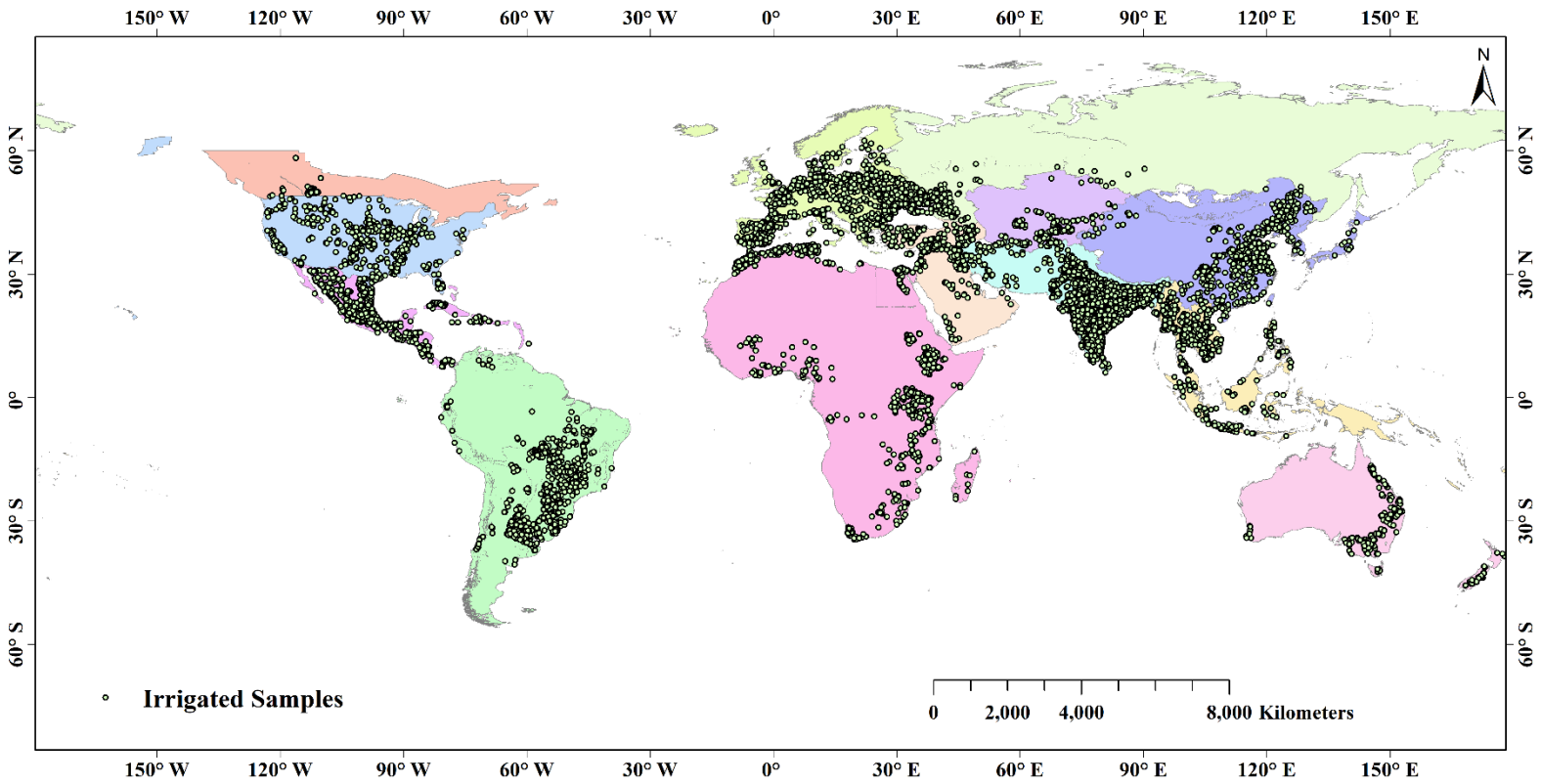

Figure 10. Reference irrigated samples for training and testing. Distribution of Reference training and testing data for irrigated croplands gathered from multiple sources that include ground surveys, published National, regional, and global maps along with interpretations using sub-meter to 5-meter very high-resolution imagery, by interpreting and finalizing. There are 7,544 samples. These samples were NOT used in validation.

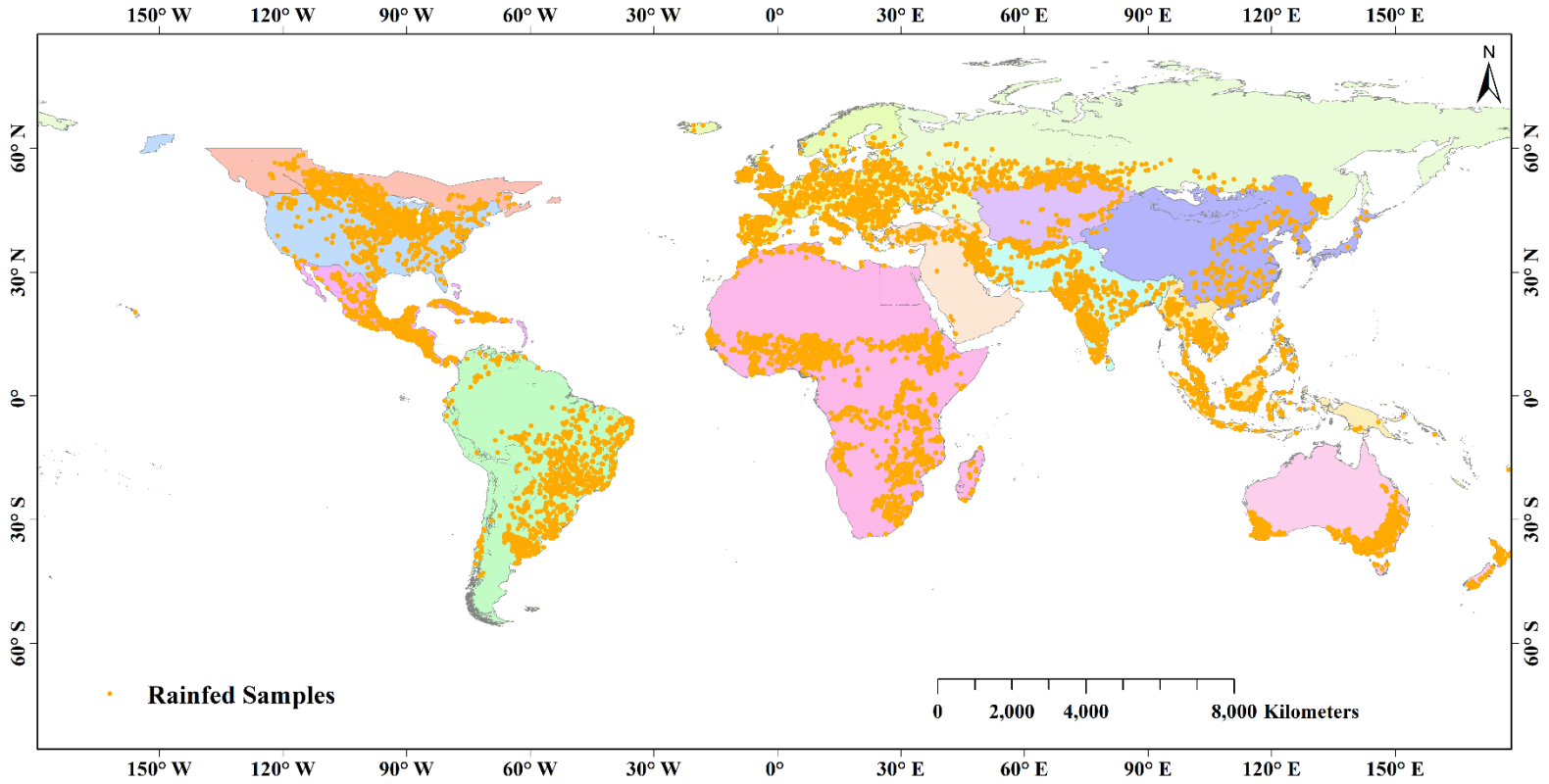

Figure 11. Reference rainfed samples for training and testing. Distribution of Reference training and testing data for rainfed croplands gathered from multiple sources that include ground surveys, published National, regional, and global maps along with interpretations using sub-meter to 5-meter very high-resolution imagery, by interpreting and finalizing. These are 8,891 samples. These samples were NOT used in validation.

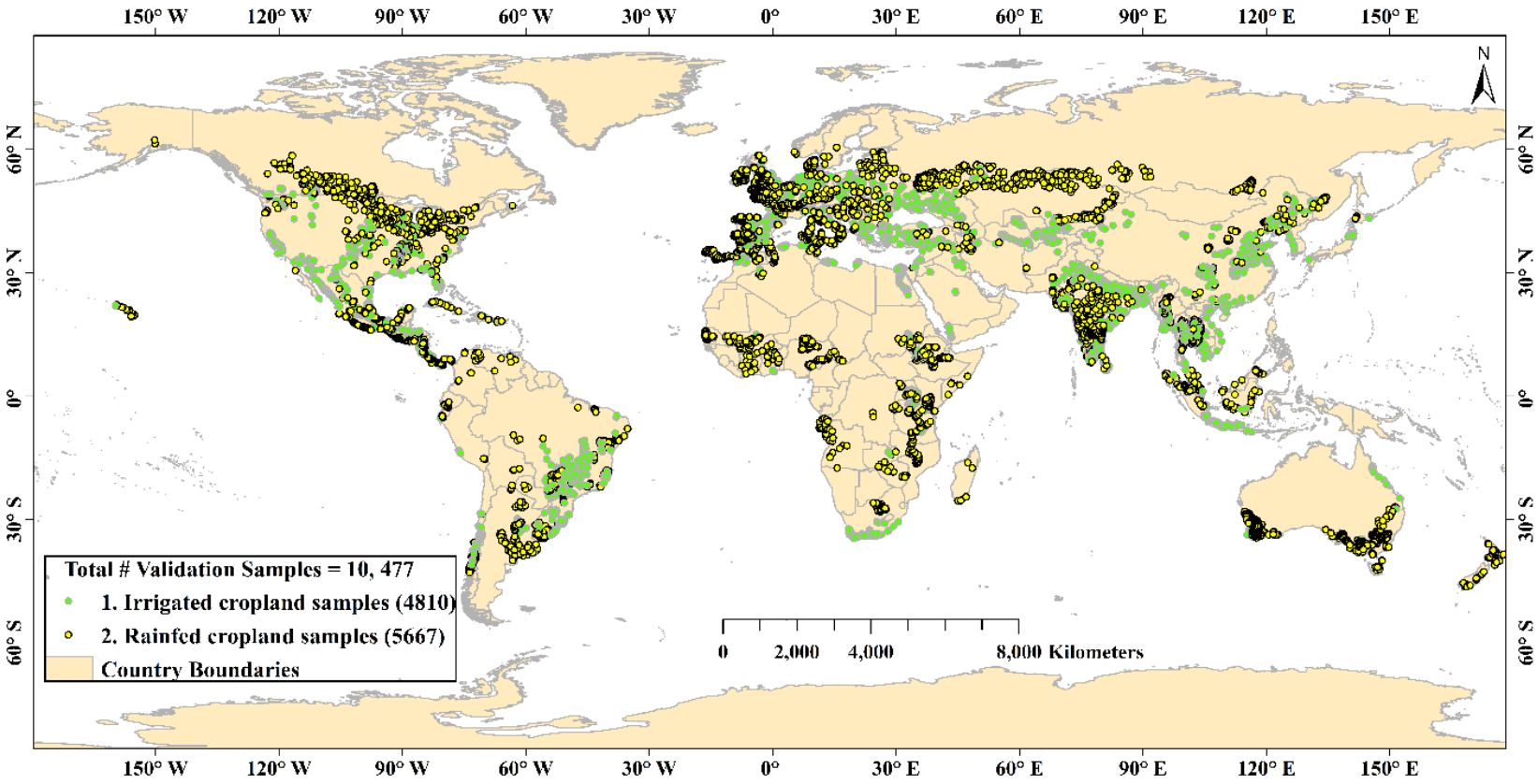

Figure 12. Reference irrigated and rainfed samples for validation. Distribution of Reference validation data used in accuracy assessments of Landsat-derived Global Rainfed and Irrigated-Cropland Product @ 30-m (LGRIP30). There were 10,477 samples of which 5,667 were rainfed and 4,810 were irrigated.

Table 4. Distribution of reference training, testing, and validation samples used in the 13 agroecological zones (AEZs). Zone wise ground reference data /samples collected for the product training and validation.

		Ground data					
Zone No	Zone Name	Training samples			Validation samples		
#	Name	Irrigated	Rainfed	Total	Irrigated	Rainfed	Total
1	United States	520	882	1402	337	575	912
2	Canada	99	372	471	63	240	303
3	Central America	699	739	1438	439	475	914
4	South America	654	730	1384	426	434	860
5	Africa	928	1581	2509	590	1015	1605
6	Europe	1003	1248	2251	653	807	1460
7	Russia	88	283	371	57	189	246
8	Central Asia	180	285	465	116	187	303
9	Middle East& WestAsia	313	91	404	206	60	266
10	SouthAsia-AFG-Iran	1750	1173	2923	1135	756	1891
11	China&Korea	520	253	773	320	142	462
12	SouthEastAsia	568	537	1105	328	332	660
13	Australia-NewZealand	222	717	939	140	455	595
	Global Total	**7544**	**8891**	**16435**	**4810**	**5667**	**10477**

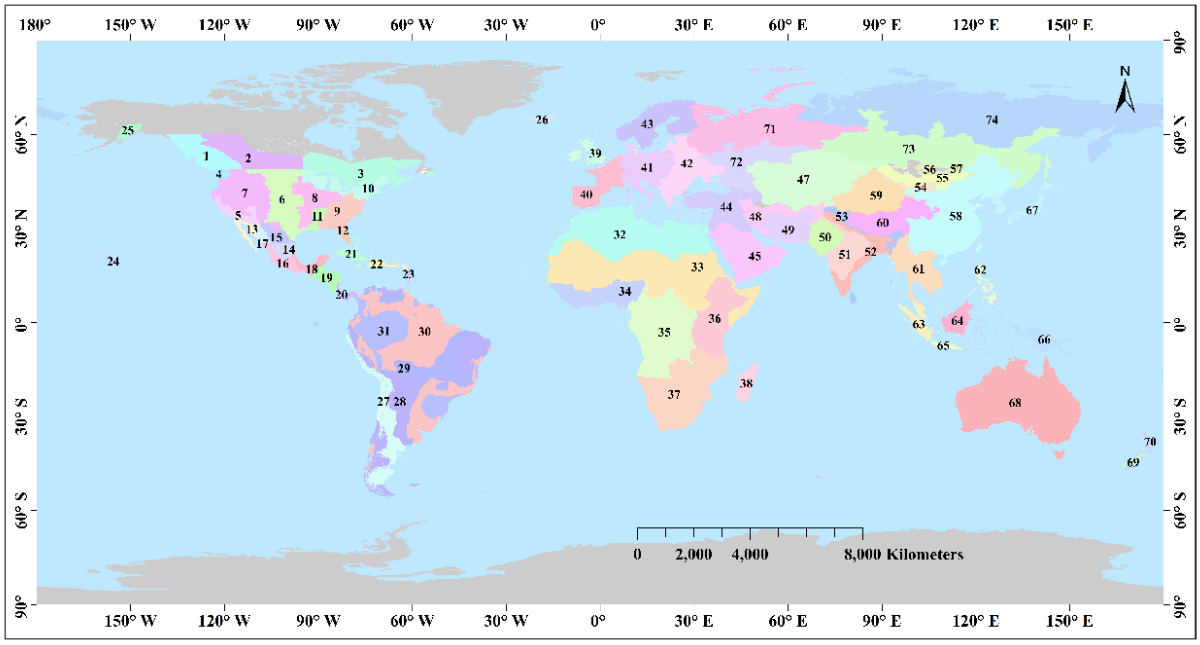

Figure 13a

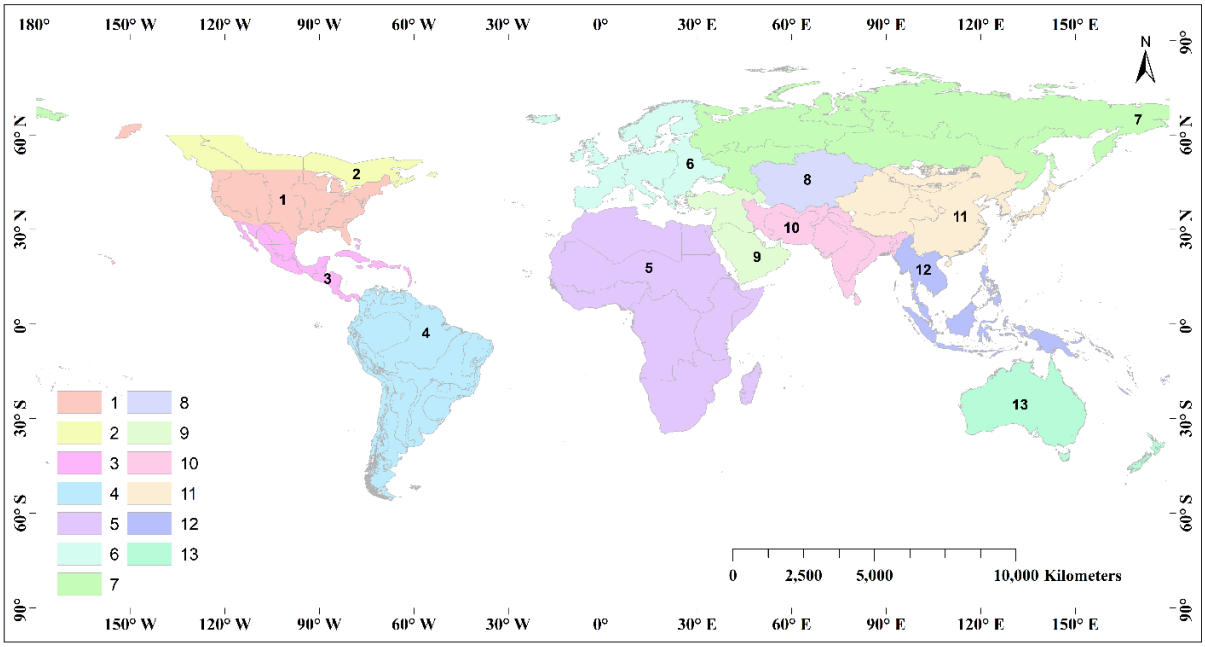

Figure 13b.

Figure 13. Agroecological zones (AEZs) of the world. The world is divided into 74 AEZs as shown in top figure (Thenkabail et al., 2021). Those 74 were reduced to 13 zones for ease of work as shown in bottom Figure. Throughout rest of the paper, we will discuss the process of developing Landsat-derived Global Rainfed and Irrigated-Cropland Product @ 30-m (LGRIP30). First LGRIP30 products were produced for each of the 13 zones and were then combined to produce a single global LGRIP30 product.

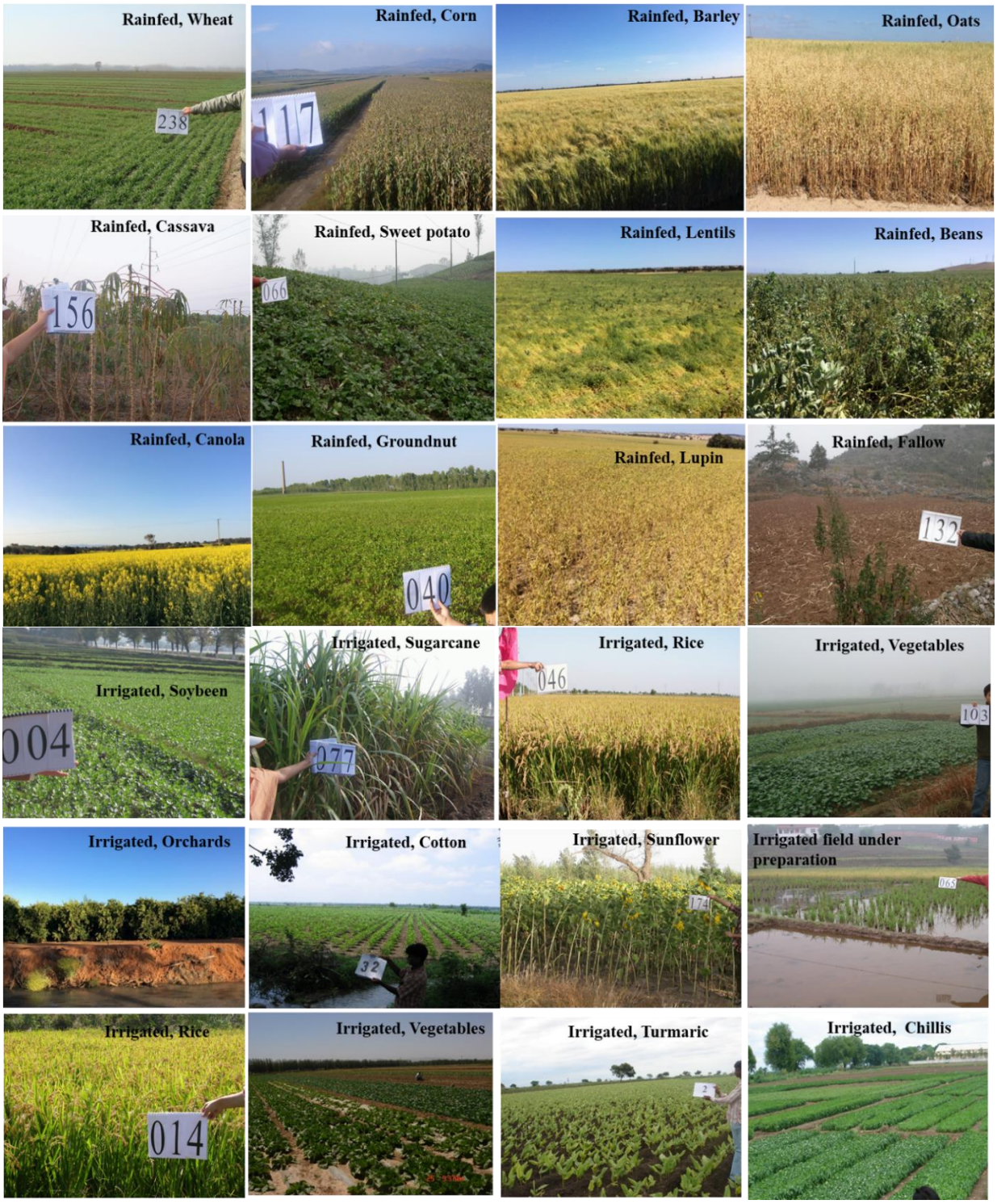

Figure 14. Ground reference data samples of rainfed and irrigated crops. These data were gathered from various sources and compiled into database (Figure 9-12). These data were used both in training and testing Landsat-derived Global Rainfed and Irrigated-Cropland Product @ 30-m (LGRIP30) during product development phase.

Figure 15. Ground reference data samples highlighting irrigated areas. These data were gathered from sub-meter to 5-m very high-resolution imagery. The sample location of these data is shown in Figure 10. Only a few samples from Figure 10 are illustrated here. These data were used both in training and testing Landsat-derived Global Rainfed and Irrigated-Cropland Product @ 30-m (LGRIP30) during product development phase.

Figure 16. Ground reference data samples highlighting rainfed areas. These data were gathered from sub-meter to 5-m very high-resolution imagery. The sample location of these data is shown in Figure 11. Only a few samples from Figure 11 are illustrated here. These data were used both in training and testing Landsat-derived Global Rainfed and Irrigated-Cropland Product @ 30-m (LGRIP30) during product development phase.

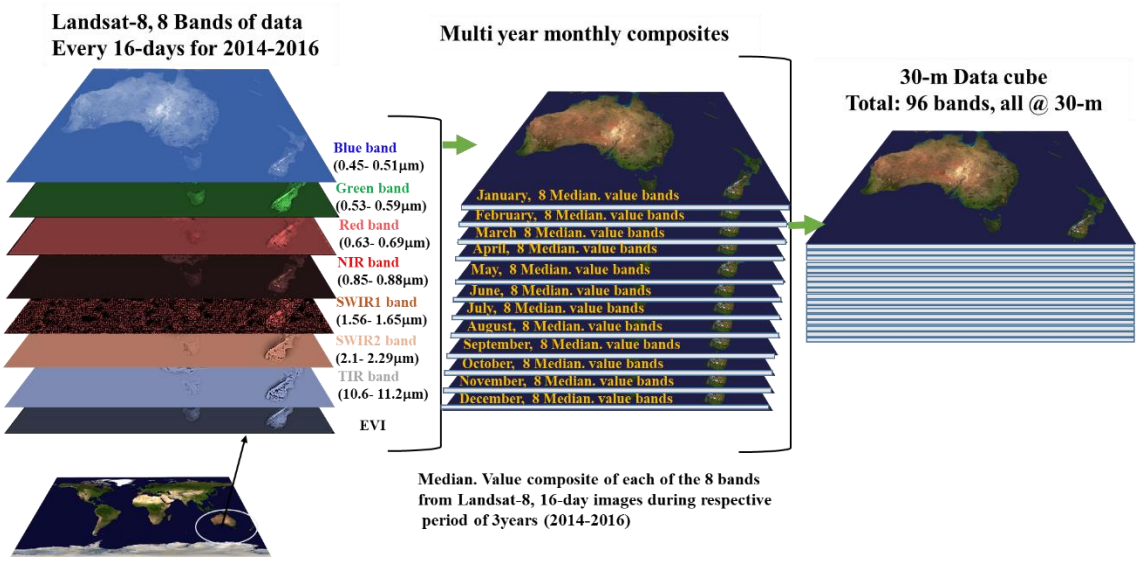

Figure 17. Analysis ready Landsat 30m data cubes (ARD30-cubes). The ARD30-cubes were developed for each of the 13 zones, classified, classes identified, and the final Landsat-derived Global Rainfed and Irrigated-Cropland Product @ 30-m (LGRIP30) was produced.

f. Landsat 30m derived on global cropland extent product (GCEP30)

In order to produce Landsat-derived Global Rainfed and Irrigated-Cropland Product @ 30-m (LGRIP30), first we produced two coarser resolution products:

1. An aggregated 2-class SPOT-Vegetation, AVHRR and other ancillary data derived global rainfed and irrigated-area product @ 1000m (GRIP1000) (Figure 2); and
2. An Aggregated 2-class MODIS-derived Global rainfed and irrigated-area product @ 250m (MGRIP250) (Figure 7).

In addition, Landsat 30m derived global cropland extent product (GCEP30) that provides croplands versus non-croplands (Figure 8) was produced as description is detailed in USGS professional paper (Thenkabail et al., 2021) and will not be repeated here. The GCEP30 product (Figure 8) is also made available for download in NASA's LP DAAC (Thenkabail et al., 2021): https://lpdaac.usgs.gov/news/release-of-gfsad-30-meter-cropland-extent-products/

VI. Methodology for mapping Landsat 30m derived global rainfed and irrigated area product (LGRIP30)

A. Overview on irrigated and rainfed cropland mapping

The irrigated and rainfed cropland mapping methods using remote sensing data have matured over the years as evidenced by growing body of scientific literature (Gumma et al., 2022, Zhang et al., 2022, Xing et al., 2022, Thenkabail et al., 2021, Nagaraj et al., 2021, Zohaib et al., 2019, Teluguntla et al., 2017, Friedl et al., 2002; Hansen et al., 2002; Loveland et al., 2000; Ozdogan and Woodcock, 2006; Thenkabail et al., 2009a; Thenkabail et al., 2009b; Wardlow and Egbert, 2008; Wardlow et al., 2006; Wardlow et al., 2007; Xiao et al., 2006). Satellite images offer the most objective data to map irrigated and rainfed cropland areas by adopting several methods and approaches. These include detecting irrigation structures and command areas, National maps that provide base maps delineating irrigated command areas or show boundaries of irrigated and rainfed areas, ground data (e.g., Figures 14), very high spatial resolution imagery (VHRI, e.g., Figure 15, 16), and distinct spectral characteristics (e.g., irrigated areas often have 2 or 3 crops annually that can easily be detected in time-series spectral reflectivity or NDVI temporal-plots).

We begin separating irrigated areas from rainfed areas starting with the Landsat-derived global cropland extent product at 30m (GCEP30) (Figure 8; Thenkabail et al., 2021). Methodology of classifying and class identification of GCEP30 (Figure 8; Thenkabail et al., 2021) into irrigated and rainfed is series of steps described in sub-sections below. It begins with:

1. utilizing the GCEP30 base map (Figure 8; Thenkabail et al. 2021) to start with.
2. studying in each of the distinct agroecological zones of the world (AEZs, Figure 13a, b), by creating ARD30 cubes, (e.g., Figure 17) for each or a combination of the AEZs.
3. creating knowledgebase (e.g., Figure 18, 19) to separate irrigated areas from rainfed areas utilizing reference data (e.g., Figures 9-11, Figures 14-16).
4. classifying ARD30 cubes (e.g., Figure 17) for each of the AEZs (Figure 13a, b) using methods (Figure 20-25) described in sub-sections below.
5. identifying classes based on spectral information (e.g., Figures 18-26), ground data (e.g., Figure 9-11, 14), and image interpretations (Figures 15-16), labeling them and then finalizing irrigated and rainfed classes (e.g., Figure 27-31).

Detailed methodology leverages on our earlier work of global cropland extent product @ 30 m (Thenkabail et al., 2021, Xiong et al., 2017a,b, Teluguntla et al., 2017) and global irrigated and rained area cropland products also by our team (Thenkabail et al., 2016, Teluguntla et al., 2015; Thenkabail et al., 2012, 2011, 2010, 2009a, 2007, Gumma et al. 2022). Leveraging on that, specific methodological steps are described below in this algorithm theoretical basis document or ATBD (Teluguntla et al., 2023a). Another LGRIP30 manuscript is currently in preparation (Teluguntla et al., 2023b). Methods adopted in this LGRIP30 are as discussed below (Page 33-57):

B. Machine learning (ML) classification methods: Supervised pixel-based

In machine learning we start with inputs and outputs and that produces a formula which is called machine learning model. There are two categories of machine learning models: pixel based and object-based models. Supervised and unsupervised are two pixel-based approaches, in supervised learning you know what outputs are called labels. In unsupervised learning you are asking model to tell the output groups are to explore analysis. We have used Radom Forest (RF), Support vector machines (SVM) supervised approaches and an unsupervised classification approach called ISO-CLASS-clustering (Lillesand et al., 2014) which detects the similar inputs.

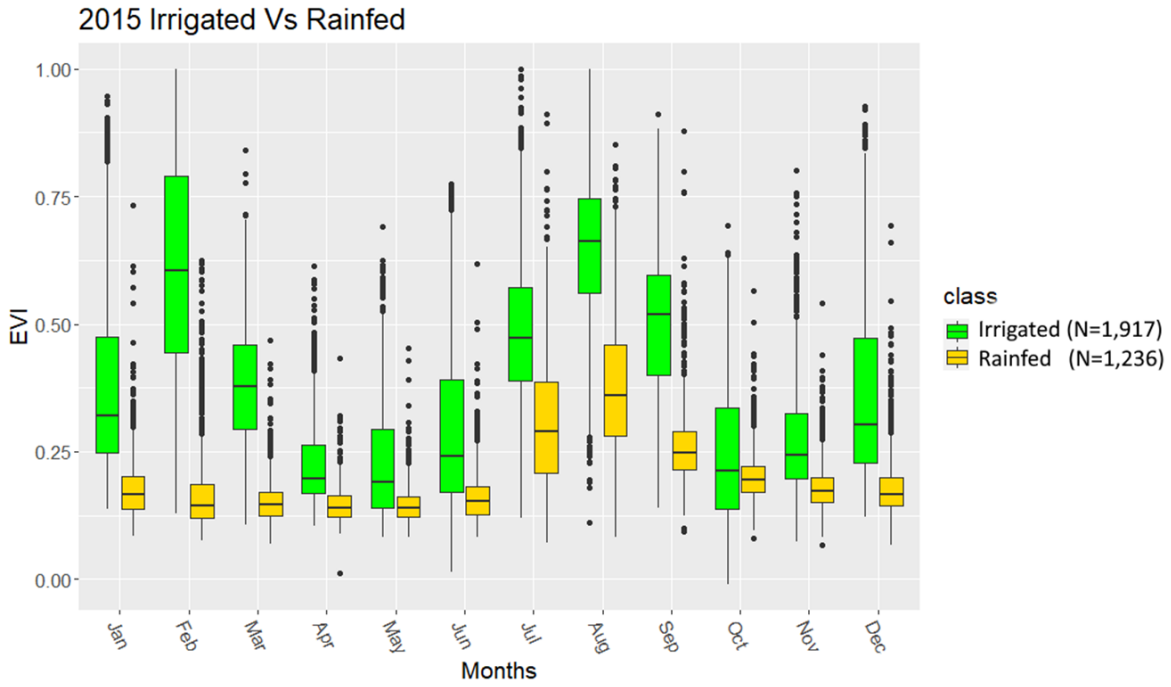

Figure 18. Irrigated *versus* rainfed cropland class separation knowledgebase. Illustration of Landsat-derived Enhanced Vegetation Index (EVI) time-series box-plot profiles for irrigated and rainfed croplands samples in an agroecological zone.

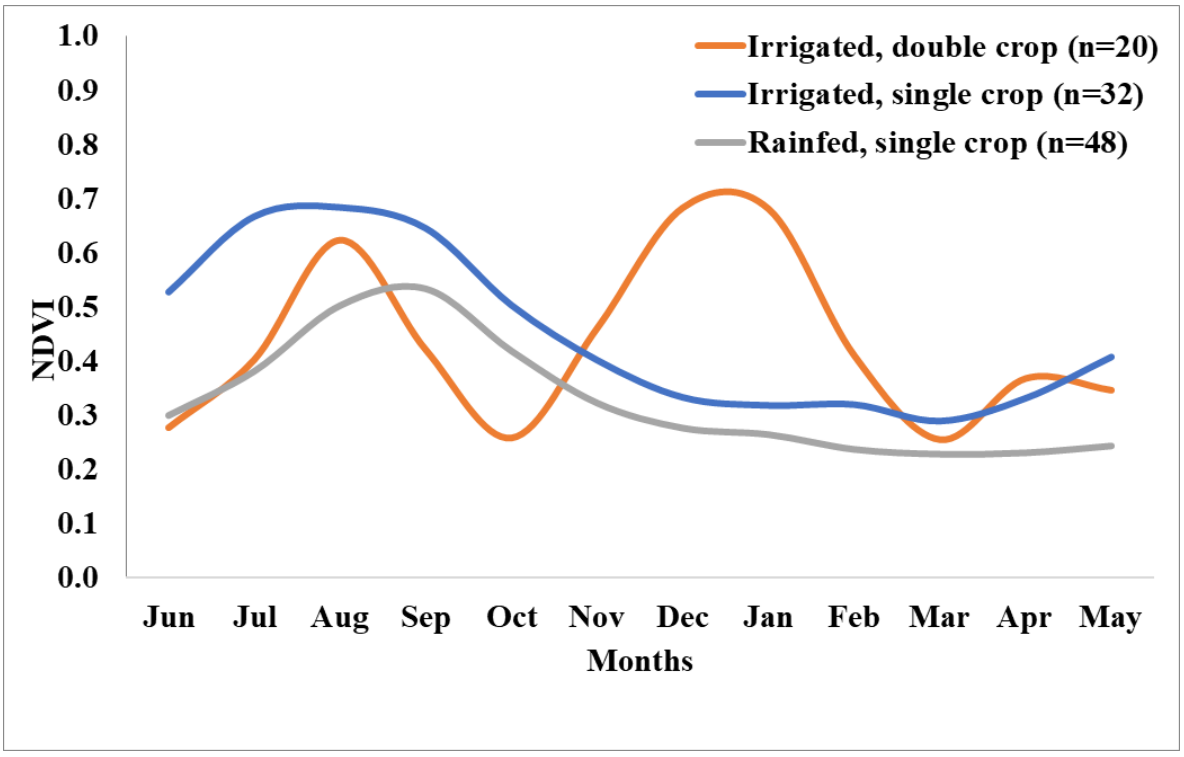

Figure 19. Irrigation versus rainfed cropland separation knowledgebase. Illustration of Landsat-derived Normalized Difference Vegetation Index (NDVI) time series profiles for irrigated and rainfed croplands in an agroecological zone.

B1. Random Forests (RF) supervised classification

Random forest (RF) machine learning algorithm (MLA) is a pixel-based supervised classification that uses multiple decision trees to assign classification labels and is generally immune to data noise and overfitting and is extremely useful in classifying remote sensing data (Figure 20). RF classifiers can successfully handle high data dimensionality and typically achieve higher accuracies in comparison with other approaches such as maximum likelihood, single decision trees (Belgiu and Drăguţ, 2016; Lawrence et al., 2006; Na et al., 2010). Random Forest classifiers construct multiple de-correlated random decision trees that are bootstrapped and aggregated to classify a dataset by using the mode of predictions from all decision trees (Breiman, 2001). The RF classifier is more robust than single decision tree (Chan and Paelinckx, 2008) and easier to be implemented than many other advanced classifiers such as Support Vector Mission (SVM) (Pelletier et al., 2016). Additionally, RF classifiers provide a quantitative measurement of each variable's contribution to the classification output, which is useful in evaluating the importance of each variable.

Random Forest classifiers have several parameters including number of classification trees, number of variables used in each classification tree, and minimum leaf population. When the number of trees increases, the overall accuracy of classification increases without overfitting (Breiman, 2001). While training sample imbalance can affect the RF classification output by over-fitting the majority class (Breiman, 2001; Chen et al., 2004), various methods such as down sampling the majority class can provide immunity against over-fitting (Sun et al., 2007). The optimized parameter values were selected by selecting the training samples (Table 4), running the RF algorithm, and testing the classification output for overall, producer's and user's accuracies in error matrix. The goal is to obtain not just the high overall accuracies, but also a good balance of producer's accuracies (or least errors of omissions) and user's accuracies (or least errors of commissions). It is not just the high number of training samples of a class that help attain optimal accuracies, but the purity (e.g., pure cropland samples instead of mixed) of the samples as well.

All supervised pixel-based classifications rely heavily on the input training samples. To discriminate croplands under various environments and conditions, two criteria are very important:
1. RF classifications need to take place in AEZs or RAEZs (e.g., Figure 13a, b), and
2. The sample size (Table 4) of the initial training dataset for the RF classifier needs to be large, especially in complex regions.

All samples were selected to represent a 90-m x 90-m polygon (Table 4). The number of iterations required for the training sample selection is a function of the complexity of the area. If the classification results were not satisfactory, we increased the training samples till we attained satisfactory classification results. Once that was achieved, accuracy assessments were performed using the independent validation data (Table 4). A product was accepted as final only when the overall, producer's and user's accuracies were adequately high (typically above 80%).

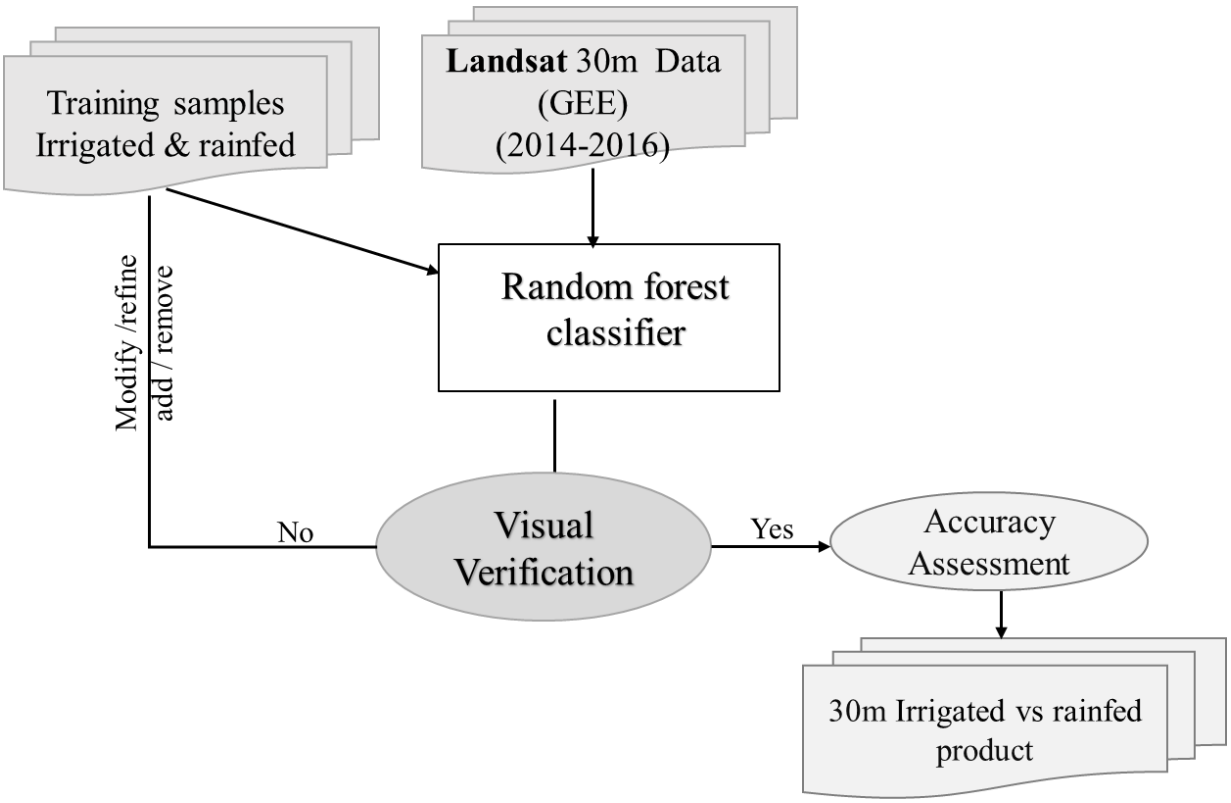

Figure 20. **Overview of methodology for irrigated vs. rainfed cropland mapping using Random Forest.** This study used a pixel-based supervised Random Forest machine learning algorithm for classification and executed on Google Earth Engine cloud-computing platform.

B2. Support vector machines (SVM)

A support-vector machine (SVM) is especially attractive when sample sizes are smaller. It can achieve good classification accuracy when only a few samples exist (Mountrakis et al., 2011), but the samples must be accurate and pure in contrast, RF ensemble decision trees require as large a sample size as possible to ensure the ensemble process has many trees from which to make best decisions for a class, which is problematic when obtaining large and well-distributed samples in a resource-constrained environment.

In this project, the sample size for irrigated cropland versus rainfed cropland was large, accurate, and well distributed, making RF an ideal classifier; however, RF still results in overfitting irrigated areas in many places, leading to large areas of rainfed croplands being classified as irrigated. Further refinement of the training data and incorporating additional MLAs was used to optimize both irrigated and rainfed cropland class accuracy.

Furthermore, despite the best efforts, the results of pixel-based classifications (RF, SVM), in practice, inevitably include "salt and pepper" noise and disjointed farm fragments. A 3x3 pixel median value smoother (nearest neighbour) was used to change the classification of isolated misclassified pixels.

The typical process of pixel-based MLAs used in this study involved the following key steps (e.g., Figure 20 illustrated for the random forest):

1. Start with a known AEZ or a combination of these AEZs (**Error! Reference source not found.** b).
2. Create high quality image ARD30 cubes over AEZs or AEZ combinations (**Error! Reference source not found.**).
3. Choose appropriate reference-training data (Table 4, Figure 9-11).
4. Generate a knowledge base to separate irrigated cropland from non-irrigated cropland (rainfed) (e.g., Figure 18-19).
5. Create pixel-based supervised MLAs such as RF and SVMs in the GEE cloud. Overview of this approach shown in Figure 20.
6. Run pixel-based MLAs (Figure 20) using the ARD30 cube (e.g., Figure 17) in the GEE cloud for each AEZ or AEZ combinations (Figure 13a, b).
7. Evaluate irrigated *versus* rainfed classes to ensure accurate classification using reference data (Figure 9-11), ancillary data (e.g., from other maps from National or regional or global systems through collaborators or published work).
8. Perform error matrices for accuracies using validation data (Figure 12, Table 4).
9. If classification accuracies are not sufficiently high, further evaluate the reference-training data and subtract samples that cause problems or add additional samples to improve the classification accuracies.
10. Reiterate steps 4 to 9.
11. Optimize classification results of RF and SVM by removing any overfitting issues.

Stop when adequate overall, producer's, and user's accuracies are achieved. Overall, supervised classification are powerful tools, yet lacked the accuracies achieved in unsupervised classifications and hence we primarily deployed unsupervised classifications as discussed below.

C. Machine learning (ML) pixel-based unsupervised classification methods:

In this research, primarily, Irrigated and rainfed croplands were separated based on four methods (Lu et al., 2021, Teluguntla et al., 2017, 2015; Thenkabail et al., 2012, 2009a, 2007, 2005) as below:

1. ISOCLASS clustering to classify images (Thenkabail et al., 2011, 2009a) (e.g., Figure 21).
2. Quantitative spectral matching techniques (SMTs) as main class identification and labeling method (Lu et al., 2021, Teluguntla et al., 2017, Thenkabail et al., 2007) (e.g., Figure 22-23).
3. Other class identification and labeling methods: (a) Decision trees (DTs) (Lin et al., 2022, Thenkabail et al., 2009a) (e.g., Figure 24b); (b) Space time spiral curves or STSCs (Thenkabail et al., 2005) (e.g., Figure 24c); and
4. Class aggregation and refinement leading to final consolidation of classes using methods SMTs, DTs, and STSCs along with reference data (Figure 9-11).

C1. ISOCLASS clustering

ISODATA is an iterative Self-Organizing Data Analysis Technique. It uses spectral distance between image pixels in feature space to classify pixels into a specified number of unique spectral groups. The ISODATA method uses minimum spectral distance to assign a cluster for each candidate pixel. The process begins with a specified number of arbitrary clusters means or the

means of existing signatures, and then it processes repetitively, so that those means shift to the means of the clusters in the data.
To perform ISODATA clustering Three parameters are considered.

1. **N –** maximum number of clusters to be considered**.** Since each cluster is the basis for a class, this number becomes the maximum number of classes to be formed. The ISO-DATA process begins by determining N arbitrary cluster means. Some clusters with too few pixels can be eliminated, leaving less than N clusters.
2. **T** – a convergence threshold, which is the maximum percentage of pixels whose class values are allowed to be unchanged between iterations.
3. **M** – maximum number of iterations to be performed

The Landsat-derived global cropland extent product @ 30m (GCEP30) (Figure 8, Thenkabail et al., 2021) formed the baseline for this product. The goal is to use GCEP30 as baseline to determine which of these croplands are irrigated and which are rainfed. The goal is to identify irrigated and rainfed classes within each AEZ (Figure 13a) or by taking a combination of AEZs (e.g., Figure 13b) depending on complexity or ease of analysis. Further, within these AEZs, we analyzed irrigated and rainfed areas by taking the coarse resolution mask of irrigated and rainfed areas (Figure 7) as a starting block. Then we develop ARD30 cubes (e.g., Figure 17) of irrigated and rainfed mask areas (Figure 7) on the Google Earth Engine (GEE) for each of the AEZs (Figure 13a) or combination of AEZs (Figure 13b). For example, we created ARD30 cubes of irrigated mask (Figure 21, top-right) for AEZ zones 48-52 (Figure 21, top-left) and used ISOCLASS clustering algorithm on ERDAS Imagine classifying this data-cube into 100 classes (Figure 21, bottom-left). The NDVI time-series signatures of these 100-classes is shown in Figure 21, bottom-right. When classifying it is good to have as many classes as possible (e.g., 100) to give us an opportunity to identify and label as many unique classes as possible.

C2. Quantitative spectral matching techniques (SMTs)
Once the classes (e.g., 100 classes in Figure 21) are obtained through classification, then class identification and labeling process begins. The primary and powerful means of class identification and labeling is by using SMTs. The SMTs (Teluguntla et al, 2017, Thenkabail et al., 2011) are innovative methods of identifying and labeling classes (Thenkabail et al., 2009a) that was first proposed for remote sensing image classification and class identification and labeling by (Thenkabail et al. 2007). For each Landsat 30-m derived class, we looked through its characteristics over time using MODIS time-series data (e.g., Figure 21). The time-series of NDVI or other metrics (Teluguntla et al., 2017, Thenkabail et al., 2005, 2007a) are analogous to spectra, where time is substituted for wavelength. The principle in SMT is to match the shape, or the magnitude or both to an ideal or target spectrum (pure class or "end-member").

We will use the following quantitative SMTs (Thenkabail et al., 2007):
(a) Spectral Correlation Similarity (SCS)-a shape measure.
(b) Spectral Similarity Value (SSV)-a shape and magnitude measure.
(c) Euclidian Distance Similarity (EDS)-a distance measure; and
(d) Modified Spectral Angle Similarity (MSAS)-a hyper angle measure.

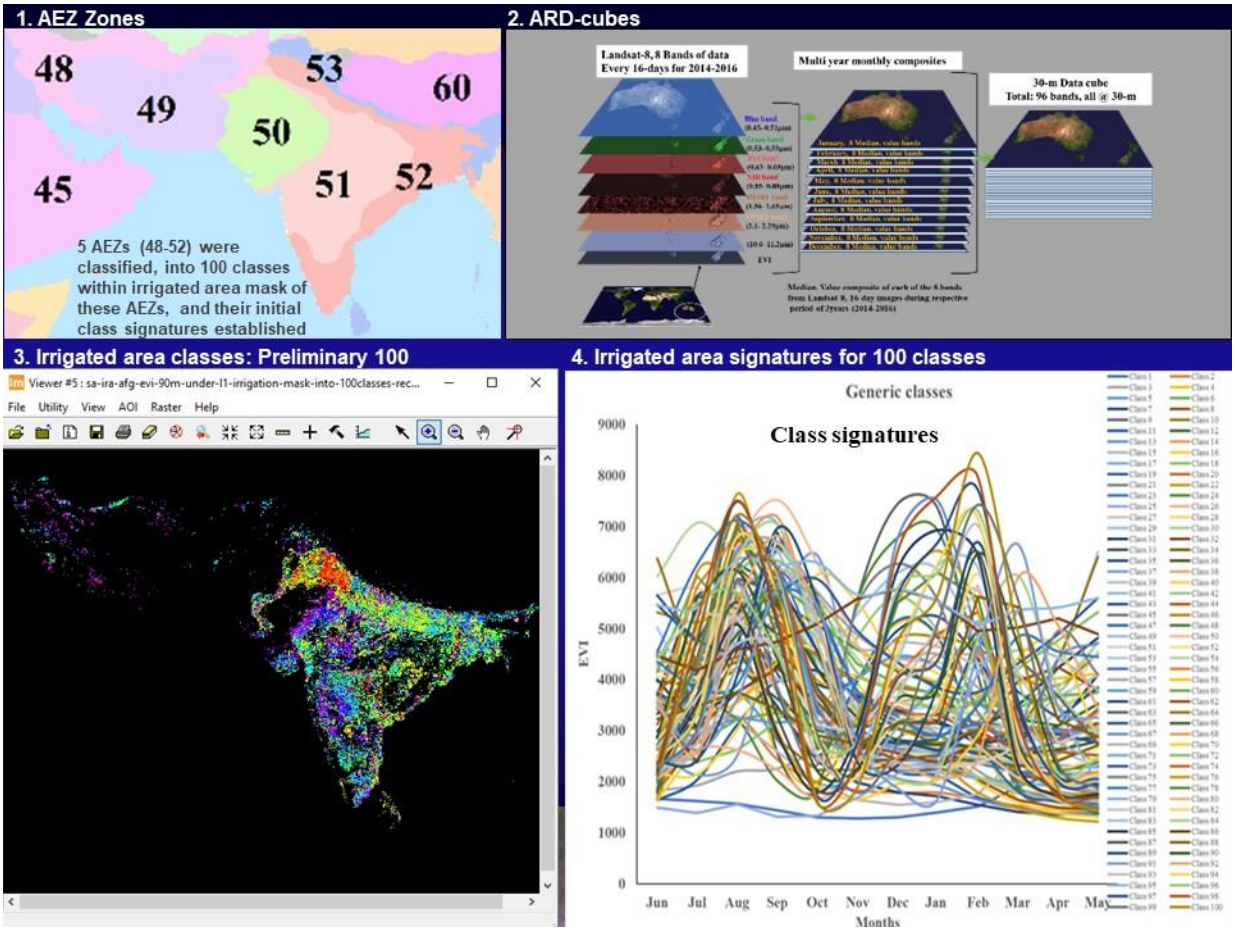

Figure 21. ISOCLASS clustering by classifying the image. The irrigated area mask of AEZ 48-52 (top-left) were classified using ARD30 cube (top right). That lead to 100 classes (bottom left), the signature of which is shown in bottom right.

C2.1. Generating class spectra:

Here we illustrate class spectra generated for AEZ 48-52 (Figure 21, top-left). All Landsat data-cubes (Figure 21, top-right) are composed on the Google Earth Engine (GEE) cloud using methods and approaches as in Thenkabail et al. (2021). These data-cubes are composed for the irrigated and rainfed mask areas (Figure 7) overlaid on cropland extent product (Figure 8). Classification is performed using ISOCLASS clustering algorithm (Thenkabail et al., 2011, 2009a) leading to 100 classes (Figure 21, bottom-left).

The time-series NDVI signatures of these classes are shown in Figure 21, bottom right. In more local applications, it is common to use field-plot data to identify and label class spectra. However, at the global scale this is not possible due to the enormous resources required to cover vast areas to identify and label classes. Therefore, we used spectral matching techniques to match similar classes by matching class spectra with ideal or target spectra (e.g., Figure 22-23) and then identify and label the classes (Thenkabail et al., 2007) as we will illustrate below.

C2.2 Ideal spectral data bank:

The term "ideal or target" spectrum refers to time-series spectral reflectivity or NDVI generated for classes for which we have precise location specific ground knowledge. We have initial ~112,000 samples on croplands and non-croplands (Figure 9) of which several thousands have irrigated or rainfed data as well. In addition, we have gathered an additional 27,396 samples of irrigated *versus* rainfed (Figure 10, 11, 12 and Table 4). Illustrations of some of these samples are shown in Figure 14-16. These signatures are synthesized and aggregated to generate a few hundred signatures (with each signature having a large sample size) that will constitute an ideal-spectral data bank of irrigated areas (ISDB IA) (e.g., Figure 22, Top-left). The ideal spectra are established by exact knowledge of the crop during field visit (ground data) or by using data sourced from reliable sources such as agricultural extension officers or reliable maps. Once the knowledge is clear, time-series satellite images are used to generate ISDB. Figure 22, top-left, it is labeled irrigated, surface water, double crop (IR, SW, DC) based on ground data.

C2.3 Matching class spectra with ideal spectra:

Any classes that are identical in class spectra (Figure 21, bottom-right) are grouped (e.g., three classes in Figure 22, top-right; these are similar classes in terms of shape and magnitude gathered from 100 classes in Figure 21, bottom-right), and then matched with the ideal spectra (Figure 22, bottom-left). Since the 3 class spectra (Figure 22, top-right) match perfectly with ideal spectra (Figure 22, bottom-left), they are merged into one single class and then matched with the ideal spectra (Figure 22, bottom-right). The most powerful and lucid of all the SMTs in land cover or cropland studies is the SCS R^2-value (Teluguntla et al., 2017, Thenkabail et al., 2007) which is a shape measure that typically produces values between 0 and 1. The greater the SCS R^2-values, the greater the similarity between class spectra and target spectra. The SCS R^2-values of Figure 22, bottom-right is 0.98. As a result of the very high SCS R^2-values, the three classes (Figure 22 top-right) that were matched with ideal spectral (Figure 22, bottom-left) and combined (Figure 22, bottom-right) were labeled same as ideal spectra: irrigated, surface water, double crop (IR, SW, DC). Figure 22 illustrates combining, identifying, and labeling classes: irrigated, surface water, single crop (IR, SW, SC). The process is repeated for all 100 classes (Figure 21, bottom-right). Once all classes are identified and labeled, they are further verified by using the reference data (Figure 9-11) and\or by verifying the class labels with other local maps and any other available information (e.g., local country partners).

C2.4 Other class identification and labeling process

The class spectra (Figure 22) also are identified using other methods like decision-trees (DTs) which involves writing a set of rules to separate irrigated areas from rainfed areas (e.g., Figure 24b) based on spectral band reflectivity of various bands or their transformed data such as NDVI. We have mapped irrigated areas using these methods in several publications (Gumma et al., 2016, Thenkabail et al., 2009a, Wu et al., 2014). Further, we have found space-time spiral-curves (STSCs; Figure 24c; Thenkabail et al., 2005) that uses time-series satellite data during the crop growing season to clearly and distinctly separate irrigated and rainfed croplands based on the trajectory in two-dimensional (e.g., Figure 24c) or multi-dimensional feature space.

The first part of the DT algorithms involve knowledge-capture to understand and map agricultural cropland dynamics by: (a) identifying croplands versus non-croplands and crop type\dominance based on spectral matching techniques, decision trees tassel cap bi-spectral plots, and very

high resolution imagery; (b) determining watering method (e.g., irrigated or rainfed) based on temporal characteristics (e.g., NDVI), crop water requirement (water use by crops), secondary data (elevation, precipitation, temperature), and irrigation structure (e.g., canals and wells); (c) establishing croplands that are large scale (i.e., contiguous) versus small scale (i.e., fragmented); (d) characterizing cropping intensities (single, double, triple, and continuous cropping); (e) interpreting MODIS NDVI Temporal bi-spectral Plots to Identify and Label Classes; and (f) using in-situ data from very high resolution imagery, field-plot data, and national statistics. The second part of the method establishes accuracy of the knowledge-captured agricultural map and statistics by comparison with national statistics, field-plot data, and very high-resolution imagery. The third part of the method makes use of the captured knowledge to code and map cropland dynamics through an automated algorithm. The fourth part of the method compares the agricultural cropland map derived using an automated algorithm (classified data) with that derived based on knowledge capture (reference map). The fifth part of the method applies the tested algorithm on an independent data set of the same area to automatically classify and identify agricultural cropland classes. The sixth part of the method assesses accuracy and validates the classes derived from independent dataset using an automated algorithm.

The space-time spiral curves (ST-SCs) (Figure 25) are introduced as an innovative approach to represent and track near continuous changes in class behavior over time and space. The dynamics of two classes (irrigated and rainfed are shown in a 2-dimentional feature space using Landsat class reflectivity in Figure 25. Each class, irrigated and rainfed, have their own territory and mostly move around within it throughout the year. In Figure 25 the rainfed class is in brightness territory, and irrigated class in greenness territory. The ST-SCs depict change over time depending on their growth and vigor. The classes shown in Figure 24 rarely overlap one another, providing an excellent opportunity to separate classes on most dates. SC-STs tell us when (what time of the year) the two classes have similar spectra and when (what time of the year) they are most separable.

Irrigated areas often have 2-3 crops grown on same cropland areas annually which can be detected using NDVI time-series plot (Figure 19) when compared to a single crop grown annually in a rainfed cropland area (e.g., Figure 19). This is overwhelmingly true in much of the world's croplands. Also, irrigated areas have higher NDVI magnitude during much of a growing season when compared with rainfed croplands (e.g., Figure 19). This is also true in much of the croplands of the world. These two indicators play a key major role in distinguishing irrigated croplands from rainfed croplands. Other methods like RF (Oliphant et al., 2019, Xiong et al., 2017b, Conrad et al., 2016) are also used in separating irrigated areas from rainfed areas.

Based on this process, the 100 classes (Figure 21) were reduced to 35 unique classes (Figure 26). Note that all these 35 classes are from the irrigated mask. Of the 35 classes in the irrigated area mask, 31 remain as irrigated, remaining 4 classes were identified as rainfed.

Adopting same methods and approaches described for irrigated area mask, rainfed area mask (Figure 27) was also classified, classes identified, and labeled. The initial 60 classes for AEZ 48-52, for the rainfed mask (Figure 27, bottom-left) were classified into 60 classes and from which 23 unique aggregated classes were identified (Figure 27). Of the 23 classes in the rainfed area mask, 18 remain as rainfed remaining 5 were identified as irrigated (Figure 27).

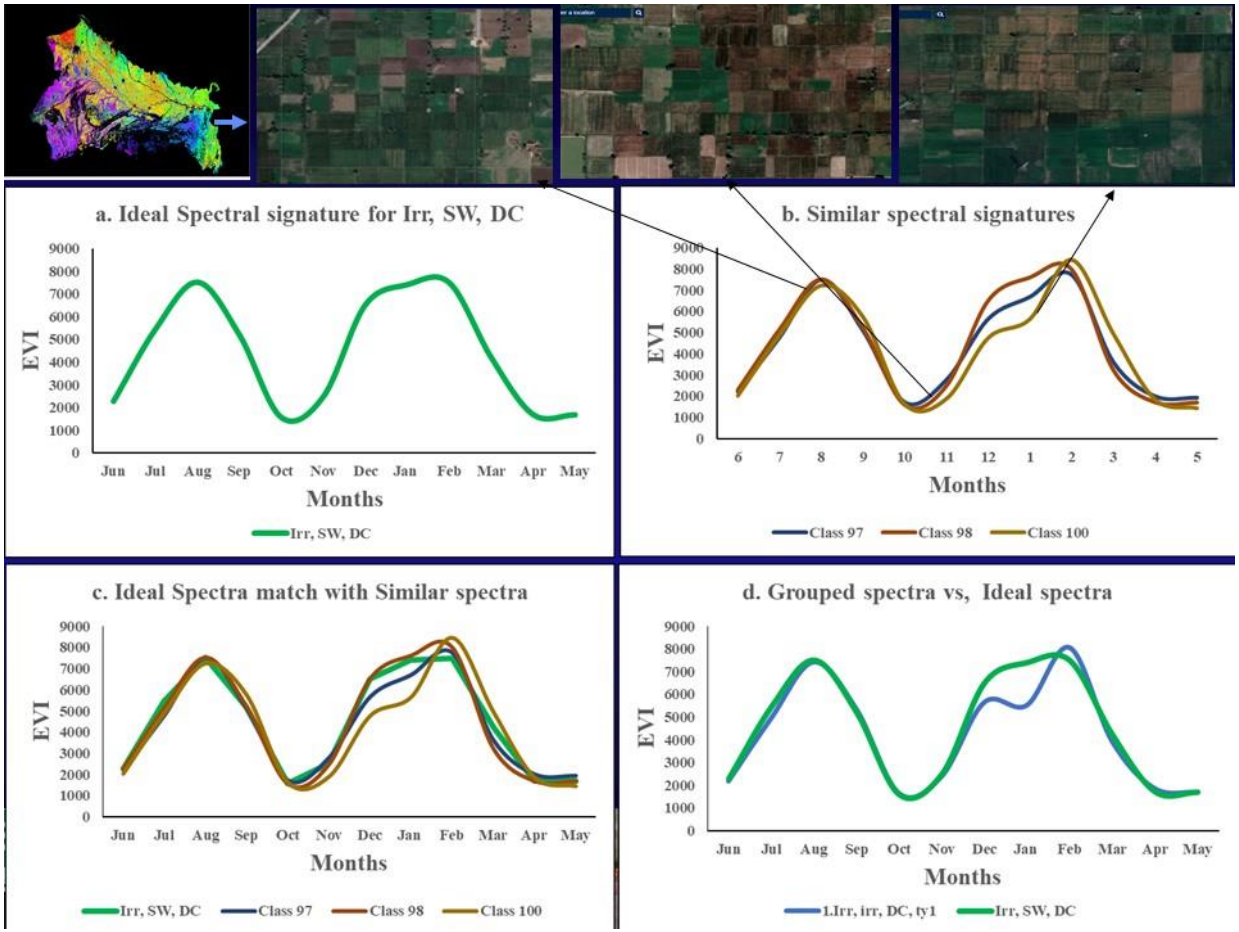

Figure 22. Spectral matching technique (SMT) for identifying and labelling classes from the irrigated area mask. The SMTs involve matching class spectra with ideal spectra. The class spectra are the time-series NDVI or spectral reflectivity profiles of the classes from the irrigated mask (e.g., 100 classes generated in Figure 21). Ideal spectra are the spectra in the knowledge-bank for which precise knowledge is known. For example, for irrigated (IR), surface water (SW), double crop (DC) the spectral signature in the signature bank in AEZ zones 48-52 is as in top-left (22a). Three similar classes (22b) from the 100 class spectra (Figure 21) were matched with the ideal spectra (22c). Since the three class spectra match well, they were combined and matched with idea spectra (22d). For quantitative methods refer to Thenkabail et al. 2007a.

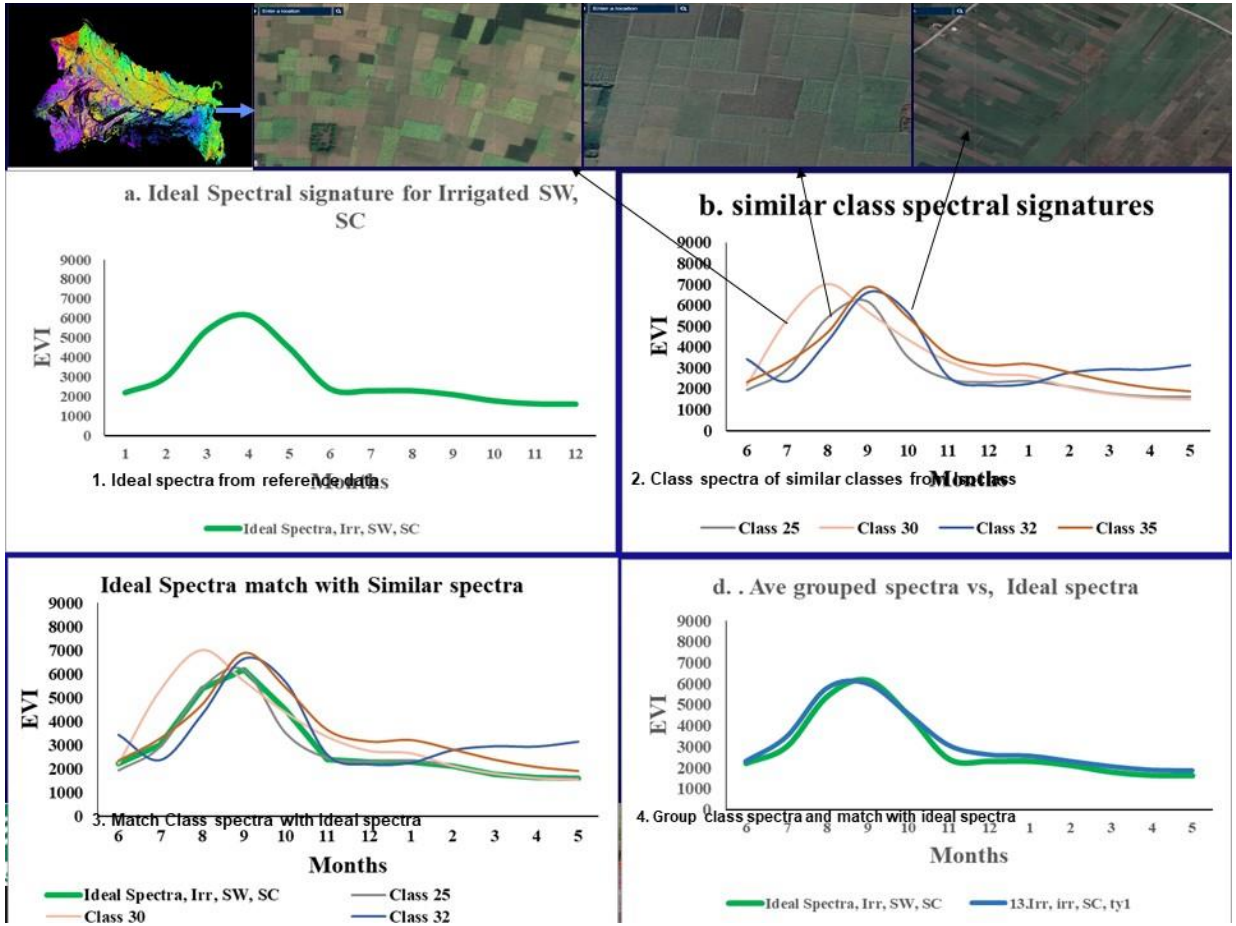

Figure 23. Spectral matching technique (SMT) for identifying and labelling classes from the irrigated area mask. The SMTs involve matching class spectra with ideal spectra. The class spectra are the time-series NDVI or spectral reflectivity profiles of the classes from irrigated mask (Figure 20). Ideal spectra are the spectra in the knowledge-bank for which precise knowledge is known. For example, irrigated (IR), surface water (SW), single crop (SC) the spectral signature in the signature bank in AEZ zones 48-52 is as in top-left (23a). Four similar classes (23b) from the 100 class spectra (Figure 21) were matched with the ideal spectra (23c). Since the three class spectra match well, they were combined and matched with idea spectra (23d). For quantitative methods refer to Thenkabail et al. 2007a.

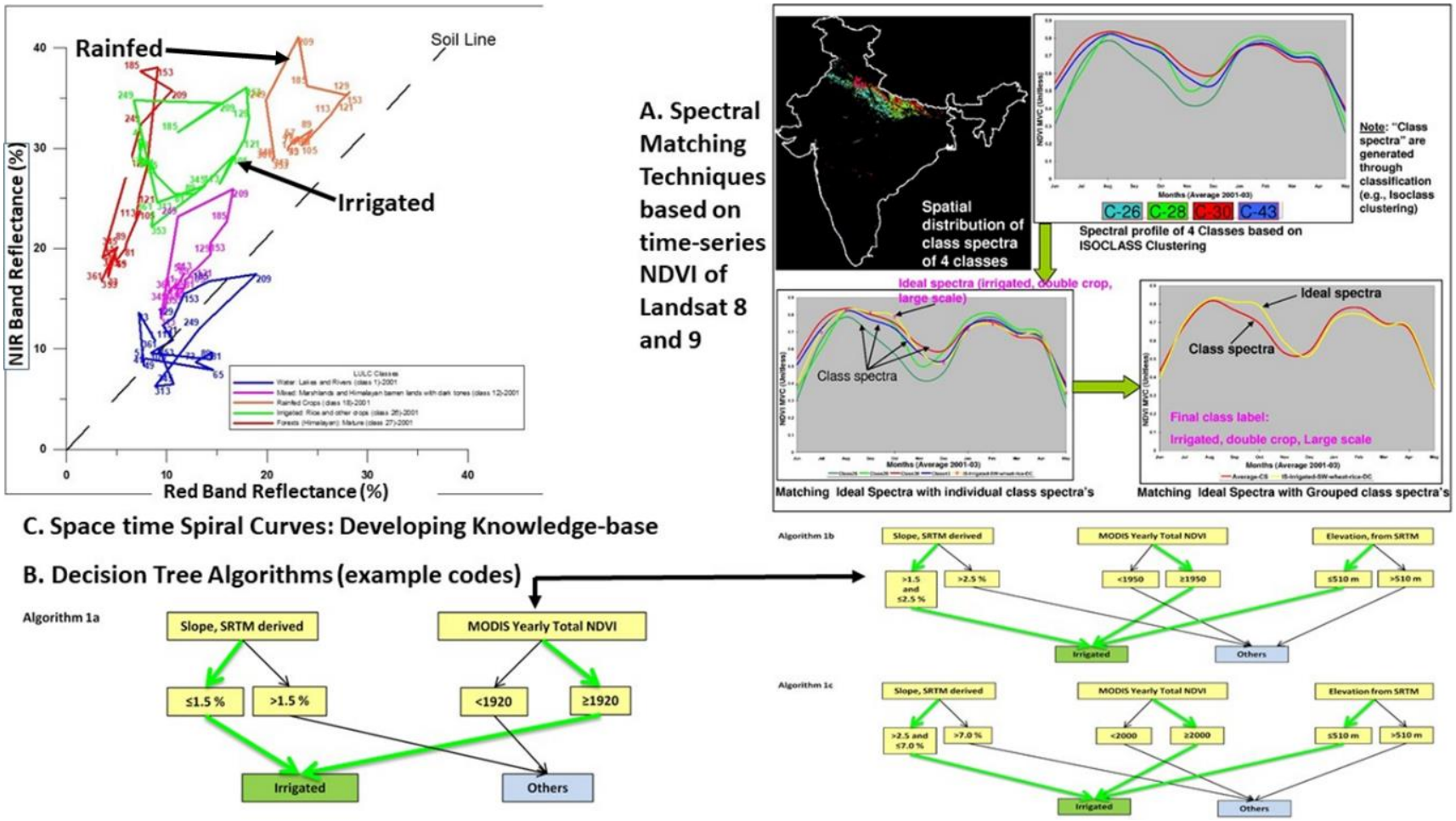

Figure 24. Irrigated *versus* rainfed cropland class identification approaches. There are various approaches to identifying and labeling classes. This includes: (a) quantitative spectral matching techniques (SMTs) (Figure 22 and 23), (b) decision trees (DTs), and (c) space-time spiral curves (STSCs).

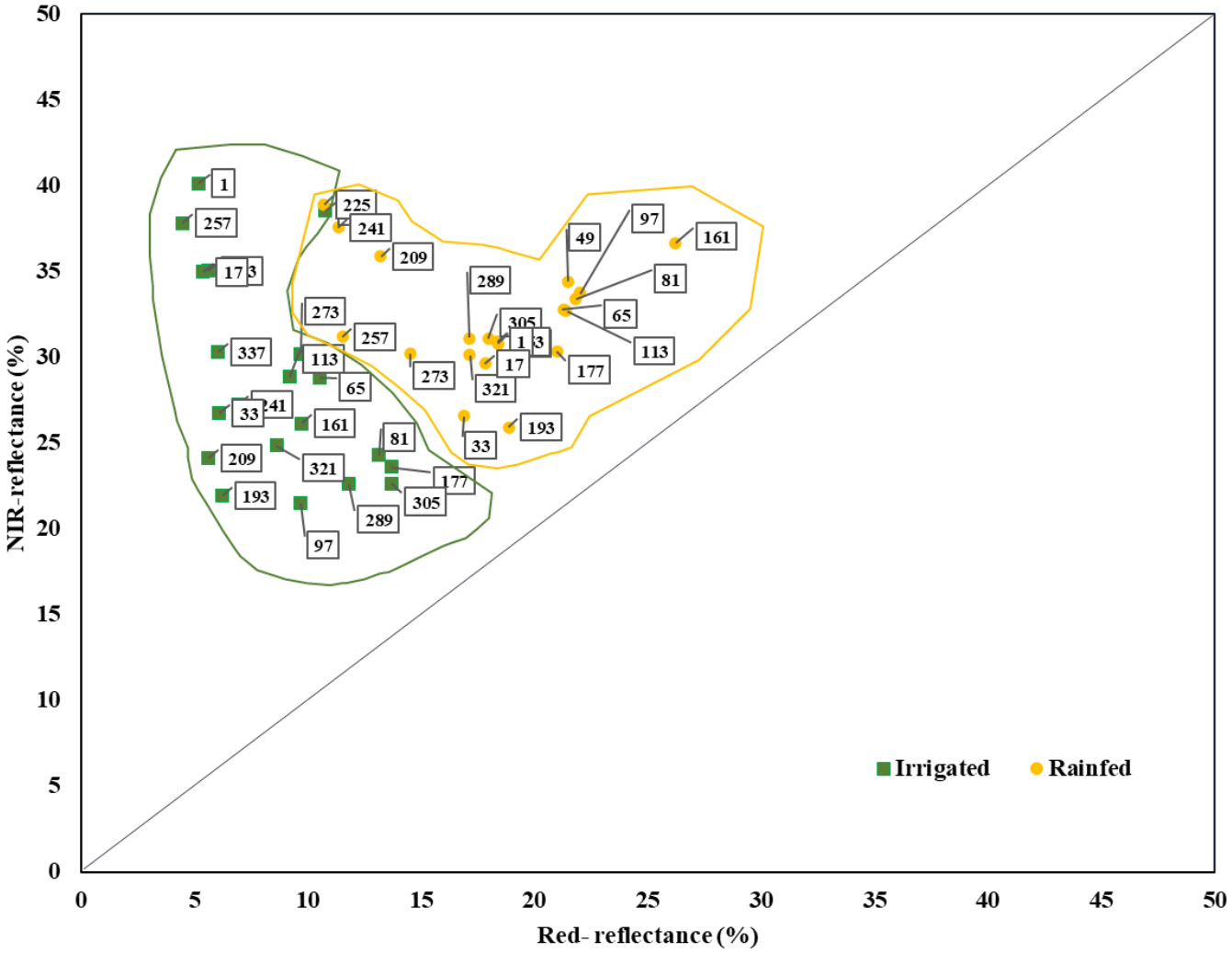

Figure 25. Space-time spectral curves (ST SCs). The NIR and red spectral reflectance of irrigated and rainfed area classes can be plotted to see how they transverse in time. The dates shown are Julian dates in a calendar year. This plot is for the Ganges basin in India. Such plots can be developed for any classes to see how they transverse in time. Over space, in different parts of the world, these will transverse differently but often having distinct separability amongst irrigated and rainfed classes at least during some dates of the calendar year.

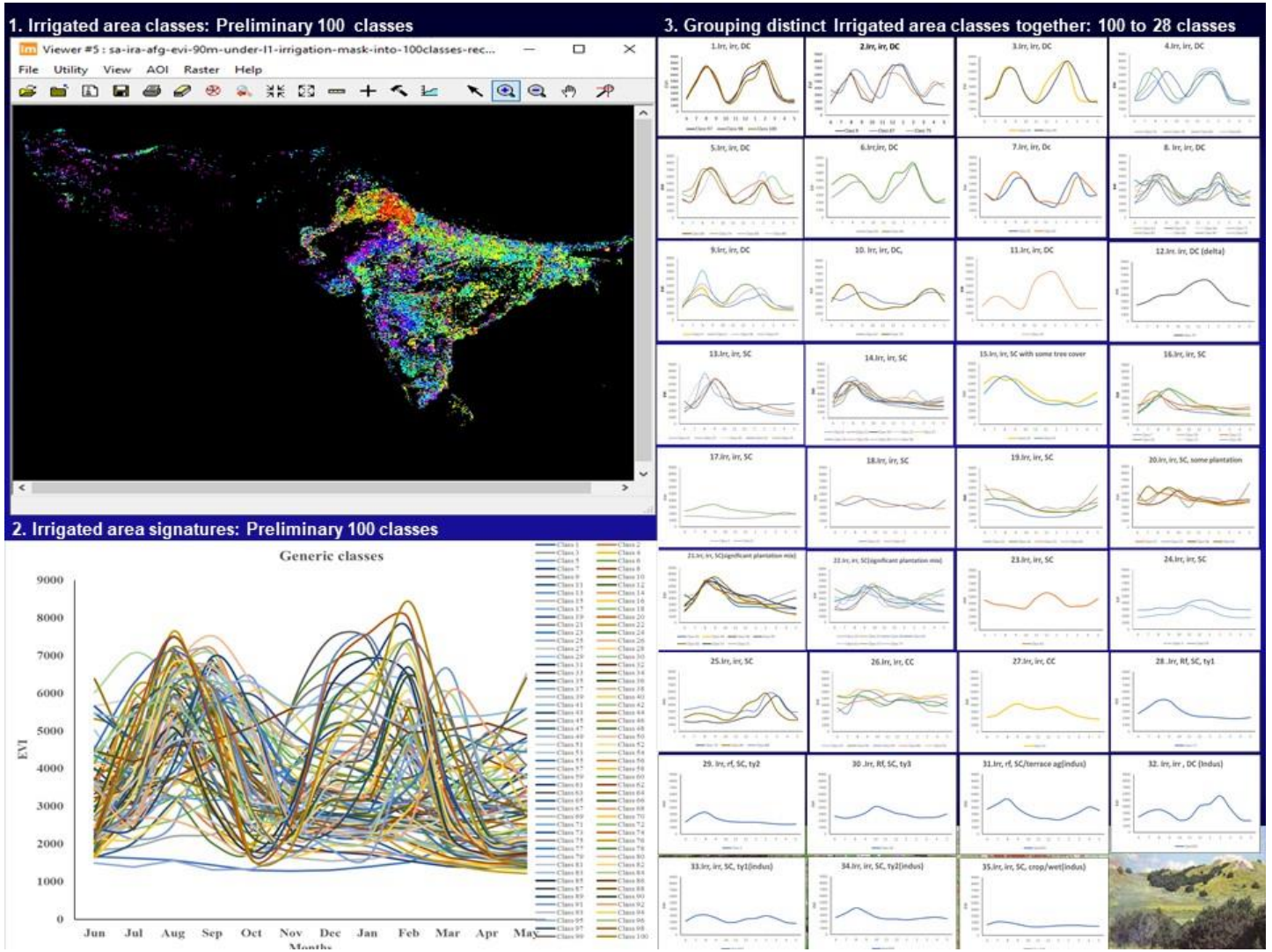

Figure 26. Grouping classes from the irrigated area mask. Based on the methods and approaches described above, all similar classes were grouped together and labeled. Here we illustrate 100 classes reduced to 35 similar classes. Of the 35 classes in the irrigated area mask, 31 remain as irrigated, remaining 4 classes were identified as rainfed.

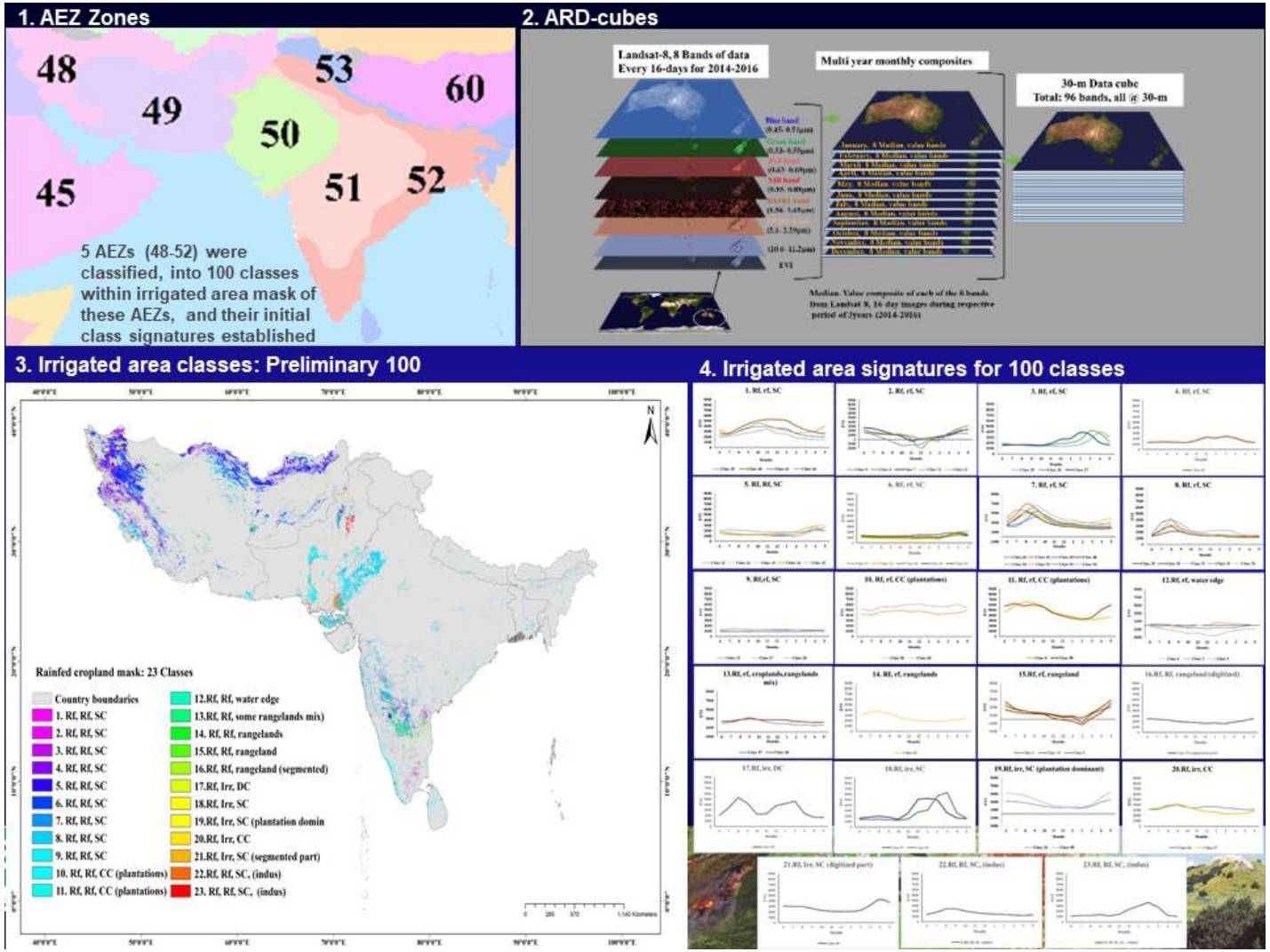

Figure 27. Grouping classes from the rainfed area mask. Adopting same methods and approaches described for irrigated area mask, this rainfed area mask for AEZ 48-52 were classified into 60 classes and from which 23 unique aggregated classes were identified. Of the 23 classes in the rainfed area mask, 18 remain as rainfed remaining 5 were identified as irrigated.

C3.0 Aggregating classes

The classes were identified, labeled and grouped in the irrigated area mask (Figure 26) and the rainfed area mask (Figure 27).

There were 35 unique classes that were identified in the irrigated area mask of AEZ 48-52. Of these 35 classes, 31 classes (classes 1-27, 32-25) were identified as irrigated and the rest 4 classes (classes 28-31) were identified as rainfed. Aggregated 35-classes are shown Figure 28.

There were 23 unique classes that were identified in the rainfed area mask of AEZ 48-52. Of these 23 Classes, 18-classes (Classes 1-16, 22-23) were identified as rainfed and the rest 5 classes (Classes 17-21) were identified as irrigated. Aggregated 23-classes are shown Figure 29.

C3.1 Level I irrigated and rainfed classes

Once the irrigated and rainfed classes are all identified in the irrigated mask (Figure 28) and Rainfed mask (Figure 29), our next goal is to create Level I irrigated area product for the AEZ 48-52.

Since there are 31 irrigated area classes in the irrigated area mask (Figure 28) and there are 5 irrigated area classes in the rainfed mask (Figure 29), we derive for AEZ 48-52:

Level I 36-class irrigated area product (Figure 30)

Since there are 4 rainfed area classes in the irrigated area mask (Figure 28) and there are 18 rainfed area classes in the rainfed mask (Figure 29), we derive for AEZ 48-52:

Level I 22-class rainfed area product (Figure 31)

When we put all the irrigated and rainfed area classes of Level I (Figure 30 and 31) together, we get for AEZ 48-52:

Level I 58-class Landsat-derived global rainfed and irrigated area product @ 30m (LGRIP30-AEZ 48-52) as shown in Figure 32.

C3.2 Level II irrigated and rainfed classes

The level II 4-class irrigated area product (Figure 33) is derived by aggregating the 36-class irrigated area product (Figure 30). The Level II 5-class rainfed area product (Figure 34) derived by aggregating the 22-class rainfed area product (Figure 31). The two Level II products (Figure 33 and 34) are combined to form the AEZ 48-52:

Level II 9-class Landsat-derived global rainfed and irrigated area product @ 30m (LGRIP30-AEZ 48-52) as shown in Figure 35.

C3.3 Level III irrigated and rainfed classes

The 9-class Level II LGRIP30-AEZ 48-52 classes (Figure 35) were aggregated to derive:

Level III 2-class Landsat-derived global rainfed and irrigated area product @ 30m (LGRIP30-AEZ 48-52) as shown in Figure 36. The process described above for to create, Level II LGRIP30-AEZ 48-52 was repeated for all AEZs to finally derived the:

Landsat-derived global rainfed and irrigated area product @ 30m (LGRIP30) for the entire world (Figure 37).

C4.0 Programming codes

The codes and models related to this work is provided a zip files.

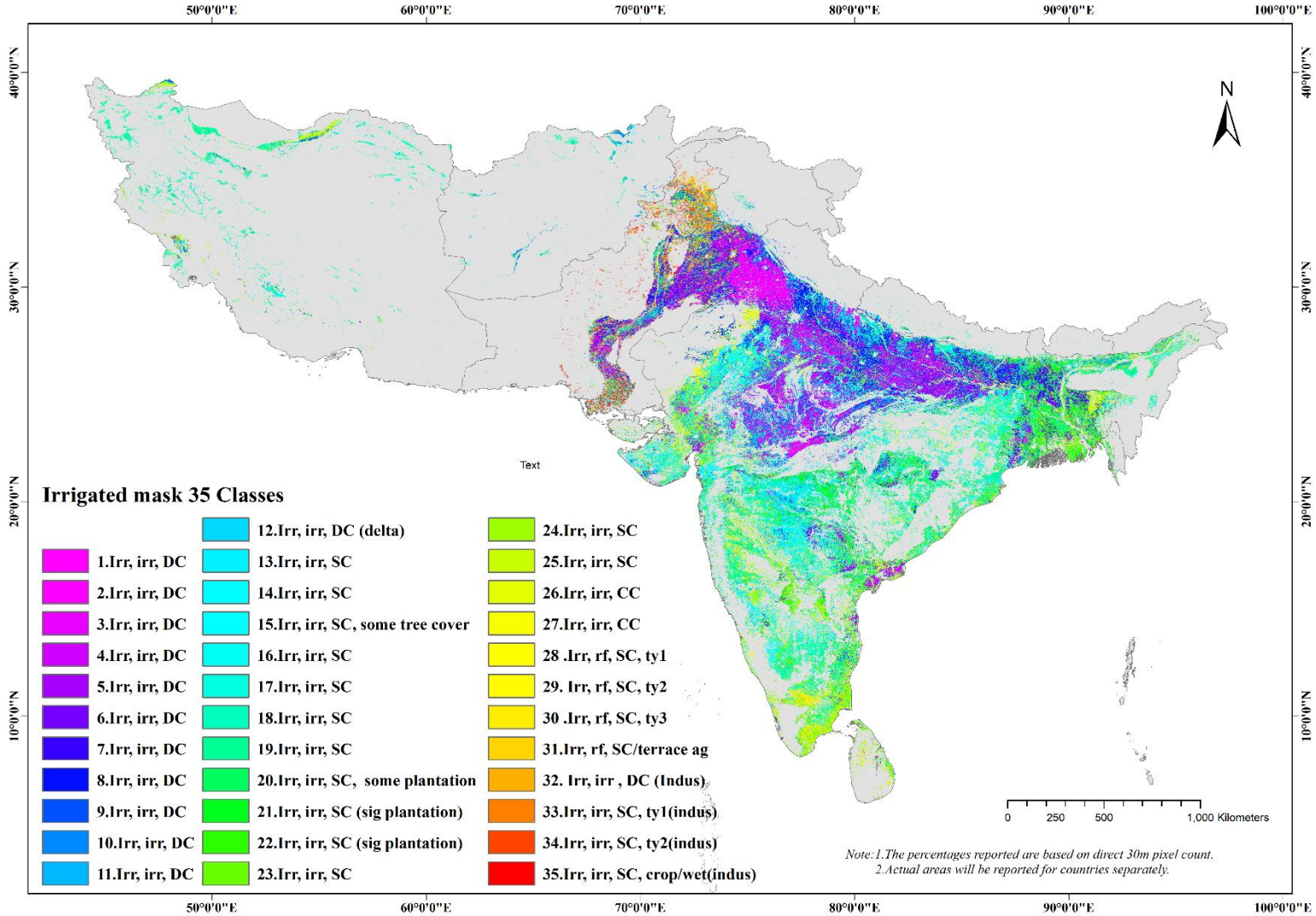

Figure 28. Aggregated 35-classes from irrigated area mask in AEZ 48-52. There were 35 unique classes that were identified in the irrigated area mask of AEZ 48-52. Of these 35 classes, 31 classes (classes 1-27, 32-35) were identified as irrigated and the rest 4 classes (classes 28-31) were identified as rainfed.

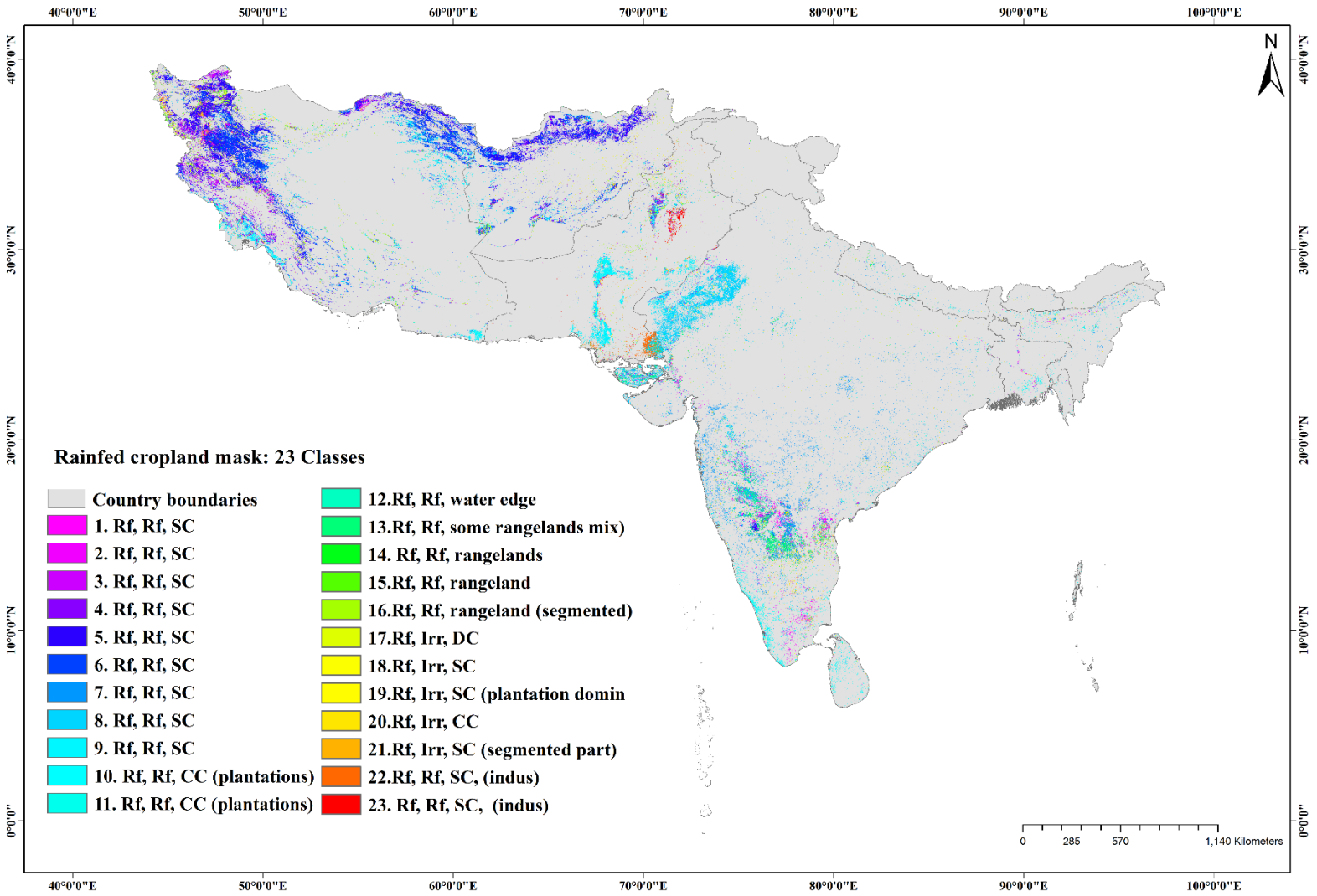

Figure 29. Aggregated 23-classes from rainfed area mask in AEZ 48-52. There were 23 unique classes that were identified in the rainfed area mask of AEZ 48-52. Of these 23 Classes, 18-classes (Classes 1-16, 22-23) were identified as rainfed and the rest 5 classes (Classes 17-21) were identified as irrigated.

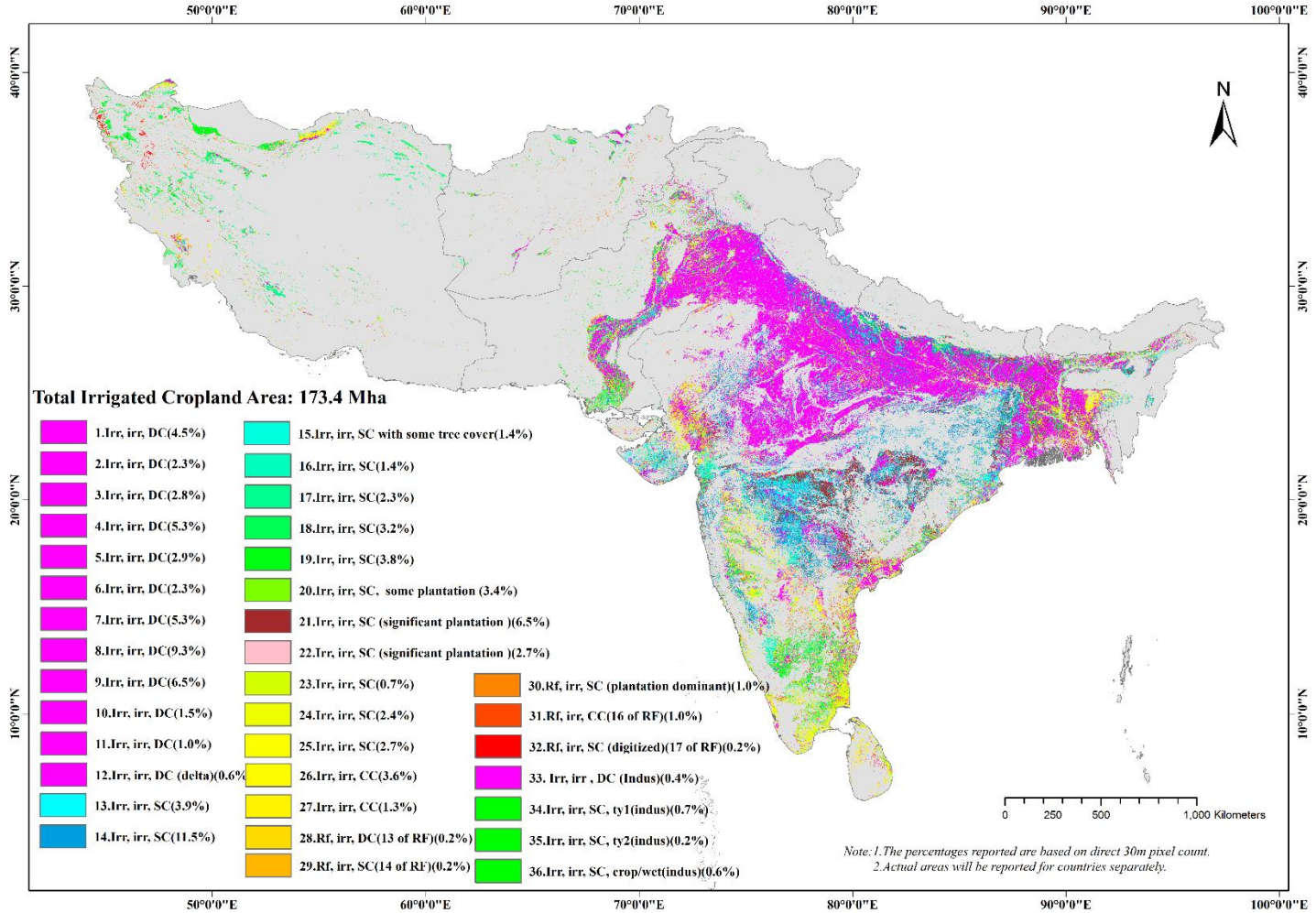

Figure 30. Level I 36-class irrigated area map @30m for AEZ 48-52. The 36-class level I irrigated area classes were derived from 31 irrigated area classes out of total 35 classes from irrigated mask (Figure 28) and 5 irrigated area classes out of total 23 classes from rainfed mask (Figure 29).

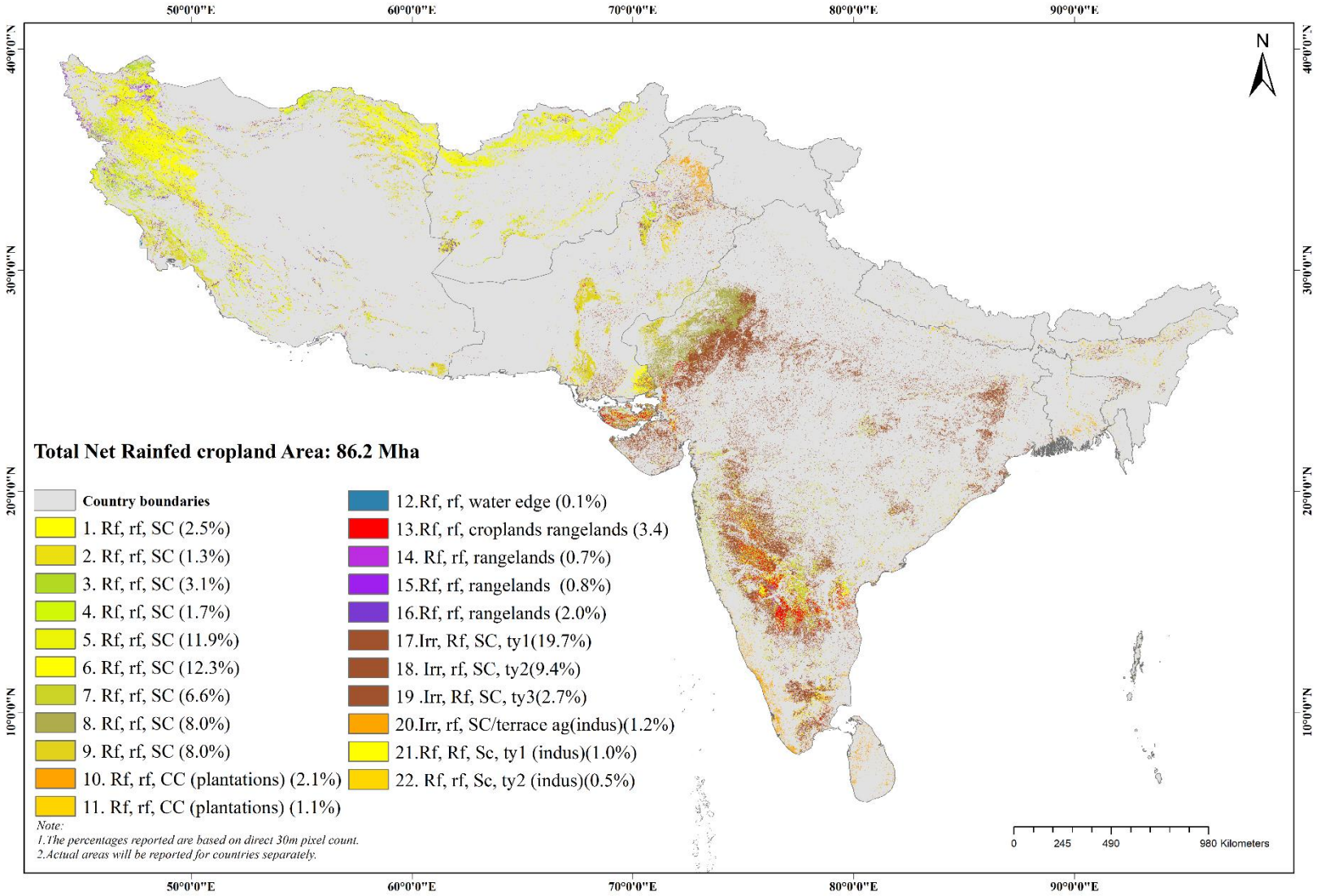

Figure 31. Level I 22-class rainfed area map @30m for AEZ 48-52. The 22-class level I rainfed area classes were derived from 18 rainfed area classes out of total 23 classes from rainfed mask (Figure 29) and 4 irrigated area classes out of total 35 classes from irrigated area mask (Figure 28).

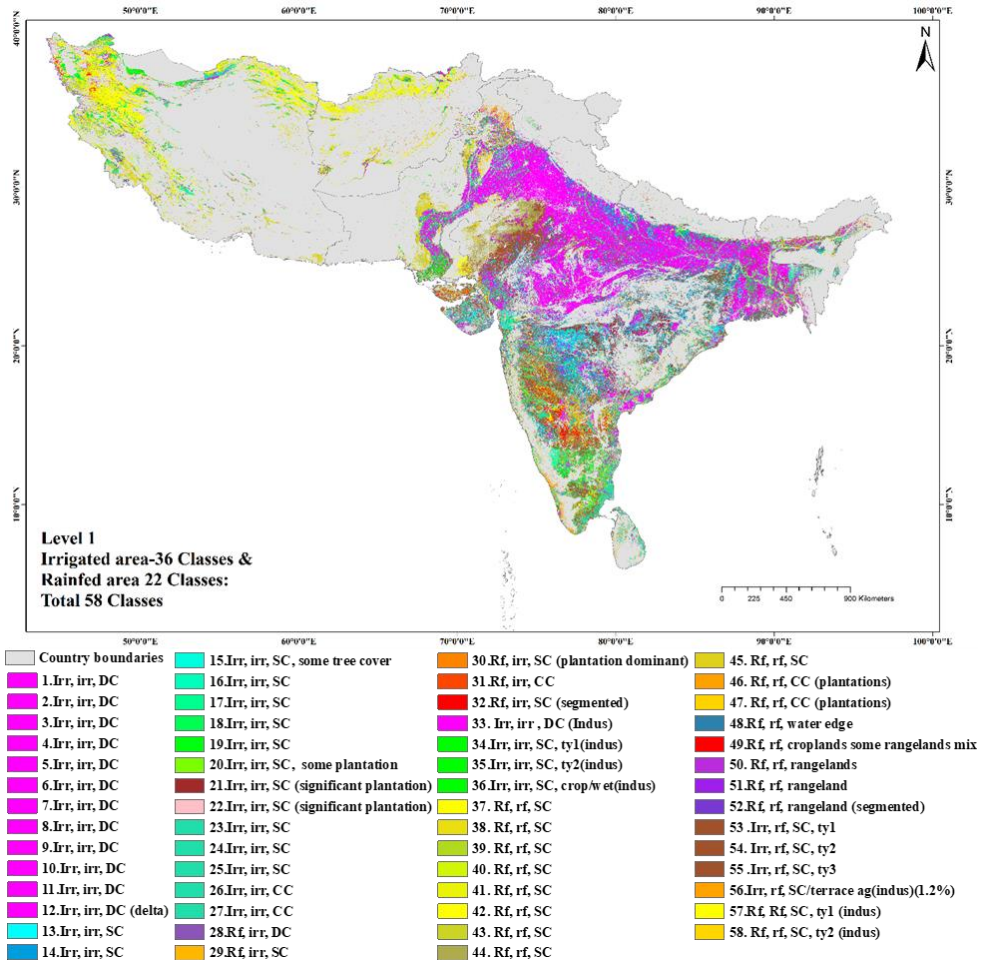

Figure 32. Level I 58-class Landsat-derived global rainfed and irrigated area map @ 30m for AEZ 48-52 (LGRIP30-AEZ48-52). The 58-class level I LGRIP30-AEZ48-52 was derived by combining the Level I 36-class irrigated area product (Figure 30) and Level I 22-class rainfed area product (Figure 31).

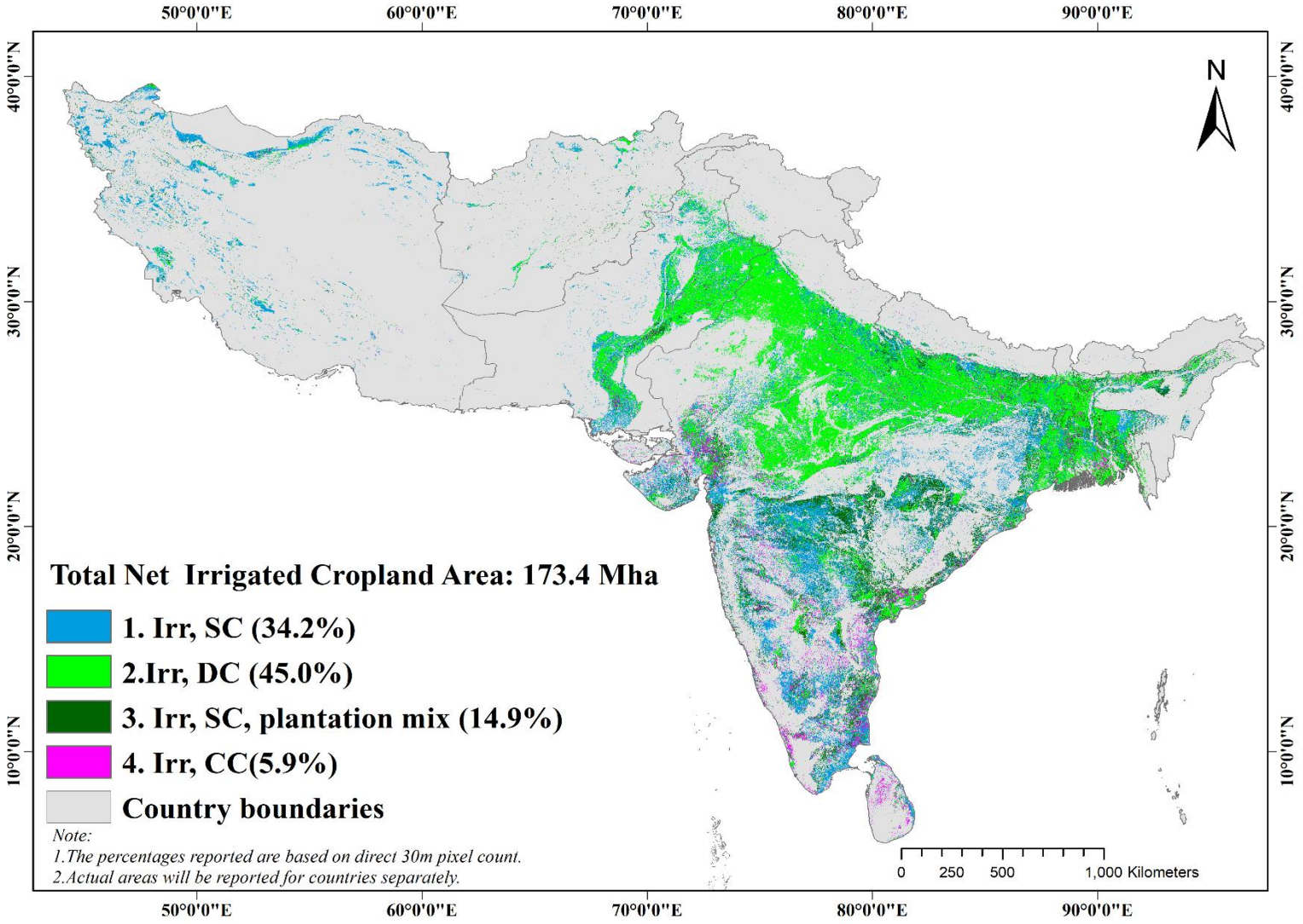

Figure 33. Level II 4 class Landsat-derived irrigated area map@30m. This 4-class Level II irrigated area map for AEZ 48-52 were derived by combining classes from Level I 36-class irrigated area map (Figure 30).

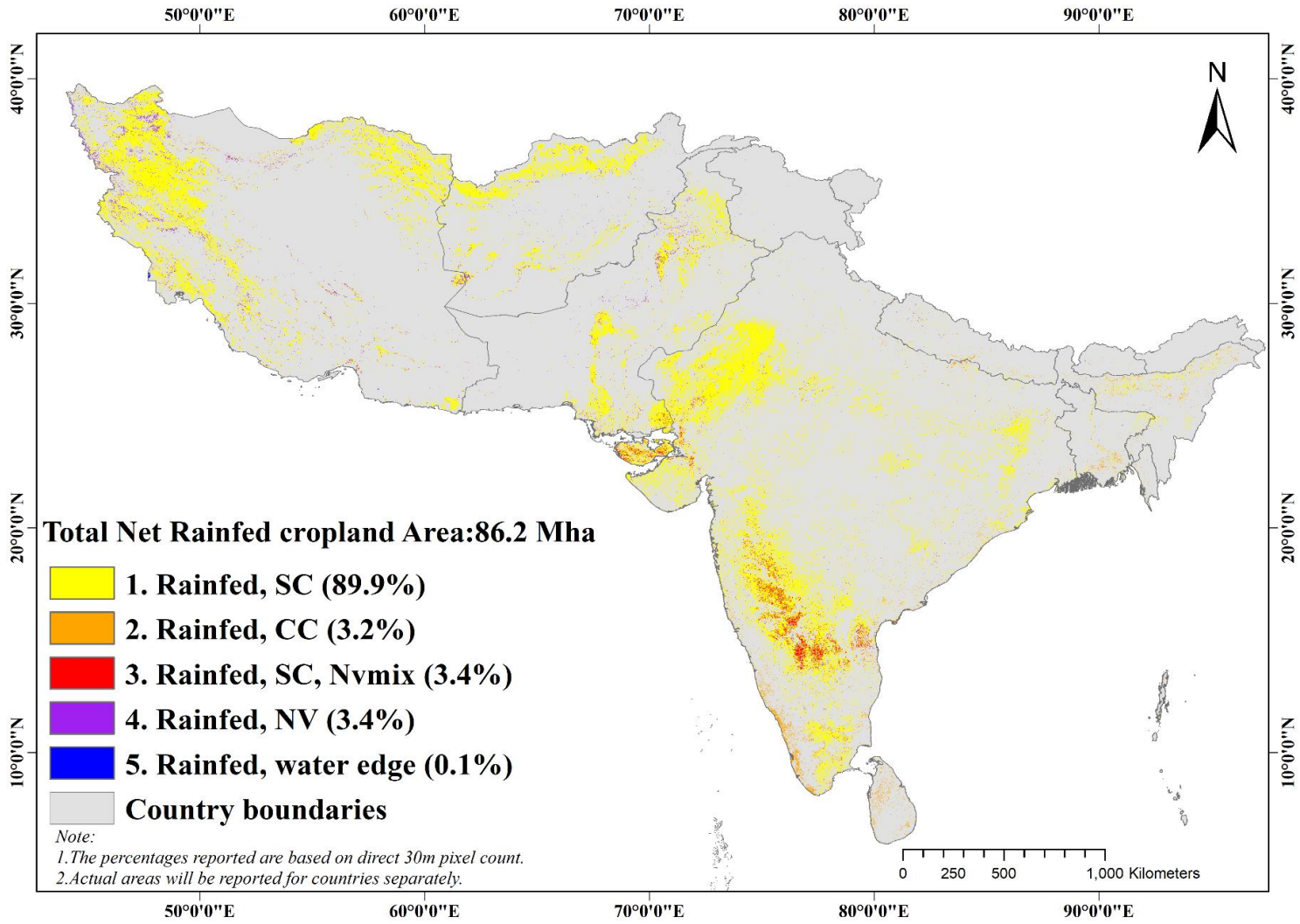

Figure 34. Level II 5 class Landsat-derived rainfed area map @30m. This 5-class Level II rainfed area map for AEZ 48-52 were derived by combining classes from Level I 22-class rainfed area map (Figure 31)

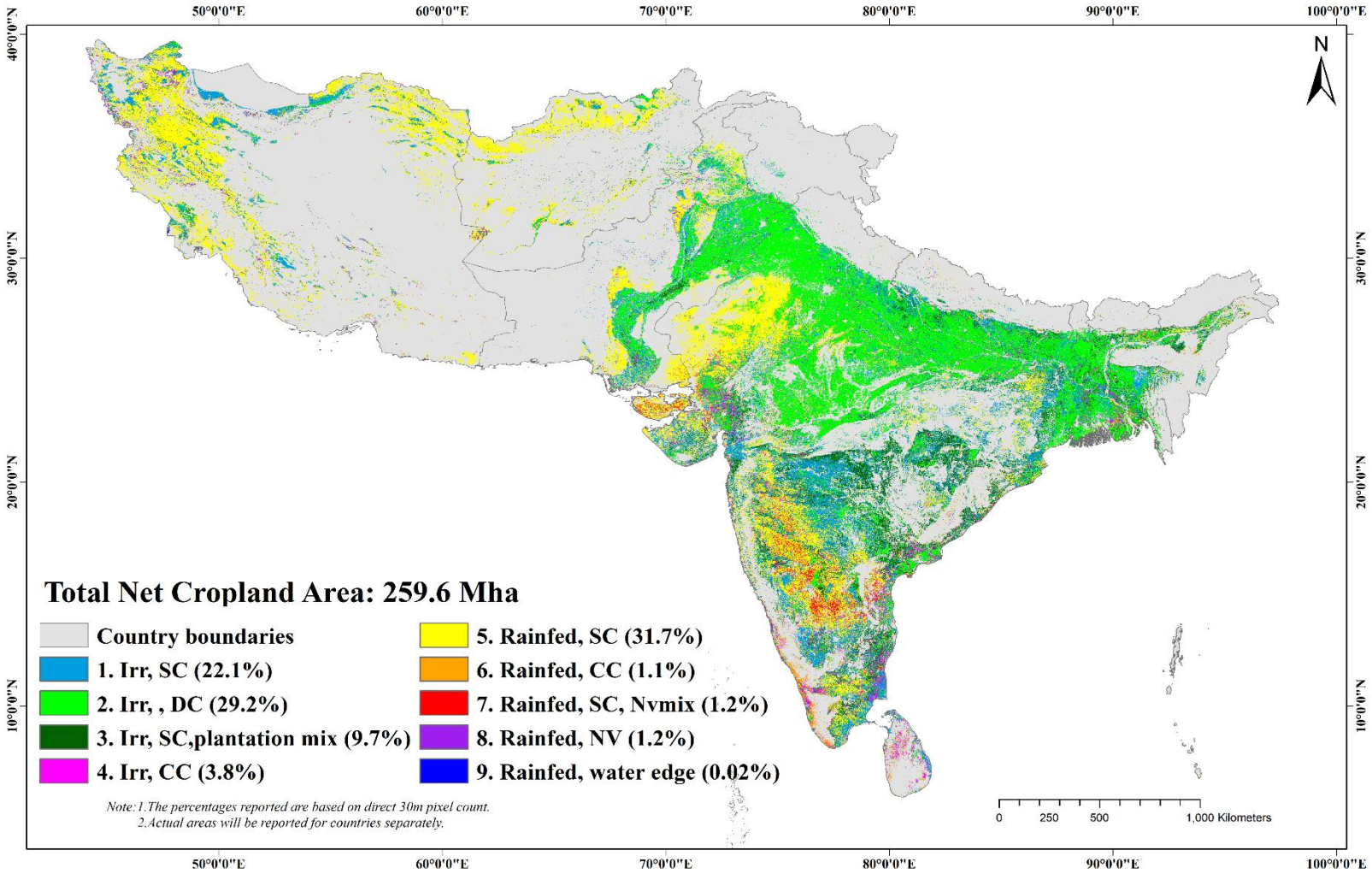

Figure 35. Level II 9-class Landsat-derived rainfed and irrigated area map@30m. The 9-class level II Landsat-derived 30m rainfed and irrigated area classes for AEZ 48-52 were derived by combining the 4-class Level II irrigated area map (Figure 33) with 5-class Level II rainfed area map.

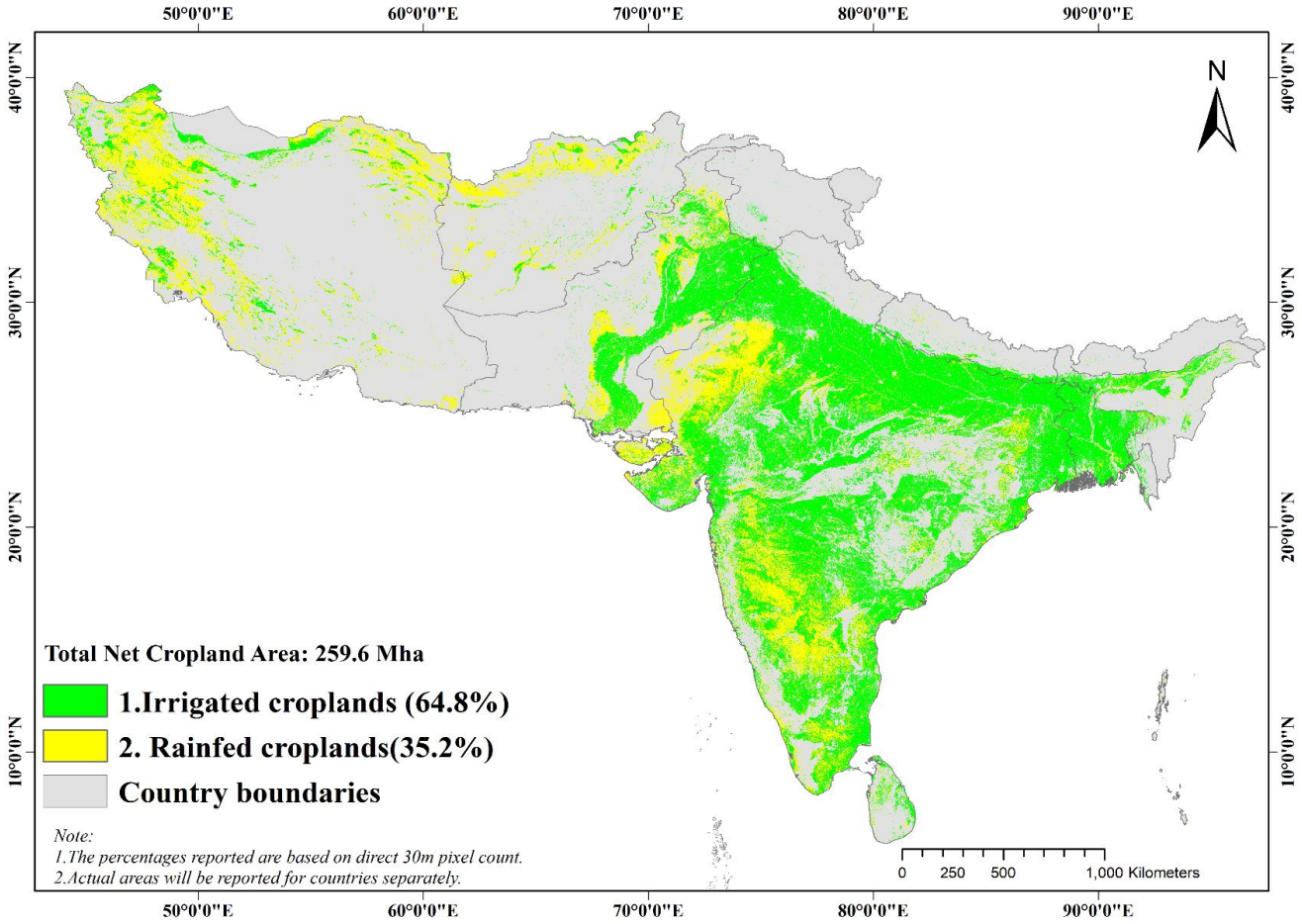

Figure 36. Level III 2-class Landsat-derived rainfed and irrigated-area map @ 30m. The 2-class level II Landsat-derived 30m rainfed and irrigated area classes for AEZ 48-52 were derived by aggregating classes from Level II 9-class rainfed and irrigated area map (Figure 35).

VII. Results

The Landsat-derived Global Rainfed and Irrigated-Cropland Product @ 30-m (LGRIP30) of the World (GFSADLGRIP30WORLD) resulted in multiple global irrigated and rainfed cropland products. This includes, maps, areas, statistics of various nature. We will discuss these in the following sections and sub-sections.

A. Global irrigated and rainfed cropland maps at 30m

The Landsat-derived Global Rainfed and Irrigated-Cropland Product @ 30-m (LGRIP30) for the nominal year 2015 is shown in Figure 37. The map shows spatial distribution of the global irrigated (green) and rainfed (yellow) areas across all the countries of the World.

Spatial distribution of LGRIP30 is illustrated for few places of the world in Figure 38 through 44. Figure 38 shows distribution of irrigated and rainfed areas over the state of Nebraska, USA, which has highest irrigated areas along with the state of California (Figure 39). Distribution of irrigated and rainfed areas are also illustrated for Italy (Figure 40), Uganda (Figure 41), Nigeria (Figure 42), parts of India (Figure 43), and Australia (Figure 44). In the images shown (Figure 38-44) rainfed areas dominate in Nigeria and Australia, irrigated areas dominate in India. In France and Uganda both irrigated and rainfed areas have almost equal presence. The full resolution view of LGRIP30 map can be viewed at:
www.usgs.gov/apps/croplands (navigate to LGRIP30 within this site)
or
www.croplands.org (navigate to LGRIP30 within this site)

B. Accuracies

Accuracy assessments of LGRIP30 (Figure 37) were performed using 10,477 validation samples (Figure 11, Table 4), of which 5,667 were rainfed samples and the rest 4,810 were irrigated samples. The resulting error matrix (Table 5) showed an overall accuracy (Congalton and Green, 2009) of 86.5%. The irrigated class has a producer's accuracy of 86.7% (errors of omissions of = 13.3%) and user's accuracy of 84.3% (errors of commissions = 15.7%). The rainfed class has a producer's accuracy of 86.3% (errors of omissions of = 13.7%) and user's accuracy of 88.4% (errors of commissions = 11.6%). For the 13 AEZs (Figure 13b) the LGRIP30 (Figure 37) showed overall accuracies to vary between 79.2 to 94.4% (Table 6). In the 13 AEZ's, the irrigated class producer's accuracies varied between 77.9 to 95% (errors of omissions of = 5 to 21.1%) and user's accuracies vary between 76.9 to 94.3% (errors of commissions = 5.7-23.1%) (Table 6). In the 13 AEZ's, the rainfed class producer's accuracies varied between 77.6 to 98.5% (errors of omissions of = 1.5 to 22.4%) and user's accuracies vary between 82 to 95.5 % (errors of commissions = 4.5-18%) (Table 6). These results clearly indicate robust and high degree of accuracies in both irrigated and rainfed cropland mapping.

Producer's accuracies of irrigated areas and rainfed areas of all the countries in the world is shown in Figure 45 and 46, respectively. User's accuracies of irrigated areas and rainfed areas of all the countries in the world is shown in Figure 47 and 48, respectively. The overall accuracies of the LGRIP30 map are shown in Figure 49.

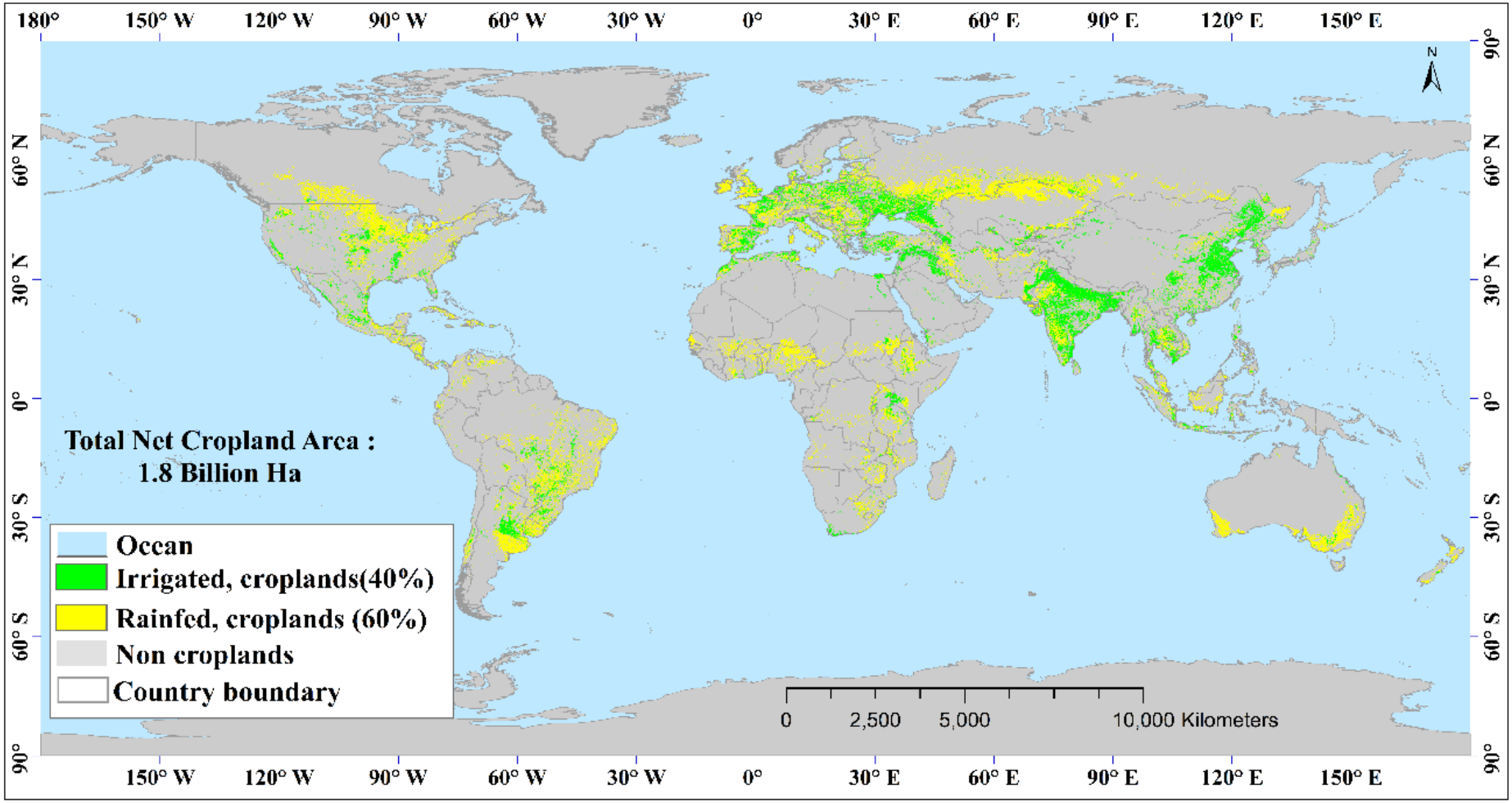

Figure 37. LGRIP30 product. The Landsat-derived Global rainfed & irrigated product @ 30m (LGRIP30) for the nominal year 2015. This product provides global rainfed and irrigated areas at 30m. View this product at: www.usgs.gov/apps/croplands (navigate to LGRIP30 within this site). The product is tiles 1 degree by 1 degree and released through NASA's LP DAAC.

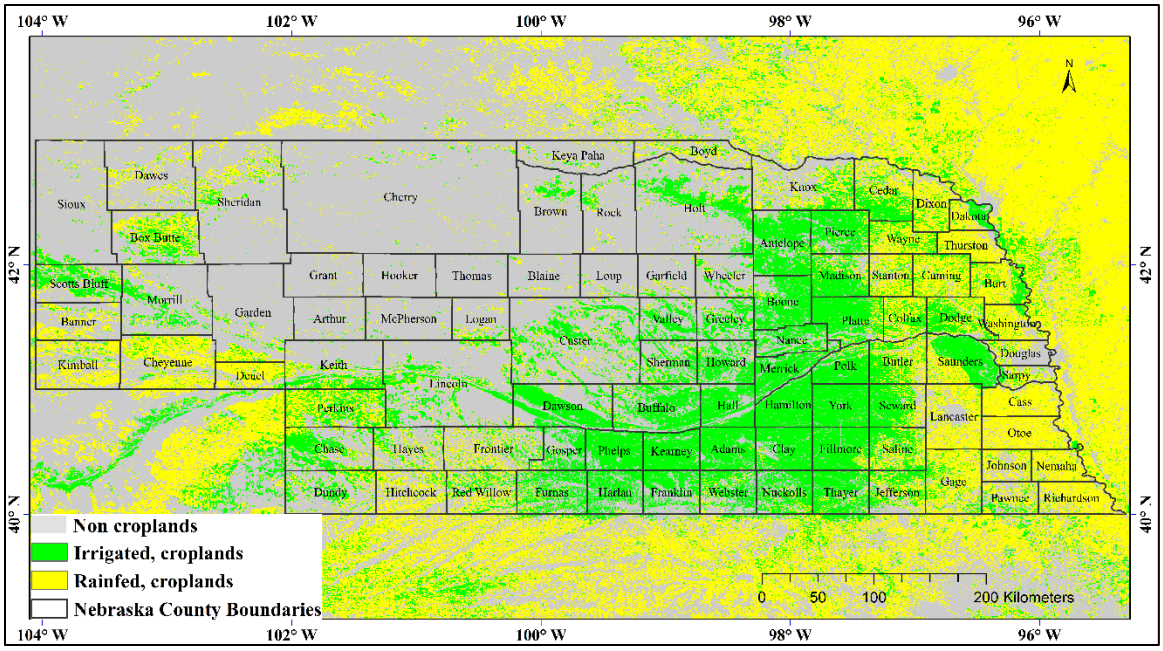

Figure 38. LGRIP30 zoom-in to Nebraska, USA. Landsat-derived Global rainfed & irrigated product @ 30m (LGRIP30) for the nominal year 2015. Zoom in views of Nebraska, USA.

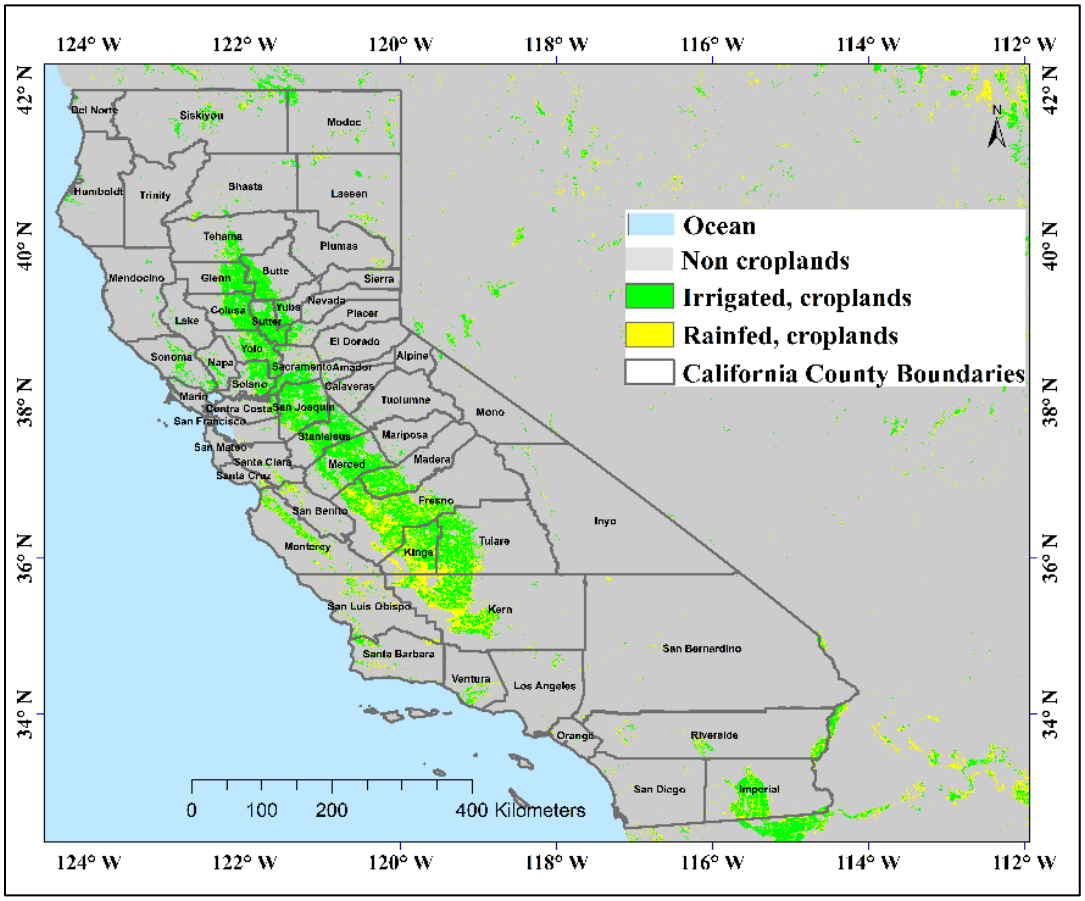

Figure 39. LGRIP30 zoom-in to California, USA. Landsat-derived Global rainfed & irrigated product @ 30m (LGRIP30) for the nominal year 2015. California, USA.

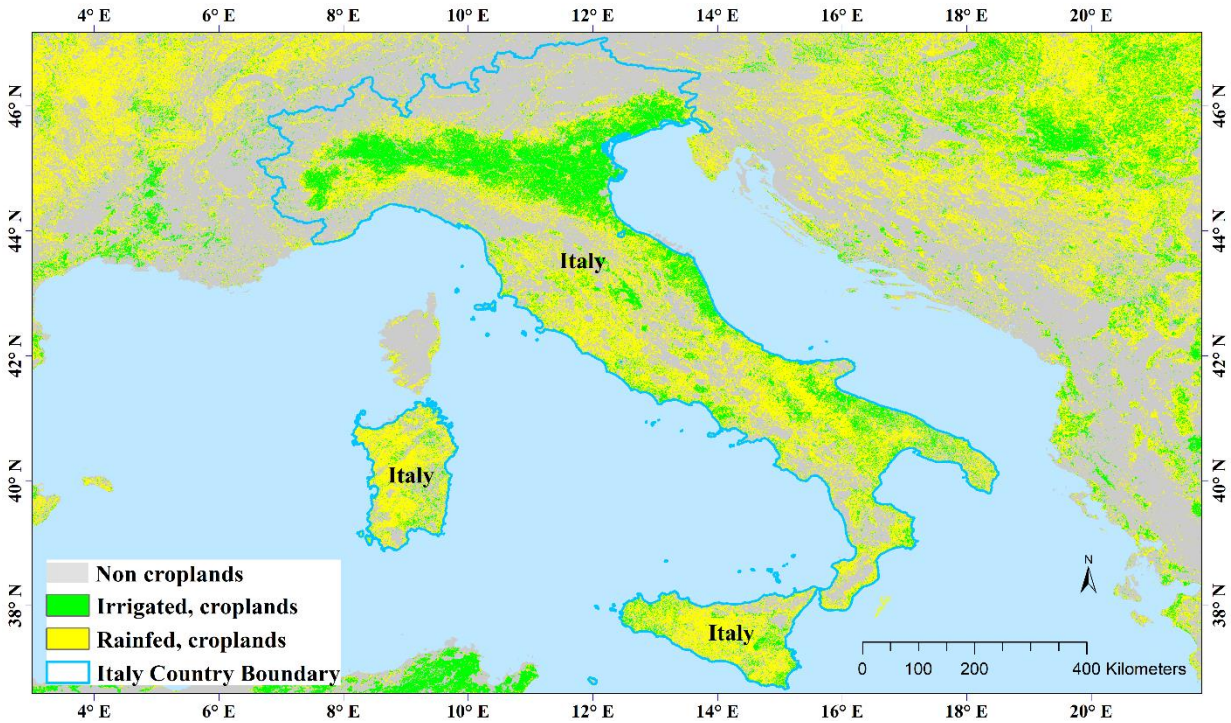

Figure 40. LGRIP30 zoom-in to France. Landsat-derived Global rainfed & irrigated product @ 30m (LGRIP30) for the nominal year 2015. France.

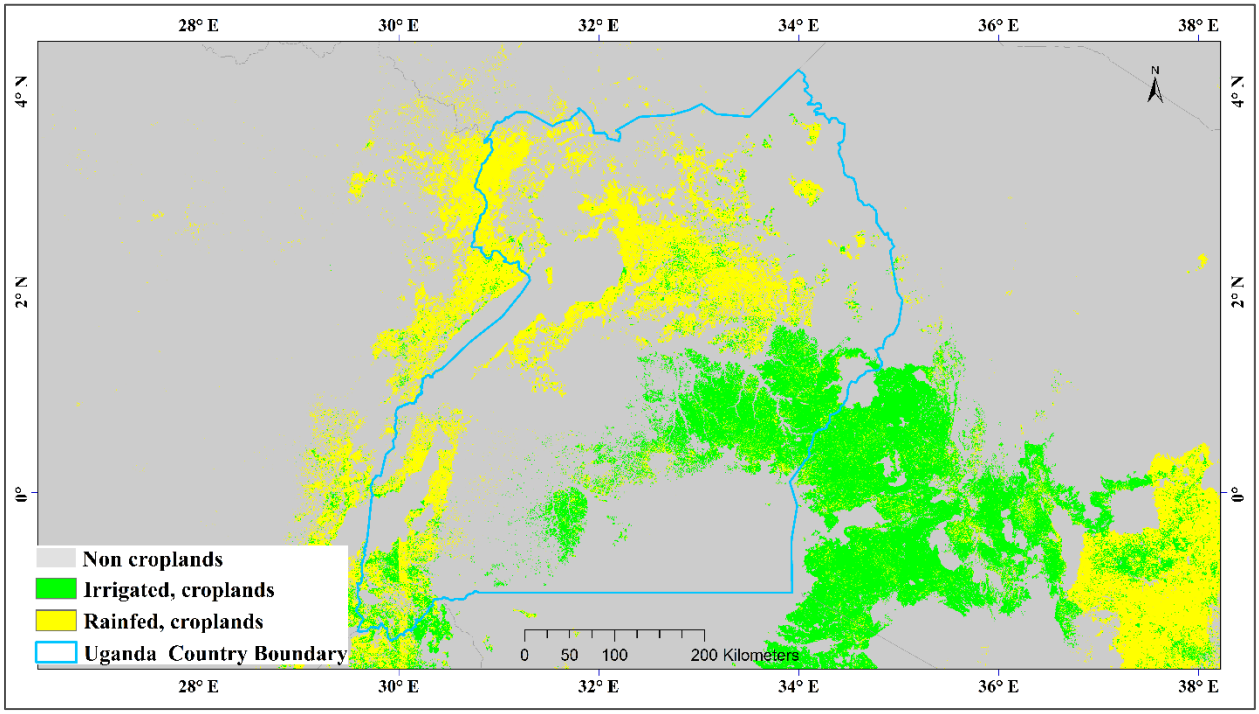

Figure 41. LGRIP30 zoom-in to Uganda. Landsat-derived Global rainfed & irrigated product @ 30m (LGRIP30) for the nominal year 2015. Uganda.

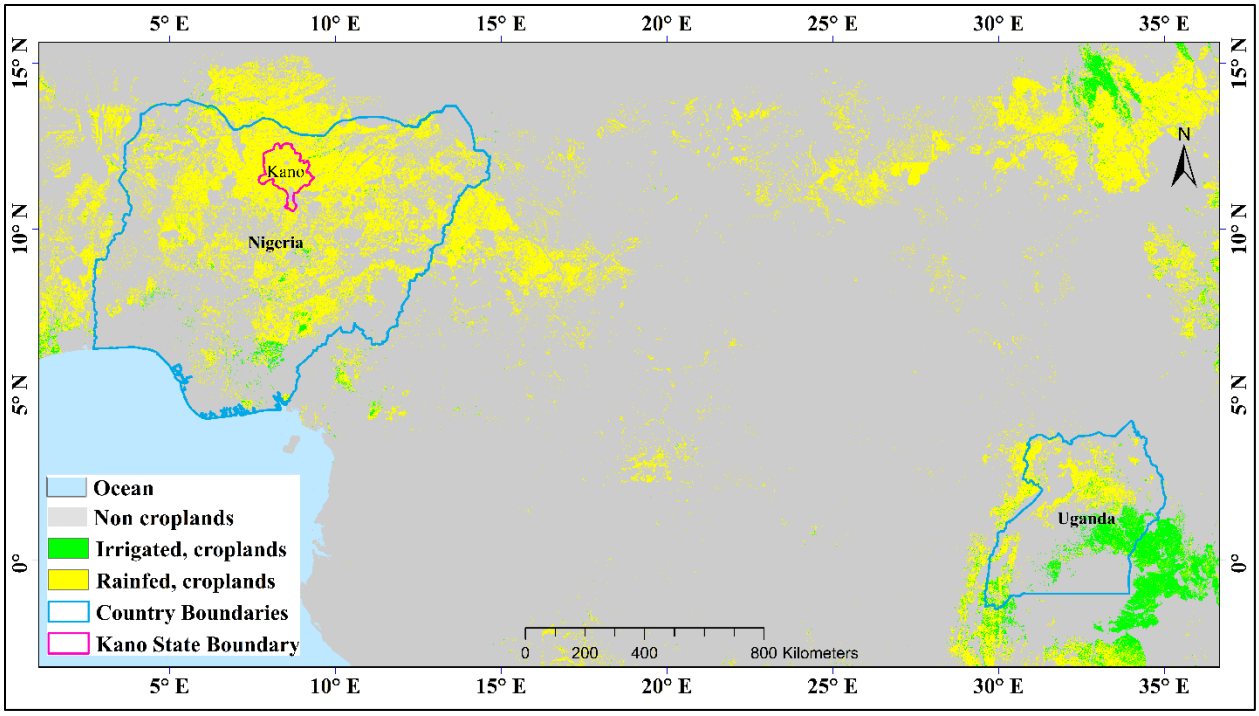

Figure 42. LGRIP30 zoom-in to Nigeria. Landsat-derived Global rainfed & irrigated product @ 30m (LGRIP30) for the nominal year 2015. Nigeria.

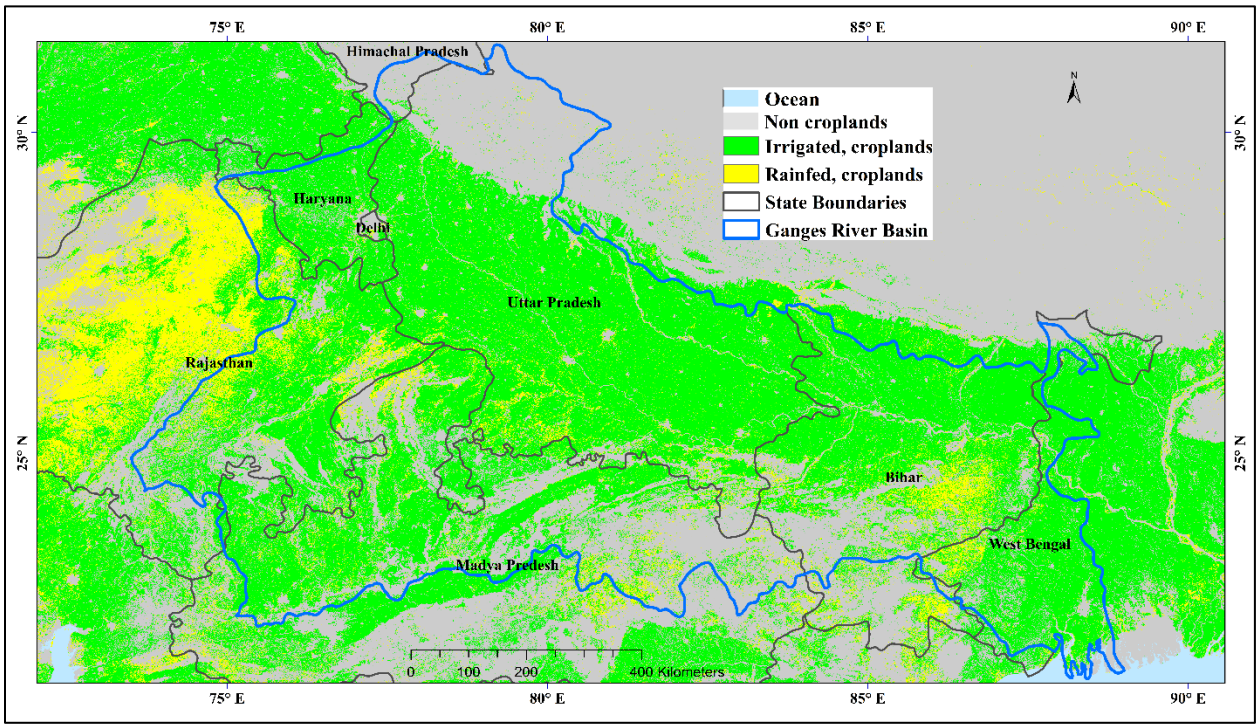

Figure 43. LGRIP30 zoom-in to Parts of India. Landsat-derived Global rainfed & irrigated product @ 30m (LGRIP30) for the nominal year 2015. Ganges, India.

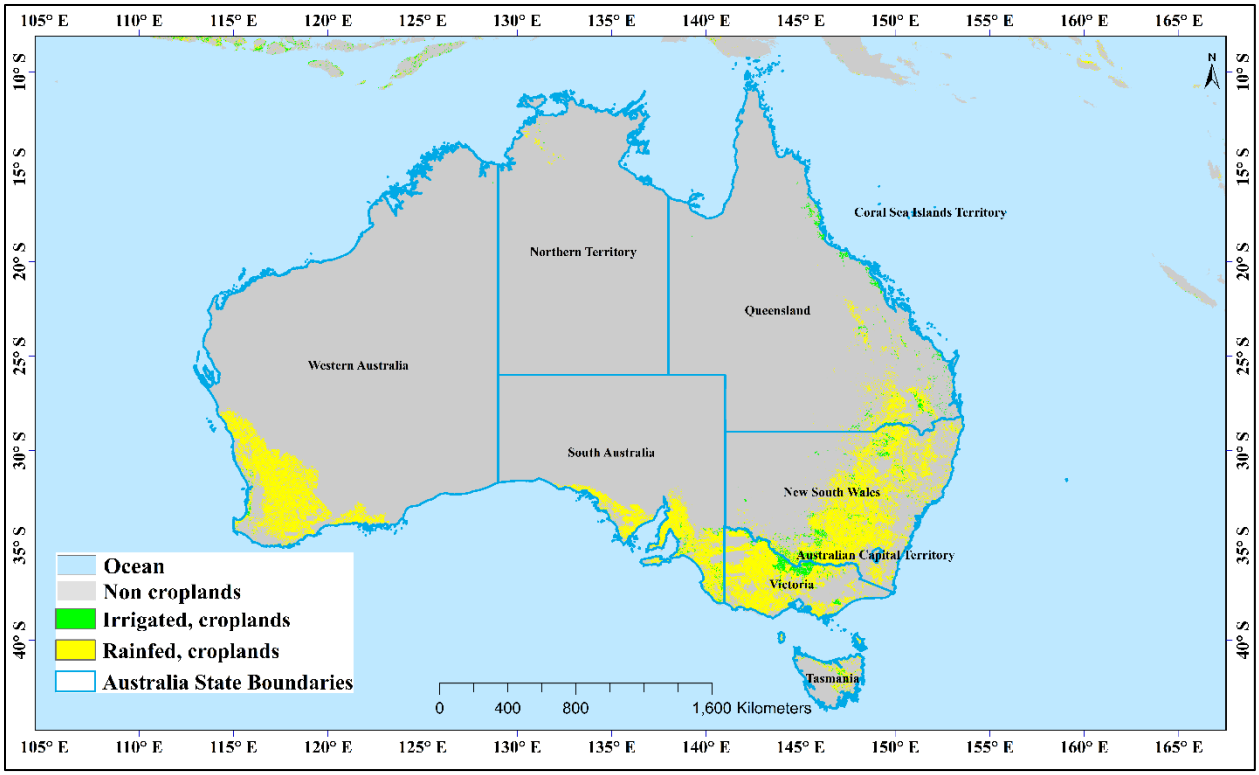

Figure 44. LGRIP30 zoom-in to Australia. Landsat-derived Global rainfed & irrigated product @ 30m (LGRIP30) for the nominal year 2015. Australia.

Table 5. LGRIP30 accuracy error matrix of the world. Global accuracy assessment error matrix showing the overall accuracies, user's accuracies, and producer's accuracies. Number of validation samples, N = 10477.

	Reference Data			
Class	Irrigated	Rainfed	Row total	Commission error
Irrigated	**4171**	774	4945	15.7%
Rainfed	639	**4893**	5532	11.6%
Column total	4810	5667	**10477**	
Omission error	13.3%	13.7%		
Producer accuracy	86.7%	86.3%		
User accuracy	84.3%	88.4%		
Overall accuracy				**86.5%**

Table 6. LGRIP30 accuracy error matrix of the world for each of the 13 zones. These accuracies of the LGRIP30 product are mapped in Figure 45-49.

		Producers Accuracy		Users Accuracy		Overall accuracy
Zone#	**Zone**	**Irrigated**	**Rainfed**	**Irrigated**	**Rainfed**	
#	**Name**	**%**	**%**	**%**	**%**	**%**
1	United States of America	84.6	85.2	77.0	90.4	85.0
2	Canada	82.5	97.5	89.7	95.5	94.4
3	Central America	77.9	87.8	85.5	81.1	83.0
4	South America	80.3	87.3	86.1	81.9	83.8
5	Africa	87.3	86.4	78.9	92.1	86.7
6	Europe	82.4	87.0	83.7	85.9	84.9
7	Russia	78.9	94.2	80.4	93.7	90.7
8	Central Asia	92.2	95.7	93.0	95.2	94.4
9	Middle east & West Asia	92.2	80.0	94.1	75.0	89.5
10	South Asia	93.7	77.4	86.1	89.0	87.1
11	China, Japan, & Korea	95.0	74.6	89.4	86.9	88.7
12	Southeast Asia	83.2	75.3	76.9	82.0	79.2
13	Australia &New Zealand	82.1	98.5	94.3	94.7	94.6
	Global	**86.7**	**86.3**	**84.3**	**88.4**	**86.5**

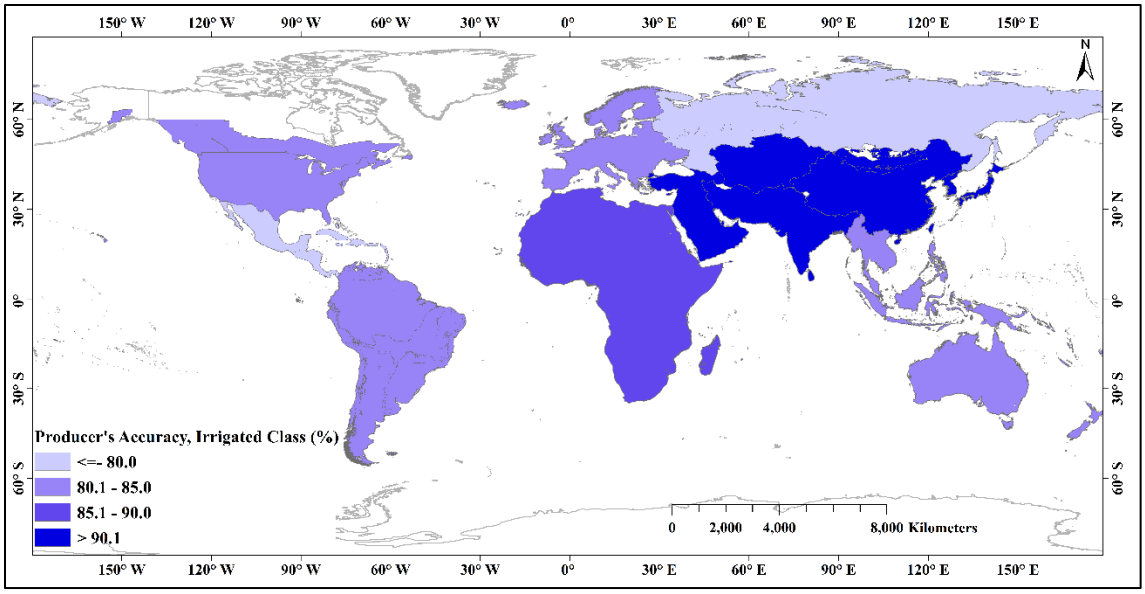

Figure 45. Producer's accuracies for LGRIP30 irrigated areas. Map showing producer's accuracies of irrigated croplands in Landsat derived global rainfed and irrigated cropland product at 30-m resolution (LGRIP30) for all 13 zones. Note that errors of omission (%) = 100 − producer's accuracy (%).

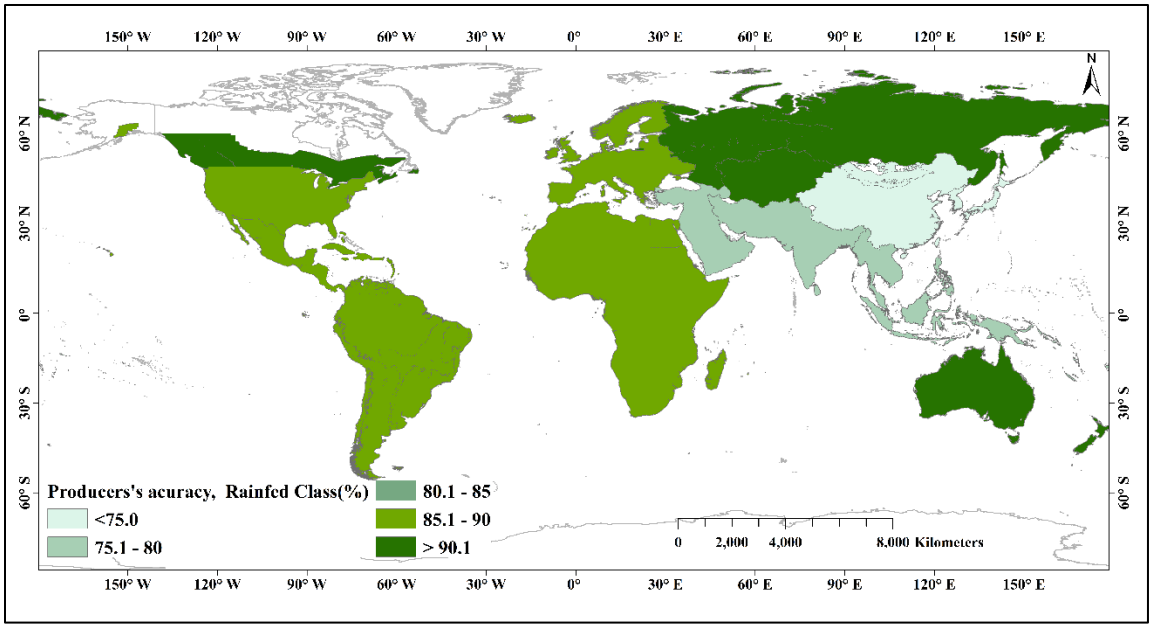

Figure 46. Producer's accuracies for LGRIP30 rainfed areas. Map showing producer's accuracies of rainfed croplands in Landsat derived global rainfed and irrigated cropland product at 30-m resolution (LGRIP30) for all 13 zones. Note that errors of omission (%) = 100 − producer's accuracy (%).

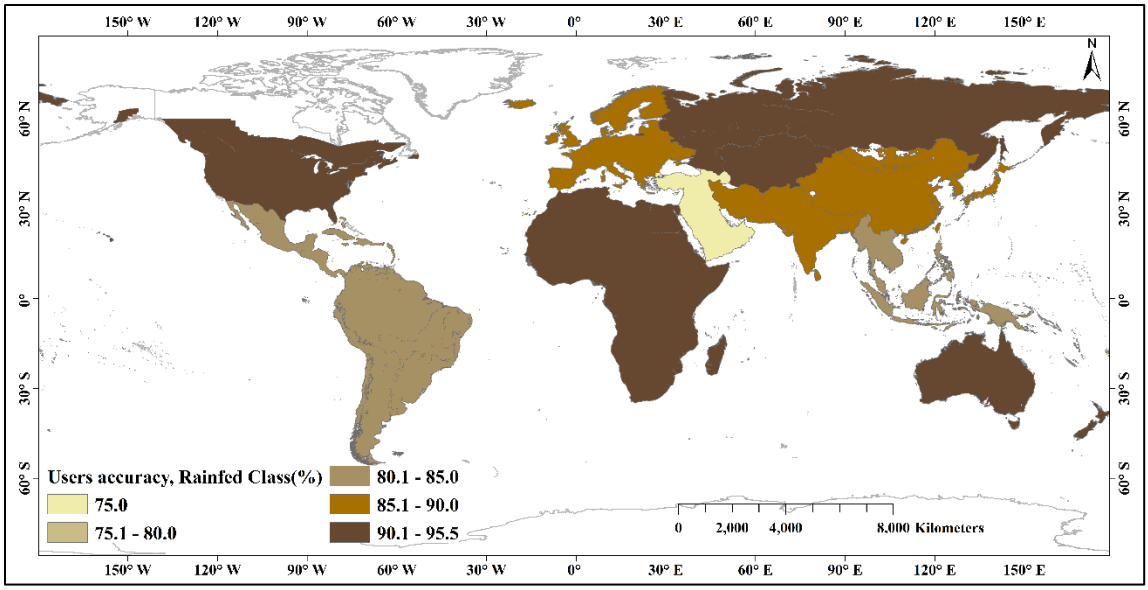

Figure 47. User's accuracies for LGRIP30 irrigated areas. Map showing user's accuracies of irrigated croplands in Landsat derived global rainfed and irrigated cropland product at 30-m resolution (LGRIP30) for all 13 zones. Note that errors of commission (%) = 100 − user's accuracy (%).

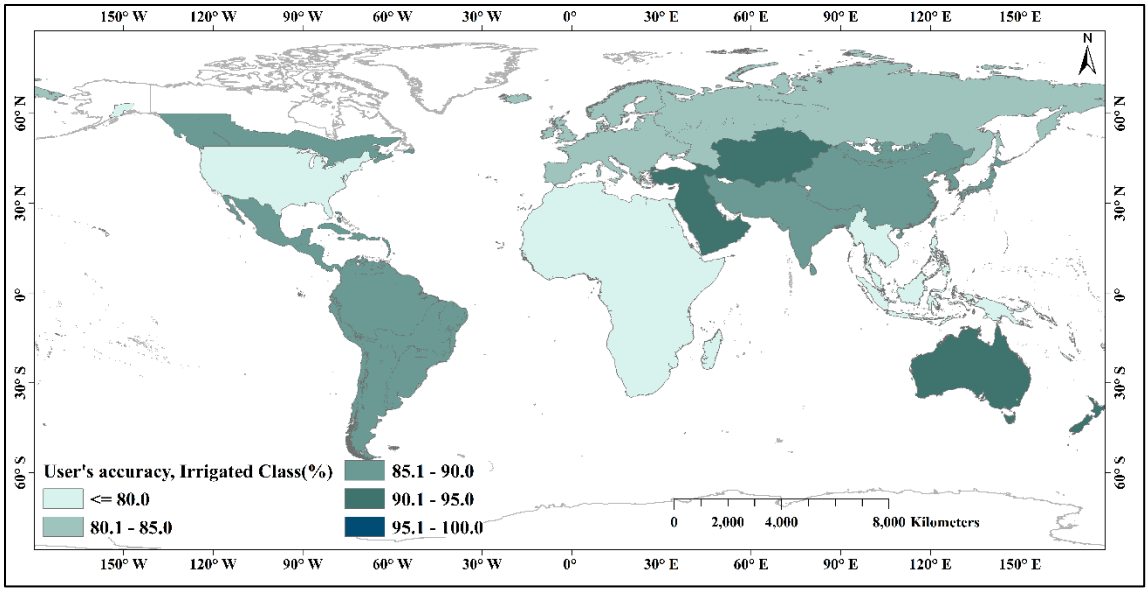

Figure 48. User's accuracies for LGRIP30 rainfed areas. Map showing user's accuracies of rainfed croplands in Landsat derived global rainfed and irrigated cropland product at 30-m resolution (LGRIP30) for all 13 zones. Note that errors of commission (%) = 100 − user's accuracy (%).

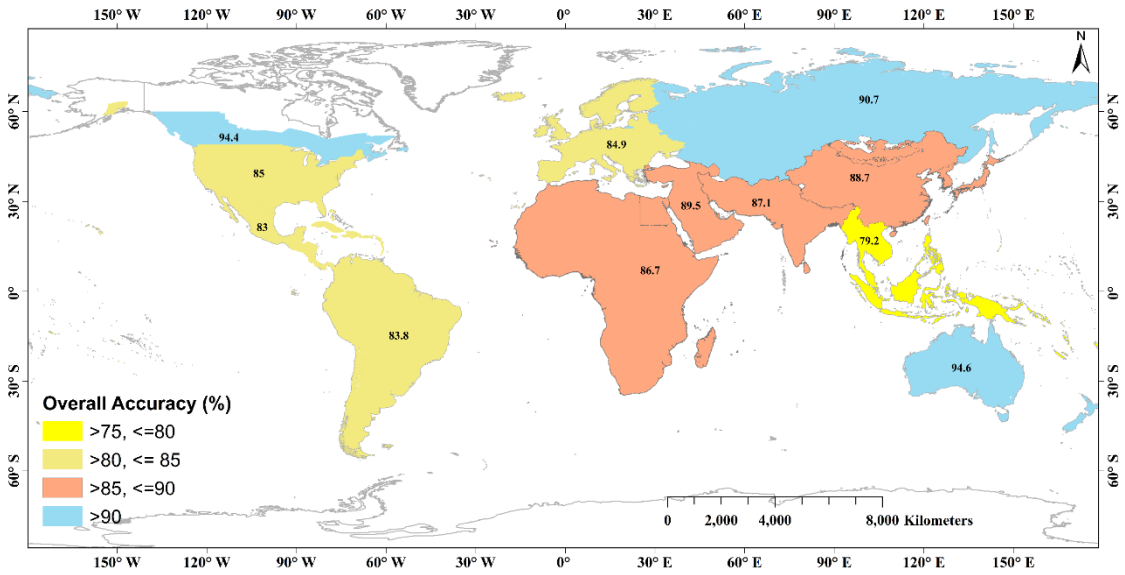

Figure 49. Overall accuracies for LGRIP30. Map showing overall accuracies of each zone for nominal-year 2015. Accuracies derived from Landsat derived global rainfed and irrigated cropland product at 30-m resolution (LGRIP30).

C. Areas

Our area calculations have two important note to consider in terms of irrigated areas. When we mean irrigated areas, they imply: 1. net irrigated areas (NIAs) and 2. equipped irrigated areas (EIAs). This study does not report gross irrigated area (GIA) or annualized irrigated areas.

The LGRIP30 (Figure 37) has a total global net irrigated area (TGNIA) of 1,802,929,008 hectares (or 1.80 billion hectares or Bha) of croplands (Table 7) of which 1,087,185,109 hectares (1.09 Bha) was rainfed and the rest 715,743,899 hectares (0.71 Bha) was irrigated (Table 7). Thereby, overall, of the 1.8 Bha of croplands 60.3% is rainfed and 39.7% is irrigated (Figure 24) (we will refer to this as 60% irrigated and 40% rainfed throughout. In earlier Landsat-derived global cropland extent product at 30 m (GCEP30) Thenkabail et al., (2021) reported global cropland of 1.873 Bha (Figure 8). Even though Figure 8, forms the basemap from which LGRIP30 (Figure 37) is derived, the areas found non-croplands in GCEP30 (Figure 8) were dropped. Also, some of the croplands missing in GCEP30 (Figure 8) were included in LGRIP30 (Figure 37). So, LGRIP30 had both subtraction and addition to GCEP30 (Figure8) leading to a LGRIP30 area of 1.8 Bha with 40% irrigated and 60% rainfed (Figure 37).

The global net irrigated areas (GNIA) reported in our study (715 Mha) is substantially higher compared to previous studies which report GNIA that varied between 307-450 Mha (Puy et al., 2020, Salmon et al., 2015, Siebert et al., 2013, 2001, FAO, 2012b, FAO, 2015, Thenkabail et al. 2012, 2011, 2009a). This is not surprising. Indeed, in a recent study by Puy et al., (2020) suggested that the amount of irrigated land could in fact increase to as high as 1.8 billion hectares by 2050. They suggested in the paper that "*Policymakers should acknowledge that irrigated areas can grow much more than previously thought in order to avoid underestimating potential environmental costs*". Puy et al. (2020) clearly demonstrate that the current models underestimate irrigated areas. Rosa et al. (2020) showed that up to 35% of the current rainfed areas have potential for irrigation expansion in a climate change scenario of temperature warming between 1.5-3

degree Celsius. Our results show that this irrigation expansion is already happening at a rapid phase. In an increasingly changing climate, complete dependance on precipitation which has wide variability is becoming unsustainable and some supplemental irrigation in the least is necessary to ensure optimal productivity and\or to sustain any productivity at all in rainfed croplands. Further, most of lower irrigated areas reported in the range around 307-450 Mha estimates were for the 2000-2005 period (Salmon et al., 2015, Thenkabail et al., 2011, 2009a). These estimates were 307-311 Mha for 2000-2008 period (Siebert et al., 2015, FAO, 2012b, Siebert and Döll, 2001, 2010, Siebert at al., 2013), 314 Mha for 2005 by Salmon et al. (2015), and 399 Mha by Thenkabail et al. (2011, 2009a) for nominal 2000.

Significantly, higher irrigated areas reported in this study are due to following reasons:
1.Definition of irrigated area: we have defined irrigated areas as those that use artificial use of water even one or more times during the crop growing season from any source (e.g., major irrigation, minor irrigation, surface water, ground water, open well, deep acquirer wells, river pumping, diver diversions, tanks or any other source). In a climate extreme of floods and droughts and lesser reliability in timely rainfall, some supplemental irrigation has become a norm. So, these irrigated areas are swiftly increasing when we consider supplemental irrigation.

2. Technological advances in water delivery to agriculture: In much of the world technological advances has created greater and greater irrigation facility. For example, most farmers these days use some form of irrigation either by pumping water directly from rivers or from open wells or from deep acquirer wells. In India, for example, between 1950 and 2010, the number of drilled tube wells increased from 1 million to nearly 30 million (World Bank, 2020). The number of deep tube wells in the country saw surge from 1.46 million to 2.6 million in just between 2006-07 and 2013-14 (Business Standard, 2017). Overwhelming proportion of tube-wells are used for irrigation. However, most of these go unaccounted from irrigated agricultural areas.

3. Equipped area for irrigation: our irrigated areas consider all irrigated areas equipped for irrigation as irrigated areas even when part of those are not irrigated at times (or left fallows). For example, significant pasture\hay are included in irrigated areas in few countries.

4. Climate factor: In an increasingly changing climate, purely rainfall dependent agriculture is reducing swiftly. Even when rainfall amount is normal, it's timeliness in delivery varies. Crops need water in timely manner and when rainfall fails to follow a pattern during the growing season, plants will need water from irrigation and hence supplemental irrigation is greatly increasing, primarily through pumping from open wells, tube-wells, and directly from rivers.

C1. Areas by countries

Table 7 provides irrigated and rainfed cropland areas for all the countries in the world. The Table 7 shows countries with ranking based on irrigated areas. Of the 1,802,929,008 hectares total global net cropland areas (TGNCAs), 1,087,185,109 hectares (1.09 Bha) was total global net rainfed areas (TGNRAs) and the rest 715,743,899 hectares (0.71 Bha) was total global net irrigated areas (TGNIAs).

The top 10 TGNIAs of the world were (Table 7): India (132.5 million hectares or Mha, 18.5% of TGNIA of 715 Mha), China (131.8 Mha; 18.4%), USA (42.3 Mha; 5.9%), Russia (33.3 Mha; 4.6%), Ukraine (30.4 Mha; 4.2%), Turkey (19.5 Mha; 2.7%), Pakistan (19.1 Mha; 2.7%), Mexico (16.3 Mha; 2.3%), Spain (15.3 Mha; 2.1%), and France (13.5 Mha; 1.9%). These 10 countries have 64 percent of TGNIAs of the world. India and China together have 37% of the TGNIAs. India with population of 1.39 billion and China with population of 1.41 billion have large, irrigated areas to feed their large populations. Also, these are ancient countries with continuous civilizations of over 7000 years of sustained populations and agricultural development. It is important to note that significant proportion of the irrigated areas in countries like India and China have two or three crops annually as weather allows for crop growth throughout the year for much of these two countries. Modern Nations like USA, much of irrigated infrastructure was built during the nineteenth Century. It is obvious from the irrigated area statistics (Table 7) that many countries of the world have significant irrigated areas. In comparison to other studies (Salmon et al., 2015, Siebert et al., 2013, 2001, FAO, 2012b, FAO, 2015, Thenkabail et al. 2012, 2011, 2009a) there is significant increase in irrigated areas in several countries throughout the world.

The top 10 TGNRAs countries of the world were (Table 7): USA (125.9 Mha, 11.6% of 1.087 Bha), Russia (121.7 Mha, 11.2%), India (46.8 Mha; 4.3%), Brazil (46.2 Mha; 4.2%), Canada (42.6 Mha; 3.9%), China (32.1 Mha; 2.9%), Nigeria (30.8 Mha; 2.8%), Australia (30.5 Mha; 2.8%), Argentina (29.4 Mha; 2.7%), and Indonesia (26.4 Mha; 2.4%). These 10 countries have 49 percent of TGNRAs of the world. USA and Russia together have 23% of the TGNRAs. Both USA and Russia have vast stretches of highly productive croplands that can only grow one crop a year as weather conditions restrict crop during rest of the year. Overwhelming proportion of these croplands do not require irrigation. However, significant proportion of these croplands may require supplemental irrigation in years ahead as a result of changing climate and climate extremes.

As Puy et al., (2020) imply the irrigated cropland expansion maybe substantially underestimated. Indeed, in a changing climate assured cropland may not be possible is a significant proportion of the existing rainfed croplands. Further additional food and nutritional demands of ballooning populations will demand cropland intensification where currently rainfed croplands may need to grow a second crop assisted by partial or full irrigation.

Table 7. LGRIP30-derived net irrigated areas (NIAs) and net rainfed areas (NRAs) of all the countries of the world[1,2].

Sno	Zone#	ADM0_CODE[1]	ADM0_NAME[1]	Irr-rank[2]	LGRIP30-Irrigated[3]	LGRIP30-Rainfed[3]	LGRIP30-Total[3]
#	#	#	Name	#	Ha	Ha	Ha
1	10	115	India	1	132,542,113	46,767,434	179,309,548
2	11	147295	China	2	131,778,217	32,118,339	163,896,556
3	1	259	USA	3	42,323,364	125,881,360	168,204,724
4	7	204	Russian Federation	4	33,276,856	121,651,518	154,928,374
5	6	254	Ukraine	5	30,408,208	12,621,600	43,029,808
6	9	249	Turkey	6	19,547,992	8,872,795	28,420,787
7	10	188	Pakistan	7	19,127,578	7,492,682	26,620,261
8	3	162	Mexico	8	16,324,519	17,865,405	34,189,923
9	6	229	Spain	9	15,355,735	12,856,514	28,212,249
10	6	85	France	10	13,519,701	18,132,629	31,652,330
11	12	240	Thailand	11	13,516,805	12,175,398	25,692,203
12	4	37	Brazil[4]	12	13,135,572	46,424,651	59,560,223
13	9	118	Iraq	13	11,537,570	350,703	11,888,273
14	6	198	Poland	14	10,649,360	8,344,592	18,993,952
15	12	116	Indonesia	15	10,015,594	26,434,913	36,450,507
16	10	23	Bangladesh	16	9,359,234	481,359	9,840,593
17	12	171	Myanmar	17	8,939,549	4,979,478	13,919,026
18	6	93	Germany	18	8,237,645	11,544,787	19,782,432
19	10	117	Iran (Islamic Republic of)	19	8,042,545	24,326,809	32,369,353
20	12	264	Viet Nam	20	7,725,984	2,812,147	10,538,131
21	9	238	Syrian Arab Republic	21	6,533,081	26,030	6,559,111
22	6	203	Romania	22	5,649,424	7,872,839	13,522,263
23	8	261	Uzbekistan	23	5,558,757	2,208,708	7,767,466
24	5	133	Kenya	24	5,224,532	3,555,088	8,779,620
25	5	257	United Republic of Tanzania	25	5,222,179	14,829,772	20,051,951
26	6	122	Italy	26	5,117,951	11,865,176	16,983,127
27	4	12	Argentina[4]	27	4,869,367	29,397,914	34,267,281
28	5	169	Morocco	28	4,765,248	3,700,828	8,466,076
29	5	4	Algeria	29	4,703,703	3,469,561	8,173,264
30	13	17	Australia[5]	30	4,557,947	30,547,846	35,105,792
31	5	40765	Egypt	31	4,249,590	452,604	4,702,194
32	6	26	Belarus	32	4,229,552	6,251,613	10,481,165
33	9	19	Azerbaijan	33	4,191,284	537,190	4,728,475
34	12	44	Cambodia	34	4,183,465	3,416,139	7,599,604
35	5	227	South Africa	35	4,080,443	13,234,658	17,315,100
36	5	79	Ethiopia	36	4,045,941	19,538,956	23,584,897
37	12	196	Philippines	37	3,004,488	3,205,429	6,209,917
38	8	132	Kazakhstan[5]	38	2,928,290	22,956,732	25,885,023
39	5	253	Uganda	39	2,606,349	3,977,090	6,583,440
40	9	215	Saudi Arabia	40	2,571,745	107,236	2,678,981
41	8	250	Turkmenistan	41	2,543,481	1,177,884	3,721,366
42	11	67	Dem People's Rep of Korea	42	2,474,461	789,101	3,263,562
43	5	248	Tunisia	43	2,437,781	2,363,821	4,801,602
44	11	126	Japan	44	2,333,268	1,196,752	3,530,020
45	6	41	Bulgaria	45	2,277,087	3,534,067	5,811,154
46	5	6	Sudan	46	2,108,841	18,463,778	20,572,619
47	6	256	U.K. of Great Britain and No	47	1,989,605	13,712,814	15,702,419
48	6	97	Greece	48	1,986,543	2,292,069	4,278,613
49	4	194	Paraguay	49	1,940,790	7,037,188	8,977,978
50	6	65	Czech Republic	50	1,891,452	2,799,278	4,690,730
51	6	177	Netherlands	51	1,825,597	440,542	2,266,139
52	6	113	Hungary	52	1,820,245	5,442,207	7,262,452
53	9	269	Yemen	53	1,750,354	412,147	2,162,501
54	10	175	Nepal	54	1,718,874	224,783	1,943,657
55	12	153	Malaysia	55	1,656,305	8,683,545	10,339,850

Sno	Zone#	ADM0_CODE[1]	ADM0_NAME[1]	Irr-rank[2]	LGRIP30-Irrigated[3]	LGRIP30-Rainfed[3]	LGRIP30-Total[3]
#	#	#	Name	#	Ha	Ha	Ha
56	10	1	Afghanistan	56	1,566,341	6,572,877	8,139,219
57	6	165	Moldova, Republic of	57	1,516,954	1,345,832	2,862,786
58	6	69	Denmark	58	1,491,313	1,848,808	3,340,121
59	4	260	Uruguay	59	1,441,529	10,557,482	11,999,011
60	9	92	Georgia	60	1,287,736	357,602	1,645,338
61	6	2648	Serbia	61	1,279,949	3,775,592	5,055,541
62	4	51	Chile	62	1,274,174	4,700,924	5,975,098
63	6	147	Lithuania	63	1,269,120	2,686,098	3,955,218
64	6	223	Slovakia	64	1,219,444	1,227,596	2,447,040
65	11	202	Republic of Korea	65	1,162,164	263,476	1,425,640
66	12	139	Lao People's Democratic Rep	66	1,087,528	1,246,341	2,333,869
67	10	231	Sri Lanka	67	1,085,920	351,863	1,437,783
68	2	46	Canada	68	1,038,976	42,594,426	43,633,402
69	5	182	Nigeria	69	915,851	30,752,427	31,668,278
70	6	18	Austria	70	913,384	1,769,040	2,682,424
71	5	68	Democratic Republic of the C	71	897,222	11,613,284	12,510,506
72	5	145	Libya	72	893,336	920,194	1,813,530
73	6	199	Portugal	73	881,055	3,343,981	4,225,036
74	6	236	Sweden	74	871,700	2,542,384	3,414,083
75	13	179	New Zealand	75	821,896	7,298,127	8,120,023
76	5	152	Malawi	76	816,280	3,796,667	4,612,947
77	8	239	Tajikistan	77	744,781	365,886	1,110,668
78	5	270	Zambia	78	730,337	6,583,386	7,313,723
79	8	138	Kyrgyzstan	79	675,227	1,445,769	2,120,997
80	5	66	CÃ´te d'Ivoire	80	626,745	5,484,524	6,111,269
81	9	121	Israel	81	624,292	3,238	627,530
82	4	33	Bolivia	82	609,476	2,898,338	3,507,814
83	3	103	Guatemala	83	603,023	3,838,157	4,441,180
84	3	63	Cuba	84	600,717	3,607,739	4,208,456
85	5	205	Rwanda	85	499,148	831,933	1,331,081
86	6	84	Finland	86	498,882	1,352,878	1,851,761
87	3	180	Nicaragua	87	492,821	4,417,631	4,910,453
88	9	130	Jordan	88	456,531	11,553	468,083
89	6	140	Latvia	89	450,665	2,169,877	2,620,542
90	5	271	Zimbabwe	90	449,584	9,748,437	10,198,021
91	9	64	Cyprus	91	449,492	52,005	501,497
92	6	62	Croatia	92	446,805	1,894,516	2,341,321
93	3	61	Costa Rica	93	440,799	1,648,444	2,089,242
94	3	111	Honduras	94	425,723	2,813,125	3,238,848
95	11	147296	Taiwan	95	421,802	109,157	530,959
96	5	94	Ghana	96	410,828	2,858,865	3,269,694
97	5	155	Mali	97	353,258	10,011,477	10,364,735
98	6	241	The former Yugoslav Republi	98	348,699	487,029	835,728
99	3	191	Panama	99	340,175	1,758,764	2,098,939
100	9	13	Armenia	100	330,652	255,125	585,777
101	6	78	Estonia	101	325,914	1,056,137	1,382,050
102	3	72	Dominican Republic	102	305,205	1,682,026	1,987,231
103	4	263	Venezuela	103	303,055	6,881,570	7,184,625
104	5	170	Mozambique	104	299,985	6,004,906	6,304,891
105	5	150	Madagascar	105	277,448	3,068,635	3,346,083
106	4	195	Peru	106	256,558	1,513,123	1,769,681
107	5	243	Togo	107	241,842	1,657,732	1,899,573
108	9	141	Lebanon	108	218,842	23,912	242,754
109	9	255	United Arab Emirates	109	215,571	7,154	222,725
110	6	3	Albania	110	209,180	460,791	669,971

Sno	Zone#	ADM0_CODE[1]	ADM0_NAME[1]	Irr-rank[2]	LGRIP30-Irrigated[3]	LGRIP30-Rainfed[3]	LGRIP30-Total[3]
#	#	#	Name	#	Ha	Ha	Ha
111	6	27	Belgium	111	206,802	1,476,243	1,683,045
112	5	45	Cameroon	112	204,248	4,407,678	4,611,927
113	4	73	Ecuador	113	200,321	2,027,725	2,228,046
114	5	226	Somalia	114	178,552	1,456,278	1,634,831
115	9	187	Oman	115	145,334	2,395	147,729
116	4	57	Colombia	116	134,755	5,536,017	5,670,771
117	3	108	Haiti	117	129,332	1,089,452	1,218,784
118	6	34	Bosnia and Herzegovina	118	121,634	1,628,530	1,750,164
119	5	235	Swaziland	119	121,272	460,840	582,111
120	5	43	Burundi	120	103,861	644,583	748,444
121	6	119	Ireland	121	102,213	5,094,203	5,196,415
122	6	186	Norway	122	86,078	774,458	860,536
123	6	237	Switzerland	123	77,078	1,235,910	1,312,988
124	5	181	Niger	124	73,207	7,752,110	7,825,317
125	4	107	Guyana	125	70,476	68,780	139,255
126	12	242	Timor-Leste	126	69,189	51,002	120,191
127	5	29	Benin	127	66,513	3,207,925	3,274,438
128	5	8	Angola	128	47,936	4,691,297	4,739,234
129	5	217	Senegal	129	46,543	3,939,082	3,985,624
130	3	28	Belize	130	44,187	319,271	363,458
131	5	106	Guinea	131	39,622	648,708	688,330
132	3	75	El Salvador	132	38,803	991,786	1,030,589
133	9	137	Kuwait	133	36,967	1,152	38,119
134	3	123	Jamaica	134	35,368	235,535	270,903
135	3	200	Puerto Rico	135	34,919	302,064	336,983
136	5	59	Congo	136	34,647	208,740	243,388
137	5	105	Guinea-Bissau	137	29,783	164,991	194,773
138	9	267	West Bank	138	29,382	212	29,594
139	5	91	Gaza Strip	139	28,905	423	29,328
140	6	2647	Montenegro	140	26,809	181,392	208,201
141	6	224	Slovenia	141	25,764	633,483	659,246
142	5	35	Botswana	142	24,678	1,594,821	1,619,499
143	12	192	Papua New Guinea	143	22,615	295,168	317,782
144	9	201	Qatar	144	20,710	1,219	21,928
145	5	42	Burkina Faso	145	20,601	5,674,965	5,695,565
146	5	50	Chad	146	19,390	5,324,980	5,344,370
147	10	31	Bhutan	147	19,035	17,064	36,099
148	3	100	Guadeloupe	148	16,180	47,777	63,957
149	5	160	Mauritius	149	15,210	51,895	67,104
150	12	83	Fiji	150	14,111	156,300	170,411
151	5	77	Eritrea	151	13,773	609,684	623,457
152	6	156	Malta	152	13,355	11,268	24,623
153	11	167	Mongolia	153	12,010	882,577	894,587
154	5	74	South Sudan	154	11,819	1,036,348	1,048,166
155	12	178	New Caledonia	155	11,759	24,094	35,854
156	5	221	Sierra Leone	156	11,219	91,125	102,344
157	4	233	Suriname	157	9,509	22,811	32,320
158	12	40	Brunei Darussalam	158	8,062	42,005	50,067
159	3	24	Barbados	159	7,222	10,728	17,950
160	5	90	Gambia	160	5,969	318,670	324,639
161	11	33364	Hong Kong	161	5,679	4,454	10,133
162	5	172	Namibia	162	5,238	884,344	889,582
163	6	148	Luxembourg	163	5,201	134,105	139,306
164	5	159	Mauritania	164	4,491	87,733	92,224
165	12	225	Solomon Islands	165	4,245	315,279	319,524

Sno	Zone#	ADM0_CODE[1]	ADM0_NAME[1]	Irr-rank[2]	LGRIP30-Irrigated[3]	LGRIP30-Rainfed[3]	LGRIP30-Total[3]
#	#	#	Name	#	Ha	Ha	Ha
166	9	21	Bahrain	166	4,099	1,990	6,089
167	5	142	Lesotho	167	3,831	695,649	699,480
168	3	158	Martinique	168	2,089	24,648	26,737
169	3	11	Antigua and Barbuda	169	2,027	5,588	7,615
170	3	208	Saint Kitts and Nevis	170	1,502	5,701	7,203
171	5	49	Central African Republic	171	1,345	744,289	745,633
172	6	213	San Marino	172	1,273	3,962	5,235
173	3	258	United States Virgin Islands	173	1,269	3,832	5,102
174	5	206	RÃ©union	174	760	9,760	10,521
175	4	246	Trinidad and Tobago	175	618	6,299	6,917
176	3	209	Saint Lucia	176	492	2,623	3,114
177	4	86	French Guiana	177	491	3,005	3,496
178	5	144	Liberia	178	445	4,853	5,298
179	3	20	Bahamas	179	418	10,233	10,651
180	12	262	Vanuatu	180	401	39,442	39,844
181	3	71	Dominica	181	389	9,585	9,974
182	3	39	British Virgin Islands	182	376	1,446	1,821
183	6	7	Andorra	183	328	468	797
184	3	211	Saint Vincent and the Grenad	184	297	3,373	3,670
185	3	99	Grenada	185	185	2,784	2,970
186	10	154	Maldives	186	146	379	525
187	5	47	Cape Verde	187	143	1,343	1,485
188	5	214	Sao Tome and Principe	188	113	732	845
189	6	146	Liechtenstein	189	104	4,266	4,370
190	3	168	Montserrat	190	39	193	232
191	5	89	Gabon	191	16	1,384	1,400
192	6	166	Monaco	192	11	618	629
193	5	58	Comoros	193	11	123	134
194	4	81	Falkland Islands (Malvinas)	194	4	1,633	1,637
195	6	114	Iceland	195	0	235,840	235,840
196	12	245	Tonga	196	0	28,582	28,582
197	12	212	Samoa	197	0	16,249	16,249
198	12	87	French Polynesia	198	0	4,499	4,499
199	5	207	Saint Helena	199	0	3,996	3,996
200	12	60	Cook Islands	200	0	2,001	2,001
201	12	266	Wallis and Futuna	201	0	1,487	1,487
202	5	268	Western Sahara	202	0	1,470	1,470
203	3	9	Anguilla	203	0	680	680
204	12	5	American Samoa	204	0	374	374
205	3	176	Netherlands Antilles	205	0	259	259
206	12	185	Northern Mariana Islands	206	0	159	159
207	5	76	Equatorial Guinea	207	0	152	152
208	4	14	Aruba	208	0	98	98
209	12	135	Kiribati	209	0	87	87
210	12	163	Micronesia (Federated States	210	0	58	58
211	12	101	Guam	211	0	43	43
212	12	189	Palau	212	0	32	32
213	6	110	Holy See	213	0	21	21
214	5	70	Djibouti	214	0	14	14
215	5	220	Seychelles	215	0	0	0
216	3	A	Saint Martin	216	0	703	703
217	3	B	Saint Eustatius	217	0	368	368
218	3	C	Bonaire	218	0	269	269
219	3	D	Curacao	219	0	244	244
220	3	E	Sint Maarten	220	0	123	123
221	3	F	Saint Barthelemy	221	0	63	63
			Total(ha)		**715,743,899**	**1,087,185,109**	**1,802,929,008**
					TGNIA[6]	**TGNRA[6]**	**TGNCA[6]**
			Total(Mha)		**716**	**1087**	**1803**

Note:

1. FAO country code and Gaul code have diffent numbers, all stats are matched using country names only.

2. Rank assigned based on LGRIP30 irrigated areas of the countries

3. Country wise irrigated and rainfed cropland areas were calculated from LGRIP30 (nominal 2015) product using FAO GAUL boundary(FAO, 2015)

4. For the two countries (Argentina, and Brazil), croplands were estimated using following equations

LGRIP30-Irr= 1.7979*FAO-Irr+631717 (equation excludes pastures from LGRIP30 irrigated area)

LGRIP30-RF= 0.8225*FAO-Rf+338084 (equation excludes pastures from LRIP30 rainfed areas)

	LGRIP-irrigated	**LGRIP-rainfed**	**LGRIP-Total1**
	Ha	**Ha**	**Ha**
Argentina	19893291	45203957	65097248
Brazil	33292139	127949544	161241684

5. For the two countries (Australia and Kazakhstan), croplands were estimated using following equations

LGRIP30-RF= 0.8225*FAO-Rf+338084 (equation excludes pastures from LRIP30 rainfed areas)

	LGRIP-irrigated	**LGRIP-rainfed**	**LGRIP-Total1**
	Ha	**Ha**	**Ha**
Australia	4557947	63634440	68192387
Kazakhstan	2928290	59328440	62256731

6. Acronyms and abbreviations

LGRIP30: Landsat derived Global rainfed and Iriigtated croplan product @30m

TGNIA: Total Global Net Irrigated cropland Area

TGNRA: Total Global Net Rainfed cropland Area

TGNCA: Total Global Net cropland Area

C2. Areas by continent and countries in each continent

Of the total global net irrigated areas (TNGIAs) of 715 Mha (Table 7, Figure 37), continentwide irrigated areas were (Table 8 to 13): Asia (56.1%), Europe (24.2%), North America (8.9%), Africa (6.7%), South America (3.4%), and Australia and Oceania (0.75%)**.**

Of the total global net rainfed areas (TNGRAs) of 1090 Mha, continentwide irrigated areas were (Table 8 to 13): Europe (26.4%), Africa (20.4%), Asia (19.7%), North America (19.3%), South America (10.7%), and Australia and Oceania (3.5%).

There are several useful maps (Figure 50 through 53) that show LGRIP30 derived irrigated and rainfed areas as percentage of the total global net irrigated areas (TGNIA) or total global net rainfed areas (TNGRA).

- Figure 50 shows the LGRIP30-derived total net irrigated areas (TNIAs) of each country as percentage of the total Net geographic areas (TNGAs) of each country.
- Figure 51 shows the LGRIP30-derived total net irrigated areas (TNIAs) of each country as percentage of the total global net irrigated areas (TGNIAs).
- Figure 52 shows the LGRIP30-derived total net rainfed areas (TNRAs) of each country as percentage of the total net geo-graphic areas (TNGAs) of each country.
- Figure 53 shows the LGRIP30-derived total net rainfed areas (TNRAs) of each country as percentage of the total global net rainfed areas (TGNRAs).

C3. Areas by district or county in selected countries

The LGRIP30 is a 30 m (1 pixel = 0.09 hectares) data. So, it's areas can be computed even at farm level if need be. So, apart from the country level statistics discussed in previous sections, we also computed state level net irrigated areas (NIAs) statistics for USA and compared that with the NIAs statistic obtained from the LANID (Xie et al., 2021, and Xie and Lark, 2021; Table 14 and Figure 51a,b). This provided an R-square value of 0.82. Overall, LGRIP30 provides significantly higher NIAs.

These relationships clearly demonstrate the ability of LGRIP30 to determine rainfed and irrigated areas at county, district, state, country and other administrative units. This implies that operational application of LGRIP30 data for determining rainfed and irrigated areas is a powerful and accurate approach.

Table 8. LGRIP30 irrigated and rainfed areas of Africa. LGRIP30-derived total net irrigated areas (TNIAs) and total net rainfed areas (TNRAs) of countries of Africa.

Africa						
Rank #	Continent Name	GAUL #	Country Name	LGRIP30 irrigated area (Ha)	LGRIP30 rainfed area (Ha)	LGRIP30 Total area (Ha)
1	Africa	133	Kenya	5,224,532	3,555,088	8,779,620
2	Africa	257	United Republic of Tanzania	5,222,179	14,829,772	20,051,951
3	Africa	169	Morocco	4,765,248	3,700,828	8,466,076
4	Africa	4	Algeria	4,703,703	3,469,561	8,173,264
5	Africa	40765	Egypt	4,249,590	452,604	4,702,194
6	Africa	227	South Africa	4,080,443	13,234,658	17,315,100
7	Africa	79	Ethiopia	4,045,941	19,538,956	23,584,897
8	Africa	253	Uganda	2,606,349	3,977,090	6,583,440
9	Africa	248	Tunisia	2,437,781	2,363,821	4,801,602
10	Africa	6	Sudan	2,108,841	18,463,778	20,572,619
11	Africa	182	Nigeria	915,851	30,752,427	31,668,278
12	Africa	68	Democratic Republic of the Congo	897,222	11,613,284	12,510,506
13	Africa	145	Libya	893,336	920,194	1,813,530
14	Africa	152	Malawi	816,280	3,796,667	4,612,947
15	Africa	270	Zambia	730,337	6,583,386	7,313,723
16	Africa	66	CÃ´te d'Ivoire	626,745	5,484,524	6,111,269
17	Africa	205	Rwanda	499,148	831,933	1,331,081
18	Africa	271	Zimbabwe	449,584	9,748,437	10,198,021
19	Africa	94	Ghana	410,828	2,858,865	3,269,694
20	Africa	155	Mali	353,258	10,011,477	10,364,735
21	Africa	170	Mozambique	299,985	6,004,906	6,304,891
22	Africa	150	Madagascar	277,448	3,068,635	3,346,083
23	Africa	243	Togo	241,842	1,657,732	1,899,573
24	Africa	45	Cameroon	204,248	4,407,678	4,611,927
25	Africa	226	Somalia	178,552	1,456,278	1,634,831
26	Africa	235	Swaziland	121,272	460,840	582,111
27	Africa	43	Burundi	103,861	644,583	748,444
28	Africa	181	Niger	73,207	7,752,110	7,825,317
29	Africa	29	Benin	66,513	3,207,925	3,274,438
30	Africa	8	Angola	47,936	4,691,297	4,739,234
31	Africa	217	Senegal	46,543	3,939,082	3,985,624
32	Africa	106	Guinea	39,622	648,708	688,330
33	Africa	59	Congo	34,647	208,740	243,388
34	Africa	105	Guinea-Bissau	29,783	164,991	194,773
35	Africa	35	Botswana	24,678	1,594,821	1,619,499
36	Africa	42	Burkina Faso	20,601	5,674,965	5,695,565
37	Africa	50	Chad	19,390	5,324,980	5,344,370
38	Africa	160	Mauritius	15,210	51,895	67,104
39	Africa	77	Eritrea	13,773	609,684	623,457
40	Africa	74	South Sudan	11,819	1,036,348	1,048,166
41	Africa	221	Sierra Leone	11,219	91,125	102,344
42	Africa	90	Gambia	5,969	318,670	324,639
43	Africa	172	Namibia	5,238	884,344	889,582
44	Africa	159	Mauritania	4,491	87,733	92,224
45	Africa	142	Lesotho	3,831	695,649	699,480
46	Africa	49	Central African Republic	1,345	744,289	745,633
47	Africa	206	RÃ©union	760	9,760	10,521
48	Africa	144	Liberia	445	4,853	5,298
49	Africa	47	Cape Verde	143	1,343	1,485
50	Africa	214	Sao Tome and Principe	113	732	845
51	Africa	89	Gabon	16	1,384	1,400
52	Africa	58	Comoros	11	123	134
53	Africa	207	Saint Helena	0	3,996	3,996
54	Africa	268	Western Sahara	0	1,470	1,470
55	Africa	76	Equatorial Guinea	0	152	152
56	Africa	70	Djibouti	0	14	14
57	Africa	220	Seychelles	0	0	0
			TOTAL	**47,941,706**	**221,639,185**	**269,580,891**

Table 9. LGRIP30 irrigated and rainfed areas of Asia. LGRIP30-derived total net irrigated areas (TNIAs) and total net rainfed areas (TNRAs) of countries of Asia.

Asia						
Rank #	Continent Name	GAUL #	Country Name	LGRIP30 irrigated area (Ha)	LGRIP30 rainfed area (Ha)	LGRIP30 Total area (Ha)
1	Asia	115	India	132,542,113	46,767,434	179,309,548
2	Asia	147295	China	131,778,217	32,118,339	163,896,556
3	Asia	188	Pakistan	19,127,578	7,492,682	26,620,261
4	Asia	240	Thailand	13,516,805	12,175,398	25,692,203
5	Asia	118	Iraq	11,537,570	350,703	11,888,273
6	Asia	116	Indonesia	10,015,594	26,434,913	36,450,507
7	Asia	23	Bangladesh	9,359,234	481,359	9,840,593
8	Asia	171	Myanmar	8,939,549	4,979,478	13,919,026
9	Asia	117	Iran (Islamic Republic of)	8,042,545	24,326,809	32,369,353
10	Asia	264	Viet Nam	7,725,984	2,812,147	10,538,131
11	Asia	238	Syrian Arab Republic	6,533,081	26,030	6,559,111
12	Asia	261	Uzbekistan	5,558,757	2,208,708	7,767,466
13	Asia	132	Kazakhstan[1]	2,928,290	22,956,732	25,885,023
14	Asia	44	Cambodia	4,183,465	3,416,139	7,599,604
15	Asia	196	Philippines	3,004,488	3,205,429	6,209,917
16	Asia	215	Saudi Arabia	2,571,745	107,236	2,678,981
17	Asia	250	Turkmenistan	2,543,481	1,177,884	3,721,366
18	Asia	67	Dem People's Rep of Korea/North K	2,474,461	789,101	3,263,562
19	Asia	126	Japan	2,333,268	1,196,752	3,530,020
20	Asia	269	Yemen	1,750,354	412,147	2,162,501
21	Asia	175	Nepal	1,718,874	224,783	1,943,657
22	Asia	153	Malaysia	1,656,305	8,683,545	10,339,850
23	Asia	1	Afghanistan	1,566,341	6,572,877	8,139,219
24	Asia	202	Republic of Korea/South Korea	1,162,164	263,476	1,425,640
25	Asia	139	Lao People's Democratic Republic	1,087,528	1,246,341	2,333,869
26	Asia	231	Sri Lanka	1,085,920	351,863	1,437,783
27	Asia	239	Tajikistan	744,781	365,886	1,110,668
28	Asia	138	Kyrgyzstan	675,227	1,445,769	2,120,997
29	Asia	121	Israel	624,292	3,238	627,530
30	Asia	130	Jordan	456,531	11,553	468,083
31	Asia	147296	Taiwan	421,802	109,157	530,959
32	Asia	141	Lebanon	218,842	23,912	242,754
33	Asia	255	United Arab Emirates	215,571	7,154	222,725
34	Asia	187	Oman	145,334	2,395	147,729
35	Asia	242	Timor-Leste	69,189	51,002	120,191
36	Asia	137	Kuwait	36,967	1,152	38,119
37	Asia	267	West Bank	29,382	212	29,594
38	Asia	91	Gaza Strip	28,905	423	29,328
39	Asia	201	Qatar	20,710	1,219	21,928
40	Asia	31	Bhutan	19,035	17,064	36,099
41	Asia	167	Mongolia	12,010	882,577	894,587
42	Asia	40	Brunei Darussalam	8,062	42,005	50,067
43	Asia	33364	Hong Kong	5,679	4,454	10,133
44	Asia	21	Bahrain	4,099	1,990	6,089
45	Asia	262	Vanuatu	401	39,442	39,844
46	Asia	154	Maldives	146	379	525
			TOTAL	**398,480,677**	**213,789,291**	**612,269,968**

Note: 1. Kazakstan total net cropland and pasture areas were 62,256,731 hactares in LGRIP30 product. The total net irrigated areas of 2,928,290 hactares was actual, derived from LGRIP30 product. The net rainfed areas of 22,956,732 hactares was calculated using the equation.

Table 10. LGRIP30 irrigated and rainfed areas of Australia and Oceania. LGRIP30-derived total net irrigated areas (TNIAs) and total net rainfed areas (TNRAs) of countries of Australia and Oceania.

Australia & Oceania						
Rank #	**Continent Name**	**GAUL #**	**Country name**	**LGRIP30 irrigated area (Ha)**	**LGRIP30 rainfed area (Ha)**	**LGRIP30 Total area (Ha)**
1	Australia & Oceania	17	Australia[1]	4,557,947	30,547,846	35,105,792
2	Australia & Oceania	179	New Zealand[2]	821,896	7,298,127	8,120,023
3	Australia & Oceania	192	Papua New Guinea	22,615	295,168	317,782
4	Australia & Oceania	83	Fiji	14,111	156,300	170,411
5	Australia & Oceania	178	New Caledonia	11,759	24,094	35,854
6	Australia & Oceania	225	Solomon Islands	4,245	315,279	319,524
7	Australia & Oceania	245	Tonga	0	28,582	28,582
8	Australia & Oceania	212	Samoa	0	16,249	16,249
9	Australia & Oceania	87	French Polynesia	0	4,499	4,499
10	Australia & Oceania	60	Cook Islands	0	2,001	2,001
11	Australia & Oceania	266	Wallis and Futuna	0	1,487	1,487
12	Australia & Oceania	5	American Samoa	0	374	374
13	Australia & Oceania	185	Northern Mariana Islands	0	159	159
14	Australia & Oceania	135	Kiribati	0	87	87
15	Australia & Oceania	163	Micronesia (Federated States of)	0	58	58
16	Australia & Oceania	101	Guam	0	43	43
17	Australia & Oceania	189	Palau	0	32	32
			TOTAL	**5,432,573**	**38,690,385**	**44,122,958**

Note:

1. Australia total net cropland and pasture areas were 68,192,387 hactares in LGRIP30 product.

The total net irrigated areas of 4,557,947 hactares was actual derived from LGRIP30 product.

The net rainfed areas of 30,547,845 hactares was calculated the using equation.

2. In Newzealand, the total net rainfed areas of 7,298,127 hactares includes significant pastures. But was not separated. Where as the irrigated areas 821,896 hectares was actual and derived from LGRIP30 product.

Table 11. LGRIP30 irrigated and rainfed areas of South America. LGRIP30-derived total net irrigated areas (TNIAs) and total net rainfed areas (TNRAs) of countries of South America.

South America						
Rank #	**Continent Name**	**GAUL #**	**Country name**	**LGRIP30 irrigated area (Ha)**	**LGRIP30 rainfed area (Ha)**	**LGRIP30 Total area (Ha)**
1	South America	37	Brazil[1]	13,135,572	46,424,651	59,560,223
2	South America	12	Argentina[2]	4,869,367	29,397,914	34,267,281
3	South America	194	Paraguay	1,940,790	7,037,188	8,977,978
4	South America	51	Chile	1,274,174	4,700,924	5,975,098
5	South America	260	Uruguay	1,441,529	10,557,482	11,999,011
6	South America	33	Bolivia	609,476	2,898,338	3,507,814
7	South America	263	Venezuela	303,055	6,881,570	7,184,625
8	South America	195	Peru	256,558	1,513,123	1,769,681
9	South America	73	Ecuador	200,321	2,027,725	2,228,046
10	South America	57	Colombia	134,755	5,536,017	5,670,771
11	South America	107	Guyana	70,476	68,780	139,255
12	South America	233	Suriname	9,509	22,811	32,320
13	South America	246	Trinidad and Tobago	618	6,299	6,917
14	South America	86	French Guiana	491	3,005	3,496
15	South America	81	Falkland Islands (Malvinas)	4	1,633	1,637
16	South America	C	Bonaire	0	269	269
17	South America	D	Curacao	0	244	244
18	South America	14	Aruba	0	98	98
			TOTAL	**24,246,695**	**117,078,071**	**141,324,765**

Note:

1. Brazil total net cropland and pasture areas were 161, 241,684 hactares in LGRIP30 product.
However since Croplands were not separated from pasture in the LGRIP30 product,
the total net LGRIP30 irrigated areas (13,135,572 hactares) and LGRIP30 rainfed areas (46,424,651 hactares) were derived using equations.

2. Argentina total cropland and pasture areas were 65,097,248 hactares in LGRIP30 product.
However since Croplands were not separated from pasture in the LGRIP30 product,
the total net LGRIP30 irrigated areas (4,869,367 hactares) and LGRIP30 rainfed areas (29,397,914 hactares) were derived using equations.

Table 12. LGRIP30 irrigated and rainfed areas of Europe. LGRIP30-derived total net irrigated areas (TNIAs) and total net rainfed areas (TNRAs) of countries of Europe

Europe						
Rank #	Continent Name	GAUL #	Country name	LGRIP30 irrigated area (Ha)	LGRIP30 rainfed area (Ha)	LGRIP30 Total area (Ha)
1		204	Russian Federation	33,276,856	121,651,518	154,928,374
2		254	Ukraine	30,408,208	12,621,600	43,029,808
3		249	Turkey	19,547,992	8,872,795	28,420,787
4		229	Spain	15,355,735	12,856,514	28,212,249
5		85	France	13,519,701	18,132,629	31,652,330
6		198	Poland	10,649,360	8,344,592	18,993,952
7		93	Germany	8,237,645	11,544,787	19,782,432
8		203	Romania	5,649,424	7,872,839	13,522,263
9		122	Italy	5,117,951	11,865,176	16,983,127
10		26	Belarus	4,229,552	6,251,613	10,481,165
11		19	Azerbaijan	4,191,284	537,190	4,728,475
12		41	Bulgaria	2,277,087	3,534,067	5,811,154
13		256	U.K. of Great Britain and Northern Irela	1,989,605	13,712,814	15,702,419
14		97	Greece	1,986,543	2,292,069	4,278,613
15		65	Czech Republic	1,891,452	2,799,278	4,690,730
16		177	Netherlands	1,825,597	440,542	2,266,139
17		113	Hungary	1,820,245	5,442,207	7,262,452
18		165	Moldova, Republic of	1,516,954	1,345,832	2,862,786
19		69	Denmark	1,491,313	1,848,808	3,340,121
20		92	Georgia	1,287,736	357,602	1,645,338
21		2648	Serbia	1,279,949	3,775,592	5,055,541
22		147	Lithuania	1,269,120	2,686,098	3,955,218
23		223	Slovakia	1,219,444	1,227,596	2,447,040
24		18	Austria	913,384	1,769,040	2,682,424
25		199	Portugal	881,055	3,343,981	4,225,036
26		236	Sweden	871,700	2,542,384	3,414,083
27		84	Finland	498,882	1,352,878	1,851,761
28		140	Latvia	450,665	2,169,877	2,620,542
29		64	Cyprus	449,492	52,005	501,497
30		62	Croatia	446,805	1,894,516	2,341,321
31		241	The former Yugoslav Republic of Maced	348,699	487,029	835,728
32		13	Armenia	330,652	255,125	585,777
33		78	Estonia	325,914	1,056,137	1,382,050
34		3	Albania	209,180	460,791	669,971
35		27	Belgium	206,802	1,476,243	1,683,045
36		34	Bosnia and Herzegovina	121,634	1,628,530	1,750,164
37		119	Ireland	102,213	5,094,203	5,196,415
38		186	Norway	86,078	774,458	860,536
39		237	Switzerland	77,078	1,235,910	1,312,988
40		2647	Montenegro	26,809	181,392	208,201
41		224	Slovenia	25,764	633,483	659,246
42		156	Malta	13,355	11,268	24,623
43		148	Luxembourg	5,201	134,105	139,306
44		213	San Marino	1,273	3,962	5,235
45		7	Andorra	328	468	797
46		146	Liechtenstein	104	4,266	4,370
47		166	Monaco	11	618	629
48		114	Iceland	0	235,840	235,840
49		110	Holy See	0	21	21
			TOTAL	**176,431,831**	**286,812,287**	**463,244,118**

Table 13. LGRIP30 irrigated and rainfed areas of North America. LGRIP30-derived total net irrigated areas (TNIAs) and total net rainfed areas (TNRAs) of countries of North America.

North America						
Rank #	**Continent Name**	**GAUL #**	**Country name**	**LGRIP30 irrigated area (Ha)**	**LGRIP30 rainfed area (Ha)**	**LGRIP30 Total area (Ha)**
1	North America	259	USA	42,323,364	125,881,360	168,204,724
2	North America	162	Mexico	16,324,519	17,865,405	34,189,923
3	North America	46	Canada	1,038,976	42,594,426	43,633,402
4	North America	103	Guatemala	603,023	3,838,157	4,441,180
5	North America	63	Cuba	600,717	3,607,739	4,208,456
6	North America	180	Nicaragua	492,821	4,417,631	4,910,453
7	North America	61	Costa Rica	440,799	1,648,444	2,089,242
8	North America	111	Honduras	425,723	2,813,125	3,238,848
9	North America	191	Panama	340,175	1,758,764	2,098,939
10	North America	72	Dominican Republic	305,205	1,682,026	1,987,231
11	North America	108	Haiti	129,332	1,089,452	1,218,784
12	North America	28	Belize	44,187	319,271	363,458
13	North America	75	El Salvador	38,803	991,786	1,030,589
14	North America	123	Jamaica	35,368	235,535	270,903
15	North America	200	Puerto Rico	34,919	302,064	336,983
16	North America	100	Guadeloupe	16,180	47,777	63,957
17	North America	24	Barbados	7,222	10,728	17,950
18	North America	158	Martinique	2,089	24,648	26,737
19	North America	11	Antigua and Barbuda	2,027	5,588	7,615
20	North America	208	Saint Kitts and Nevis	1,502	5,701	7,203
21	North America	258	United States Virgin Islands	1,269	3,832	5,102
22	North America	209	Saint Lucia	492	2,623	3,114
23	North America	20	Bahamas	418	10,233	10,651
24	North America	71	Dominica	389	9,585	9,974
25	North America	39	British Virgin Islands	376	1,446	1,821
26	North America	211	Saint Vincent and the Grenadin	297	3,373	3,670
27	North America	99	Grenada	185	2,784	2,970
28	North America	168	Montserrat	39	193	232
29	North America	A	Saint Martin	0	703	703
30	North America	9	Anguilla	0	680	680
31	North America	B	Saint Eustatius	0	368	368
32	North America	176	Netherlands Antilles	0	259	259
33	North America	E	Sint Maarten	0	123	123
34	North America	F	Saint Barthelemy	0	63	63
			TOTAL	**63,210,417**	**209,175,891**	**272,386,308**

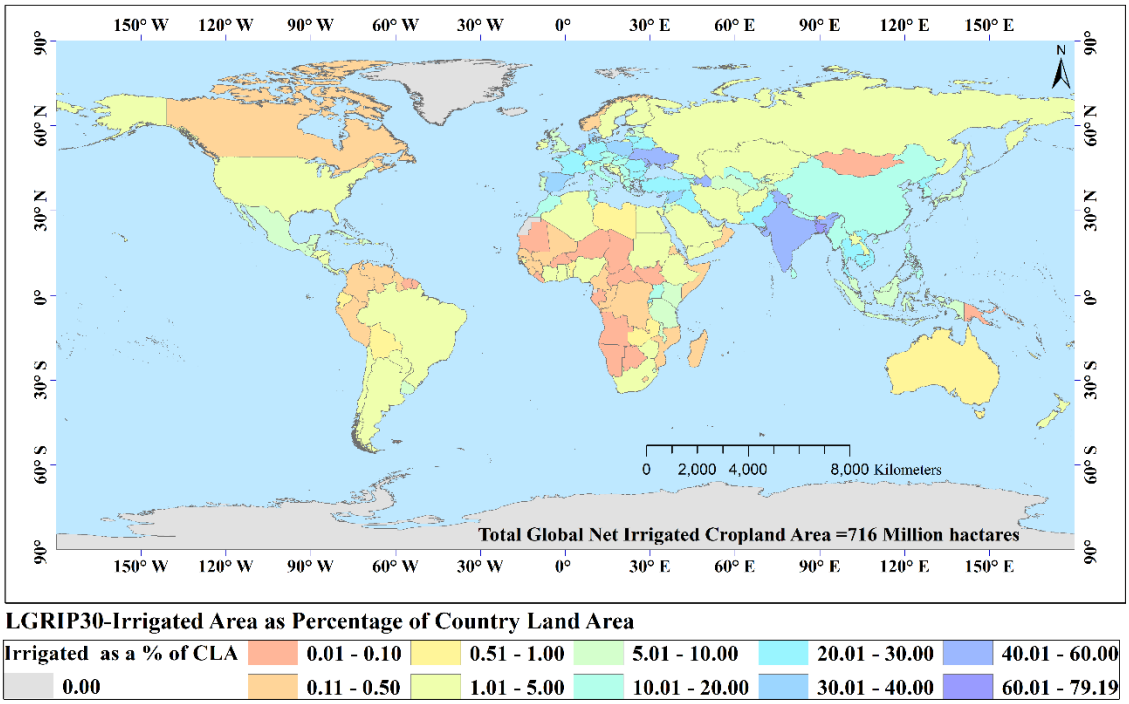

Figure 50. LGRIP30 irrigated areas as percentage of TNGAs of the countries. The LGRIP30-derived net irrigated areas (NIAs) of each country as percentage of the total Net geographic areas (TNGAs) of the country.

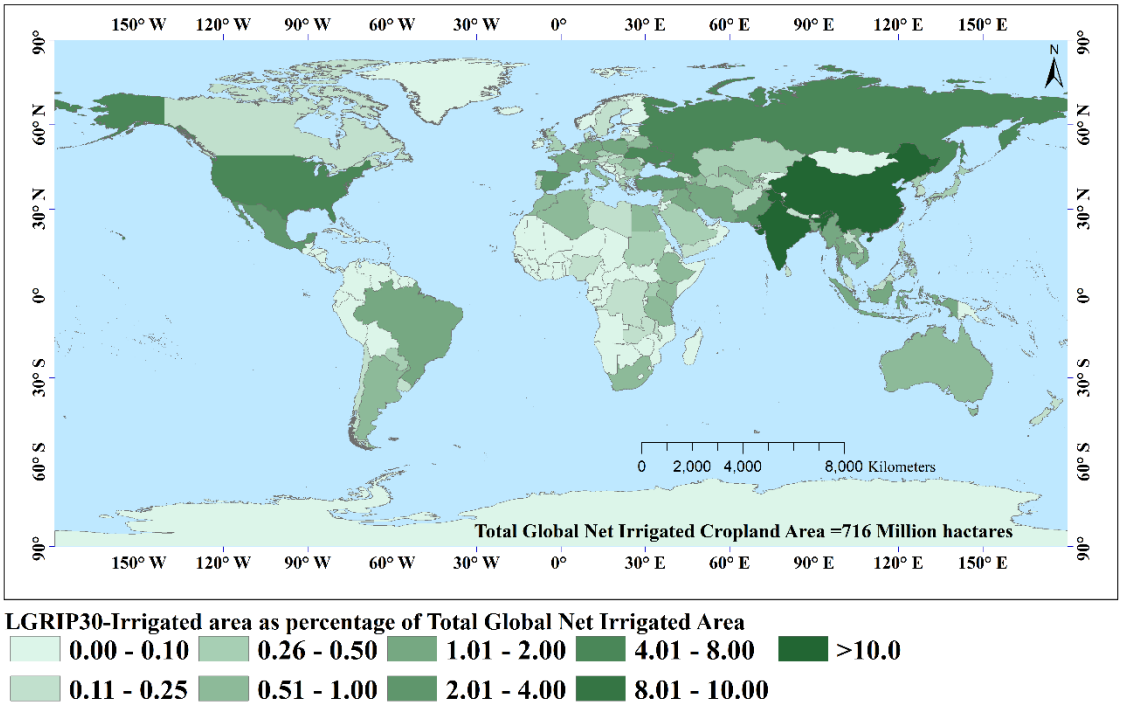

Figure 51. LGRIP30 irrigated areas as percentage of TGNIAs. The LGRIP30-derived net irrigated areas (NIAs) of each country as percentage of the total global net irrigated areas (TGNIAs).

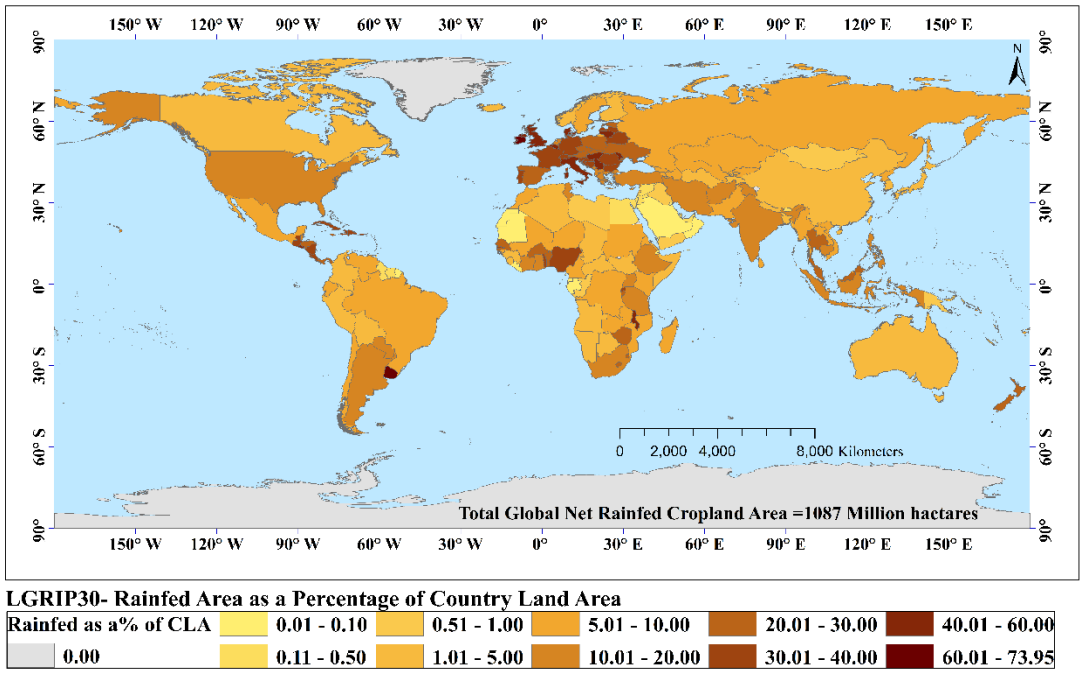

Figure 52. LGRIP30 rainfed areas as percentage of TNGAs of the countries. The LGRIP30-derived net rainfed areas (NRAs) of each country as percentage of the total net geo-graphic areas (TNGAs) of the country.

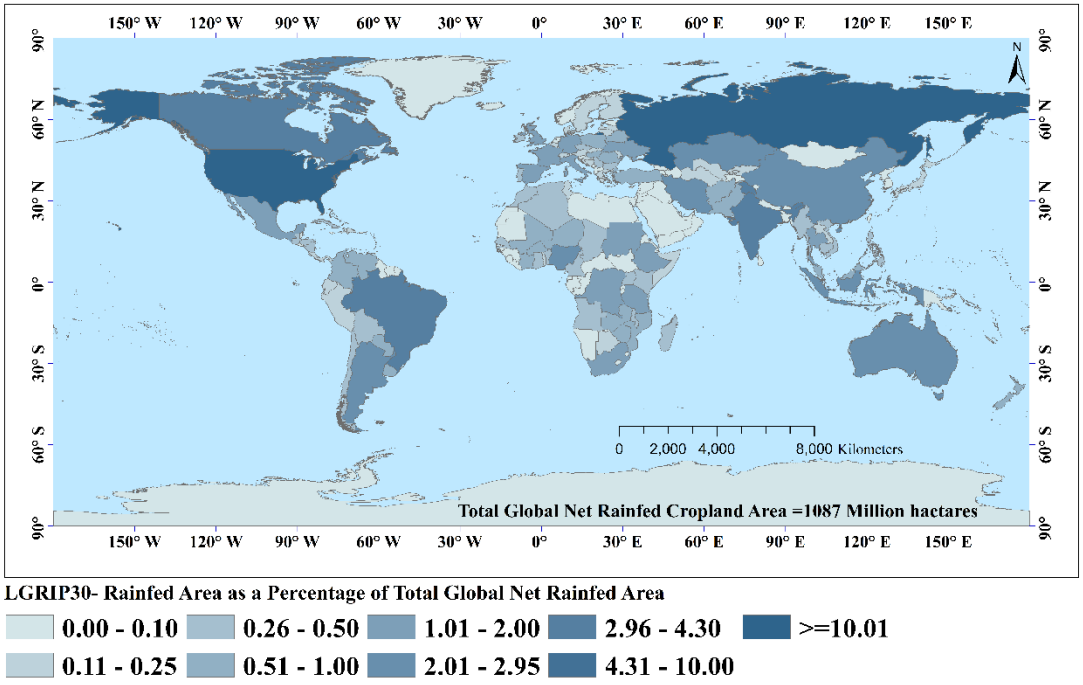

Figure 53. LGRIP30 rainfed areas as percentage of the TGNRAs of the countries. he LGRIP30-derived net rainfed areas (NRAs) of each country as percentage of the total global net rainfed areas (TGNRAs).

Table 14. LGRIP30 area statistics for the states of USA. State by state LGRIP30-derived net irrigated areas (NIAs) for the United States of America (USA).

Sno	State Name	Irrigated(Mha)	Rainfed(Mha)	Total (Mha)
1	Alabama	0.137	1.047	1.183
2	Alaska	0.000	0.010	0.010
3	Arizona	0.315	0.415	0.730
4	Arkansas	2.853	0.337	3.190
5	California	3.435	1.345	4.781
6	Colorado	0.994	3.093	4.087
7	Connecticut	0.001	0.058	0.058
8	Delaware	0.066	0.164	0.230
9	District of Columbia	0.000	0.000	0.000
10	Florida	0.847	1.326	2.173
11	Georgia	1.159	1.013	2.172
12	Hawaii	0.015	0.259	0.275
13	Idaho	1.712	0.995	2.707
14	Illinois	2.104	7.822	9.926
15	Indiana	0.987	4.436	5.424
16	Iowa	1.058	10.430	11.488
17	Kansas	3.076	8.172	11.248
18	Kentucky	0.155	1.684	1.839
19	Louisiana	1.624	0.408	2.032
20	Maine	0.002	0.193	0.196
21	Maryland	0.070	0.736	0.806
22	Massachusetts	0.002	0.074	0.076
23	Michigan	0.264	3.919	4.182
24	Minnesota	0.263	9.576	9.839
25	Mississippi	1.355	0.927	2.282
26	Missouri	1.513	3.354	4.867
27	Montana	1.239	6.249	7.488
28	Nebraska	5.058	3.764	8.822
29	Nevada	0.169	0.144	0.313
30	New Hampshire	0.000	0.044	0.044
31	New Jersey	0.028	0.236	0.264
32	New Mexico	0.265	0.521	0.786
33	New York	0.021	1.979	2.001
34	North Carolina	0.289	1.972	2.260
35	North Dakota	0.656	11.163	11.819
36	Ohio	0.578	4.234	4.812
37	Oklahoma	1.139	2.838	3.977
38	Oregon	1.170	0.774	1.945
39	Pennsylvania	0.027	2.303	2.330
40	Rhode Island	0.000	0.008	0.008
41	South Carolina	0.071	0.988	1.059
42	South Dakota	0.314	7.324	7.638
43	Tennessee	0.527	1.443	1.970
44	Texas	4.427	8.691	13.118
45	Utah	0.428	0.340	0.769
46	Vermont	0.003	0.161	0.164
47	Virginia	0.058	0.884	0.942
48	Washington	1.226	2.584	3.810
49	West Virginia	0.002	0.094	0.096
50	Wisconsin	0.114	4.624	4.738
51	Wyoming	0.510	0.682	1.192
	Grand Total	**42.327**	**125.840**	**168.167**

VIII. Constraints and Limitations and way forward

GFSADLGRIP30WORLD product has demonstrated the power of using time-series Landsat data to map global rainfed and irrigated areas. The LGRIP30 product (Figure 37) mapped the entire world's net irrigated areas and net rainfed areas. The product was produced with an overall accuracy of 86.5%. The irrigated class has a producer's accuracy of 86.7% (errors of omissions of = 13.3%) and user's accuracy of 84.3% (errors of commissions = 15.7%). The rainfed class has a producer's accuracy of 86.3% (errors of omissions of = 13.7%) and user's accuracy of 88.4% (errors of commissions = 11.6%). The study demonstrated that rainfed and irrigated areas can be accurately computed at the global, National, state, and other administrative units like the counties or districts.

The main limitation of the work will be in obtaining the reference training and validation data year after year. That will take coordination, trained personnel, and resources. Globally, this can be a significant constraint when taking National cooperation into consideration. However, such constraints can be overcome by partnering with international organizations such as the Food and Agricultural Organization of the United Nations (UN FAO) or CGIAR (Consultative Group on International Agricultural Research). Further, data can be relayed using Mobile apps from anywhere in the world. This is feasible with a good network of partners who can send sample reference data and need partnering with National agricultural extension institutes. An alternative approach for the reference data will be to acquire sub-meter to 5-meter very high spatial resolution imagery (VHRI) remote sensing data from sources such as Doves for Skysat from Planetscope LLc. and other similar sources. For global reach this is more feasible proposition as it involves less cooperation or coordination from numerous partners from around the world that can even be complex for International Institutions. However, VHRI reference data, even when sampled from 1000s of locations for the world can be costly.

LGRIP30 maps irrigated and rainfed areas at 0.09 hectares (1 pixel = 30m) compared to other existing products like GFSAD1000 that map irrigated and rainfed at 100 hectares (1 pixel = 1000m). So, LGRIP30 provides 1,111 times greater resolution compared to GFSAD1000 or other 1000m products.

Once the product is released it will be downloaded by various users worldwide and they will conduct their own evaluations and\or provide comments. As the reviewer of this manuscript suggested, in his visit to South Africa, he will further evaluate the product by field observation and through local partners. Where we get field data or maps from the ground for individual countries or regions, we will further evaluate and update the maps. The goal is to release an update 2020 LGRIP30 (LGRIP30-2020) in about 2-3 years. This will involve refining local or regional components of LGRIP30 based on maps, ground reference data, and comments received from users.

The LGRIP30-2020 product will also make use of newer generation of data such as a fusion of Landsat-8, 9, and Sentinel-2A&2B (S2) surface reflectance (SR) products on GEE, and NASA's Harmonized Landsat Sentinel-2 (HLS) Landsat product (HLSL30) for 2013-present and HLS Sentinel-2 product (HLSS30) for 2015-present, that together have sub-5-days global coverage (Masek, et al., 2021, 2022) at nominal 30m resolution.

IX. Publications

a. Peer-reviewed publications relevant to this study

Thenkabail, P.S., Teluguntla, P.G., Xiong, J., Oliphant, A., Congalton, R.G., Ozdogan, M., Gumma, M.K., Tilton, J.C., Giri, C., Milesi, C., Phalke, A., Massey, R., Yadav, K., Sankey, T., Zhong, Y., Aneece, I., and Foley, D., 2021, Global cropland-extent product at 30-m resolution (GCEP30) derived from Landsat satellite time-series data for the year 2015 using multiple machine-learning algorithms on Google Earth Engine cloud: U.S. Geological Survey Professional Paper 1868, 63 p., https://doi.org/10.3133/pp1868.

Teluguntla, P., Thenkabail, P.S., Oliphant, A., Xiong, J., Gumma, M.K., Congalton, R.G., Yadav, K. and Huete, A., 2018. A 30-m landsat-derived cropland extent product of Australia and China using random forest machine learning algorithm on Google Earth Engine cloud computing platform. *ISPRS Journal of Photogrammetry and Remote Sensing*, *144*, pp.325-340.

Gumma, M.K., Thenkabail, P.S., Panjala, P., Teluguntla, P., Yamano, T., Mohammed, I. 2022. Multiple Agricultural Cropland Products of South Asia Developed using Landsat-8 30 m and MODIS 250 m Data using Machine Learning on the Google Earth Engine Cloud and Spectral Matching Techniques (SMTs) in Support of Food and Water Security. GIScience and Remote Sensing. In press. IP-135578

Teluguntla, P., Thenkabail, P.S., Xiong, J., Gumma, M.K., Congalton, R.G., Oliphant, A., Poehnelt, J., Yadav, K., Rao, M., and Massey, R. 2017. Spectral matching techniques (SMTs) and automated cropland classification algorithms (ACCAs) for mapping croplands of Australia using MODIS 250-m time-series (2000–2015) data, International Journal of Digital Earth. DOI:10.1080/17538947.2016.1267269.IP-074181, http://dx.doi.org/10.1080/17538947.2016.1267269.

Teluguntla, P., Thenkabail, P., Xiong, J., Gumma, M.K., Giri, C., Milesi, C., Ozdogan, M., Congalton, R., Yadav, K., 2015. CHAPTER 6 - Global Food Security Support Analysis Data at Nominal 1 km (GFSAD1km) Derived from Remote Sensing in Support of Food Security in the Twenty-First Century: Current Achievements and Future Possibilities, in: Thenkabail, P.S. (Ed.), Remote Sensing Handbook (Volume II): Land Resources Monitoring, Modeling, and Mapping with Remote Sensing. CRC Press, Boca Raton, London, New York., pp. 131–160. Link.

Gumma, M. K., Thenkabail, P. S., Teluguntla, P. G., Oliphant, A., Xiong, J., Giri, C., ... & Whitbread, A. M. (2019). Agricultural cropland extent and areas of South Asia derived using Landsat satellite 30-m time-series big-data using random forest machine learning algorithms on the Google Earth Engine cloud. GIScience & Remote Sensing, 1-21. https://doi.org/10.1080/15481603.2019.1690780

Oliphant, A. J., Thenkabail, P. S., Teluguntla, P., Xiong, J., Gumma, M. K., Congalton, R. G., & Yadav, K. (2019). Mapping cropland extent of Southeast and Northeast Asia using multi-year time-series Landsat 30-m data using a random forest classifier on the Google Earth Engine Cloud. International Journal of Applied Earth Observation and Geoinformation, 81, 110-124. https://doi.org/10.1016/j.jag.2018.11.014

Xiong, J., Thenkabail, P., Tilton, J., Gumma, M., Teluguntla, P., Oliphant, A., Congalton, R., Yadav, K., & Gorelick, N. (2017a). Nominal 30-m Cropland Extent Map of Continental Africa by Integrating Pixel-Based and Object-Based Algorithms Using Sentinel-2 and Landsat-8 Data on Google Earth Engine. *Remote Sensing, 9*, 1065

Xiong, J., Thenkabail, P.S., Gumma, M.K., Teluguntla, P., Poehnelt, J., Congalton, R.G., Yadav, K., Thau, D. 2017. Automated cropland mapping of continental Africa using Google Earth Engine cloud computing, ISPRS Journal of Photogrammetry and Remote Sensing, Volume 126, April 2017, Pages 225-244, ISSN 0924-2716, https://doi.org/10.1016/j.isprsjprs.2017.01.019.

b. Peer-reviewed publications within GFSAD project

Congalton, R.G., Gu, J., Yadav, K., Thenkabail, P.S., and Ozdogan, M. 2014. Global Land Cover Mapping: A Review and Uncertainty Analysis. Remote Sensing Open Access Journal. Remote Sens. 2014, 6, 12070-12093; http://dx.doi.org/10.3390/rs61212070.

Congalton, R.G, 2015. Assessing Positional and Thematic Accuracies of Maps Generated from Remotely Sensed Data. Chapter 29, In Thenkabail, P.S., (Editor-in-Chief), 2015. "Remote Sensing Handbook" Volume I: Volume I: Data Characterization, Classification, and Accuracies: Advances of Last 50 Years and a Vision for the Future. Taylor and Francis Inc.\CRC Press, Boca Raton, London, New York. Pp. 900+. In Thenkabail, P.S., (Editor-in-Chief), 2015. "Remote Sensing Handbook" Volume I: **): Remotely Sensed Data Characterization, Classification, and Accuracies**. Taylor and Francis Inc.\CRC Press, Boca Raton, London, New York. ISBN 9781482217865 - CAT# K22125. Print ISBN: 978-1-4822-1786-5; eBook ISBN: 978-1-4822-1787-2. Pp. 678.

Gumma, M.K., Thenkabail, P.S.,Teluguntla, P., Rao, M.N., Mohammed, I.A., and Whitbread, A.M. 2016. Mapping rice-fallow cropland areas for short-season grain legumes intensification in South Asia using MODIS 250 m time-series data. International Journal of Digital Earth, http://dx.doi.org/10.1080/17538947.2016.1168489

Massey, R., Sankey, T.T., Congalton, R.G., Yadav, K., Thenkabail, P.S., Ozdogan, M., Sánchez Meador, A.J. 2017. MODIS phenology-derived, multi-year distribution of conterminous U.S. crop types, Remote Sensing of Environment, Volume 198, 1 September 2017, Pages 490-503, ISSN 0034-4257, https://doi.org/10.1016/j.rse.2017.06.033.

Massey, R., Sankey, T.T., Yadav, K., Congalton, R.G. and Tilton, J.C., 2018. Integrating cloud-based workflows in continental-scale cropland extent classification. *Remote Sensing of Environment*, *219*, pp.162-179.

Phalke, A.R., Özdoğan, M., Thenkabail, P.S., Erickson, T., Gorelick, N., Yadav, K. and Congalton, R.G., 2020. Mapping croplands of Europe, middle east, russia, and central asia using landsat, random forest, and google earth engine. *ISPRS Journal of Photogrammetry and Remote Sensing*, *167*, pp.104-122.

Phalke, A.R. and Özdoğan, M., 2018. Large area cropland extent mapping with Landsat data and a generalized classifier. *Remote sensing of environment*, *219*, pp.180-195.

Teluguntla, P., Thenkabail, P.S., Xiong, J., Gumma, M.K., Congalton, R.G., Oliphant, A., Poehnelt, J., Yadav, K., Rao, M., and Massey, R. 2017. Spectral matching techniques (SMTs) and automated cropland classification algorithms (ACCAs) for mapping croplands of Australia using MODIS 250-m time-series (2000–2015) data, International Journal of Digital Earth. DOI:10.1080/17538947.2016.1267269.IP-074181, http://dx.doi.org/10.1080/17538947.2016.1267269.

Teluguntla, P., Thenkabail, P., Xiong, J., Gumma, M.K., Giri, C., Milesi, C., Ozdogan, M., Congalton, R., Yadav, K., 2015. CHAPTER 6 - Global Food Security Support Analysis Data at Nominal 1 km (GFSAD1km) Derived from Remote Sensing in Support of Food Security in the Twenty-First Century: Current Achievements and Future Possibilities, in: Thenkabail, P.S. (Ed.), Remote Sensing Handbook (Volume II): Land Resources Monitoring, Modeling, and Mapping with Remote Sensing. CRC Press, Boca Raton, London, New York., pp. 131–160. Link.

Xiong, J., Thenkabail, P., Tilton, J., Gumma, M., Teluguntla, P., Oliphant, A., Congalton, R., Yadav, K., & Gorelick, N. (2017a). Nominal 30-m Cropland Extent Map of Continental Africa by Integrating Pixel-Based and Object-Based Algorithms Using Sentinel-2 and Landsat-8 Data on Google Earth Engine. *Remote Sensing, 9*, 1065

Xiong, J., Thenkabail, P.S., Gumma, M.K., Teluguntla, P., Poehnelt, J., Congalton, R.G., Yadav, K., Thau, D. 2017. Automated cropland mapping of continental Africa using Google Earth Engine cloud computing, ISPRS Journal of Photogrammetry and Remote Sensing, Volume 126, April 2017, Pages 225-244, ISSN 0924-2716, https://doi.org/10.1016/j.isprsjprs.2017.01.019.

c. Web sites and Data portals:

http://croplands.org (30-m global croplands visualization tool)
http://geography.wr.usgs.gov/science/croplands/index.html (GFSAD30 web portal and dissemination)
http://geography.wr.usgs.gov/science/croplands/products.html#LPDAAC (dissemination on LP DAAC)
http://geography.wr.usgs.gov/science/croplands/products.html (global croplands on Google Earth Engine)
croplands.org (crowdsourcing global croplands data)

d. Other relevant past publications prior to GFSAD project

Biggs, T., Thenkabail, P.S., Krishna, M., GangadharaRao Rao, P., and Turral, H., 2006. Vegetation phenology and irrigated area mapping using combined MODIS time-series, ground surveys, and agricultural census data in Krishna River Basin, India. International Journal of Remote Sensing. 27(19):4245-4266.

Biradar, C.M., Thenkabail, P.S., Noojipady, P., Yuanjie, L., Dheeravath, V., Velpuri, M., Turral, H., Gumma, M.K., Reddy, O.G.P., Xueliang, L. C., Schull, M.A., Alankara, R.D., Gunasinghe, S., Mohideen, S., Xiao, X. 2009. A global map of rainfed cropland areas (GMRCA) at the end of last millennium using remote sensing. International Journal of Applied Earth Observation and Geoinformation. 11(2). 114-129. doi:10.1016/j.jag.2008.11.002. January, 2009.

Dheeravath, V., Thenkabail, P.S., Chandrakantha, G, Noojipady, P., Biradar, C.B., Turral. H., Gumma, M.1, Reddy, G.P.O., Velpuri, M. 2010. Irrigated areas of India derived using MODIS 500m data for years 2001-2003. ISPRS Journal of Photogrammetry and Remote Sensing. http://dx.doi.org/10.1016/j.isprsjprs.2009.08.004. 65(1): 42-59.

Thenkabail, P.S. 2012. Special Issue Foreword. Global Croplands special issue for the August 2012 special issue for Photogrammetric Engineering and Remote Sensing. PE&RS. 78(8): 787-788.Thenkabail, P.S. 2012. Guest Editor for Global Croplands Special Issue. Photogrammetric Engineering and Remote Sensing. PE&RS. 78(8).

Thenkabail, P.S., Biradar C.M., Noojipady, P., Cai, X.L., Dheeravath, V., Li, Y.J., Velpuri, M., Gumma, M., Pandey, S. 2007a. Sub-pixel irrigated area calculation methods. Sensors Journal (special issue: Remote Sensing of Natural Resources and the Environment (Remote Sensing SensorsEdited by Assefa M. Melesse). 7:2519-2538. http://www.mdpi.org/sensors/papers/s7112519.pdf.

Thenkabail, P.S., Biradar C.M., Noojipady, P., Dheeravath, V., Li, Y.J., Velpuri, M., Gumma, M., Reddy, G.P.O., Turral, H., Cai, X. L., Vithanage, J., Schull, M., and Dutta, R. 2009a. Global irrigated area map (GIAM), derived from remote sensing, for the end of the last millennium. International Journal of Remote Sensing. 30(14): 3679-3733. July, 20, 2009.

Thenkabail, P.S., Biradar, C.M., Turral, H., Noojipady, P., Li, Y.J., Vithanage, J., Dheeravath, V., Velpuri, M., Schull M., Cai, X. L., Dutta, R. 2006. An Irrigated Area Map of the World (1999) derived from Remote Sensing. Research Report # 105. International Water Management Institute. Pp. 74. Also, see under documents in: http://www.iwmigiam.org.

Thenkabail, P. S.; Dheeravath, V.; Biradar, C. M.; Gangalakunta, O. P.; Noojipady, P.; Gurappa, C.; Velpuri, M.; Gumma, M.; Li, Y. 2009b. Irrigated Area Maps and Statistics of India Using Remote Sensing and National Statistics. Journal Remote Sensing. 1:50-67. http://www.mdpi.com/2072-4292/1/2/50.

Thenkabail, P.S., GangadharaRao, P., Biggs, T., Krishna, M., and Turral, H., 2007b. Spectral Matching Techniques to Determine Historical Land use/Land cover (LULC) and Irrigated Areas using Time-series AVHRR Pathfinder Datasets in the Krishna River Basin, India. Photogrammetric Engineering and Remote Sensing. 73(9): 1029-1040. (Second Place Recipients of the 2008 John I. Davidson ASPRS President's Award for Practical papers).

Thenkabail, P.S., Hanjra, M.A., Dheeravath, V., Gumma, M.K. 2010. A Holistic View of Global Croplands and Their Water Use for Ensuring Global Food Security in the 21st Century through Advanced Remote Sensing and Non-remote Sensing Approaches. Remote Sensing open access journal. 2(1):211-261. doi:10.3390/rs2010211. http://www.mdpi.com/2072-4292/2/1/211

Thenkabail P.S., Knox J.W., Ozdogan, M., Gumma, M.K., Congalton, R.G., Wu, Z., Milesi, C., Finkral, A., Marshall, M., Mariotto, I., You, S. Giri, C. and Nagler, P. 2012. Assessing future risks to agricultural productivity, water resources and food security: how can remote sensing

help? Photogrammetric Engineering and Remote Sensing, August 2012 Special Issue on Global Croplands: Highlight Article. 78(8): 773-782.

Thenkabail, P.S., Schull, M., Turral, H. 2005. Ganges and Indus River Basin Land Use/Land Cover (LULC) and Irrigated Area Mapping using Continuous Streams of MODIS Data. Remote Sensing of Environment. Remote Sensing of Environment, 95(3): 317-341.

Velpuri, M., Thenkabail, P.S., Gumma, M.K., Biradar, C.B., Dheeravath, V., Noojipady, P., Yuanjie, L.,2009. Influence of Resolution or Scale in Irrigated Area Mapping and Area Estimations. Photogrammetric Engineering and Remote Sensing (PE&RS). 75(12): December 2009 issue.

e. Books and Book Chapters

Teluguntla, P., Thenkabail, P.S., Xiong, J., Gumma, M.K., Giri, C., Milesi, C., Ozdogan, M., Congalton, R.,Tilton, J.,Sankey,T.R., Massey, R., Phalke, A., and Yadav, K. 2015. Global Food Security Support Analysis Data at Nominal 1 km (GFSAD1 km) Derived from Remote Sensing in Support of Food Security in the Twenty-First Century: Current Achievements and Future Possibilities, Chapter 6. In Thenkabail, P.S., (Editor-in-Chief), 2015. "Remote Sensing Handbook" (Volume II): Land Resources Monitoring, Modeling, and Mapping with Remote Sensing. Taylor and Francis Inc. Press, Boca Raton, London, New York. ISBN 9781482217957 - CAT# K22130. Pp. 131-160

Biradar, C.M., Thenkabail. P.S., Noojipady, P., Li, Y.J., Dheeravath, V., Velpuri, M., Turral, H., Cai, X.L., Gumma, M., Gangalakunta, O.R.P., Schull, M., Alankara, R.D., Gunasinghe, S., and Xiao, X. 2009. Book Chapter 15: Global map of rainfed cropland areas (GMRCA) and stastistics using remote sensing. Pp. 357-392. In the book entitled: "Remote Sensing of Global Croplands for Food Security" (CRC Press- Taylor and Francis group, Boca Raton, London, New York. Pp. 475. Published in June, 2009. (Editors: Thenkabail. P., Lyon, G.J., Biradar, C.M., and Turral, H).

Gangalakunta, O.R.P., Dheeravath, V., Thenkabail, P.S., Chandrakantha, G., Biradar, C.M., Noojipady, P., Velpuri, M., and Kumar, M.A. 2009. Book Chapter 5: Irrigated areas of India derived from satellite sensors and national statistics: A way forward from GIAM experience. Pp. 139-176. In the book entitled: "Remote Sensing of Global Croplands for Food Security" (CRC Press- Taylor and Francis group, Boca Raton, London, New York. Pp. 475. Published in June, 2009. (Editors: Thenkabail. P., Lyon, G.J., Biradar, C.M., and Turral, H.).

Li, Y.J., Thenkabail, P.S., Biradar, C.M., Noojipady, P., Dheeravath, V., Velpuri, M., Gangalakunta, O.R., Cai, X.L. 2009. Book Chapter 2: A history of irrigated areas of the world. Pp. 13-40. In the book entitled: "Remote Sensing of Global Croplands for Food Security" (CRC Press- Taylor and Francis group, Boca Raton, London, New York. Pp. 475. Published in June, 2009. (Editors: Thenkabail. P.,Lyon, G.J., Biradar, C.M., and Turral, H.).

Thenkabail, P.S., Lyon, G.J., and Huete, A. 2011. Book Chapter # 1: Advances in Hyperspectral Remote Sensing of Vegetation. In Book entitled: "Remote Sensing of Global Croplands for Food Security" (CRC Press- Taylor and Francis group, Boca Raton, London, New York. Edited by Thenkabail, P.S., Lyon, G.J., and Huete, A. Pp. 3-38.

Thenkabail, P.S., Hanjra, M.A., Dheeravath, V. and Gumma, M., 2011. *Global croplands and their water use from remote sensing and nonremote sensing perspectives* (pp. 383-419). Florida: CRC Press, Taylor and Francis Group.

Thenkabail. P.S., Biradar, C.M., Noojipady, P., Dheeravath, V., Gumma, M., Li, Y.J., Velpuri, M., Gangalakunta, O.R.P. 2009c. Book Chapter 3: Global irrigated area maps (GIAM) and statistics using remote sensing. Pp. 41-120. In the book entitled: "Remote Sensing of Global Croplands for Food Security" (CRC Press- Taylor and Francis group, Boca Raton, London, New York. Pp. 475. Published in June, 2009. (Editors: Thenkabail. P., Lyon, G.J., Biradar, C.M., and Turral, H.).

Thenkabail. P., Lyon, G.J., Turral, H., and Biradar, C.M. (Editors) 2009d. Book entitled: "Remote Sensing of Global Croplands for Food Security" (CRC Press- Taylor and Francis group, Boca Raton, London, New York. Pp. 556 (48 pages in color). Published in June, 2009.
Reviews of this book:
http://www.crcpress.com/product/isbn/9781420090093
http://gfmt.blogspot.com/2011/05/review-remote-sensing-of-global.html

Thenkabail, P.S. and Lyon, J.G. 2009. Book Chapter 20: Remote sensing of global croplands for food security: way forward. Pp. 461-466. In the book entitled: "Remote Sensing of Global Croplands for Food Security" (CRC Press- Taylor and Francis group, Boca Raton, London, New York. Pp. 475. Published in June, 2009. (Editors: Thenkabail. P., Lyon, G.J., Biradar, C.M., and Turral, H.).

Turral, H., Thenkabail, P.S., Lyon, J.G., and Biradar, C.M. 2009. Book Chapter 1: Context, need: The need and scope for mapping global irrigated and rain-fed areas. Pp. 3-12. In the book entitled: "Remote Sensing of Global Croplands for Food Security" (CRC Press- Taylor and Francis group, Boca Raton, London, New York. Pp. 475. Published in June, 2009. (Editors: Thenkabail. P., Lyon, G.J., Biradar, C.M., and Turral, H.).

X. Acknowledgements

The project was initially funded by the National Aeronautics and Space Administration (NASA) grant number: NNH13AV82I through its MEaSUREs (Making Earth System Data Records for Use in Research Environments) initiative. The United States Geological Survey (USGS) provided supplemental funding from other direct and indirect means through the Climate and Land Use Change Mission Area, including the Land Change Science (LCS) and Land Remote Sensing (LRS) programs. The project was led by United States Geological Survey (USGS) in collaboration with the International Crops Research Institute for the Semi-Arid Tropics (ICRISAT). Authors gratefully acknowledge the excellent support and guidance received from the LP DAAC team members (Bradford Wirt, Scott Saxon, Chris Torbert, and Tom Maiersperger) when releasing these data. We also like to thank Susan Benjamin, Director of USGS Western Geographic Science Center (WGSC), WGSC administrative officer David Penisten, and WGSC budget analyst Emily Yamamoto for their cheerful support and encouragement throughout the project.

XI. Contact Information

LP DAAC User Services
U.S. Geological Survey (USGS)
Center for Earth Resources Observation and Science (EROS)
47914 252nd Street
Sioux Falls, SD 57198-0001
Phone Number: 605-594-6116
Toll Free: 866-573-3222 (866-LPE-DAAC)
Fax: 605-594-6963
Email: lpdaac@usgs.gov
Web: https://lpdaac.usgs.gov

For the Principal Investigators, feel free to write to:
Prasad S. Thenkabail at pthenkabail@usgs.gov

For the LGRIP30-m product, please contact:
Pardhasaradhi Teluguntla at pteluguntla@usgs.gov
Prasad S. Thenkabail at pthenkabail@usgs.gov
Adam Oliphant at aoliphant@usgs.gov
More details about the GFSAD30 project and products can be found at: **globalcroplands.org**

XII. Citations

P. Teluguntla, P. Thenkabail, A. Oliphant, M. Gumma, I. Aneece, D.Foley and R.McCormick, (2023a). Landsat-derived Global Rainfed and Irrigated-Cropland Product @ 30-m (LGRIP30) of the World (GFSADLGRIP30WORLD). The Land Processes Distributed Active Archive Center (LP DAAC) of NASA and USGS. Pp. 103. IP-148728.
DOI: https://doi.org/10.5067/Community/LGRIP/LGRIP30.001

XIII. References

Badami, M.G., Ramankutty, N. 2015. Urban agriculture and food security: A critique based on an assessment of urban land constraints. Global food security, 4: 8-15.

Belgiu, M., & Drăguţ, L. (2016). Random forest in remote sensing: A review of applications and future directions. *ISPRS Journal of Photogrammetry and Remote Sensing, 114*, 24-31

Biradar, C.M., Thenkabail, P.S., Noojipady, P., Li, Y., Dheeravath, V., Turral, H., Velpuri, M., Gumma, M.K., Gangalakunta, O.R.P., & Cai, X.L. 2009. A global map of rainfed cropland areas GMRCA at the end of last millennium using remote sensing. International Journal of Applied Earth Observation and Geoinformation, 11, 114-129

Boden, T.A., Marland, G., and Andres, R.J. 2017. National CO_2 Emissions from Fossil-Fuel Burning, Cement Manufacture, and Gas Flaring: 1751-2014. Carbon Dioxide Information Analysis Center, Oak Ridge National Laboratory, U.S. Department of Energy.
doi 10.3334/CDIAC/00001_V2017.

Bodirsky, B.L., Rolinski, S., Biewald, A., Weindl, I., Popp, A., and Lotze-Campen, H. 2015. Global food demand scenarios for the 21 st century. PloS one, 10(11): e0139201.

Bourne Jr. B.K. 2022. War in Ukraine could plunge world into food shortages with far less Ukrainian and Russian grain and fertilizer entering global markets, experts fear that a bleak period of scarcer, pricier food will arrive this year. The National Geographic. Accessed May 6, 2022.

Breiman, L. (2001). Random forests. *Machine learning, 45*, 5-32

Buchhorn, M. ; Lesiv, M. ; Tsendbazar, N. - E. ; Herold, M. ; Bertels, L. ; Smets, B. Copernicus Global Land Cover Layers-Collection 2. Remote Sensing 2020, 12Volume 108, 1044.

Business Standard, 2017. Number of deep tube wells rose by 1.1 mn in 7 yrs in India. Business Standard, Press Trust of India, December 23, 2017.

Campbell, B.M., Thornton, P., Zougmoré, R., Van Asten, P., and Lipper, L. 2014. Sustainable intensification: What is its role in climate smart agriculture? Current Opinion in Environmental Sustainability, 8: 39-43.

Chan, J. C. W., & Paelinckx, D. (2008). Evaluation of Random Forest and Adaboost tree-based ensemble classification and spectral band selection for ecotope mapping using airborne hyperspectral imagery. *Remote Sensing of Environment, 112*(6), 2999-3011

Chen, C., Liaw, A., & Breiman, L. (2004). Using random forest to learn imbalanced data. *University of California, Berkeley, 110*

Congalton, R. and K. Green. 2009. Assessing the Accuracy of Remotely Sensed Data: Principles and Practices. 2nd Edition. CRC/Taylor & Francis, Boca Raton, FL 183p

Congalton, R.G. 2015. Assessing positional and thematic accuracies of maps generated from remotely sensed data."Remote Sensing Handbook" three-volume set: Remotely Sensed Data Characterization, classification, and accuracies, Taylor and Francis Inc.\CRC Press, Boca Raton, London, New York. Pp. 800+. Pp. 625-662.

Congalton, R., Yadav, K., McDonnell, K., Poehnelt, J., Stevens, B., Gumma, M., Teluguntla, P., and Thenkabail, P. 2017. GFSAD30VAL v001—Global food security-support analysis data (GFSAD) cropland extent 2015 validation 30m: U.S. Geological Survey–National Aeronautics and Space Administration Land Processes Distributed Active Archive Center website, https://doi.org/10.5067/MEaSUREs/GFSAD/GFSAD30VAL.001.

Conrad, C., Lamers, J., Ibragimov, N., Löw, F., and Martius, C. 2016. Analysing irrigated crop rotation patterns in arid Uzbekistan by the means of remote sensing: A case study on post-Soviet agricultural land use. Journal of Arid Environments 124, 150-159.

Enenkel, M., See, L., Bonifacio, R., Boken, V., Chaney, N., Vinck, P., You, L., Dutra, E., and Anderson, M. 2015. Drought and food security–Improving decision-support via new technologies and innovative collaboration. Global Food Security, 4: 51-55.

Fanzo, J., 2015. Ethical issues for human nutrition in the context of global food security and sustainable development. Global Food Security, 7: 15-23.

FAO, 2012a. Food and Agricultural Organization of the United Nations and International Institute of Applied System Analysis, 2012, Global agro-ecological zones (GAEZ ver. 3.0)—Model documentation: Laxenburg, Austria, and Rome, Italy, International Institute of Applied System Analysis (IIASA) and Food and Agricultural Organization of the United Nations (FAO), 179 p., accessed April 2020 at http://www.fao.org/nr/gaez/en/.

FAO, 2012b. FAOSTAT online database. Accessed in September 2012.

FAO. 2015. GlobWat – A global water balance model to assess water use in irrigated agriculture. Rome. By: Hoogeveen, J.; Faurès, J. M.; Peiser, L. ; Burke, J.;Van de Giesen, N.. FAO/World Bank/Delft University of Technology.

FAO GAUL, 2015. Food and Agricultural Organization of the United Nations. Global Administrative Unit Layers (GAUL). http://www.fao.org/geonetwork.

FAO. 2021a. Climate-smart agriculture case studies 2021 – Projects from around the world. The Food and Agricultural Organization of the United Nations (FAO UN), Rome, Italy. Pp. 86. https://doi.org/10.4060/cb5359en

FAO. 2021b. World Food and Agriculture – Statistical Yearbook 2021. Rome, Italy. https://doi.org/10.4060/cb4477en

Foley, D.J., Thenkabail, P.S., Aneece, I., and Teluguntla, P. 2019. A meta-analysis of global crop water productivity of three leading world crops (wheat, corn, and rice) in the irrigated areas over three decades. International Journal of Digital Earth, DOI: 10.1080/17538947.2019.1651912
To link to this article: https://doi.org/10.1080/17538947.2019.1651912 IP-105160 .

Friedl, M.A., McIver, D.K., Hodges, J.C., Zhang, X.Y., Muchoney, D., Strahler, A.H., Woodcock, C.E., Gopal, S., Schneider, A., Cooper, A. and Baccini, A., 2002. Global land cover mapping from MODIS: algorithms and early results. *Remote sensing of Environment*, *83*(1-2), pp.287-302.

Friedl, M.A., Sulla-Menashe, D., Tan, B., Schneider, A., Ramankutty, N., Sibley, A. and Huang, X. 2010. MODIS Collection 5 global land cover: Algorithm refinements and characterization of new datasets. Remote sensing of Environment, 114(1): 168-182.

Fuss, S., Havlík, P., Szolgayová, J., Schmid, E., Reuter, W.H., Khabarov, N., Obersteiner, M., Ermoliev, Y., Ermolieva, T., and Kraxner, F. 2015. Global food security & adaptation under crop yield volatility. Technological Forecasting and Social Change, 98: 223-233.

Gartland, K. and Gartland, J. 2016. Green biotechnology for food security in climate change. Reference Module in Food Science, Elsevier. DOI:10.1016/B978-0-08-100596-5.03071-7.

Gbegbelegbe, S., Chung, U., Shiferaw, B., Msangi, S., and Tesfaye, K. 2014. Quantifying the impact of weather extremes on global food security: A spatial bio-economic approach. Weather and Climate Extremes, 4: 96-108.

Girotto, F., Alibardi, L. and Cossu, R. 2015. Food waste generation and industrial uses: a review. Waste Management, 45: 32-41.

Gorelick, N., Hancher, M., Dixon, M., Ilyushchenko, S., Thau, D. and Moore, R., 2017. Google Earth Engine: Planetary-scale geospatial analysis for everyone. Remote Sensing of Environment.
Huang, C., Davis, L.S., Townshend, J.R.G., 2010. An assessment of support vector machines for land cover classification. International Journal of Remote Sensing 23, 725–749.

Glauber, J., and Laborde, D. 2022. How will Russia's invasion of Ukraine affect global food security?. IFPRI Blog : Issue Post. FEBRUARY 24, 2022. OPEN ACCESS | CC-BY-4.0

Gumma, M.K., Thenkabail, P.S., Panjala, P., Teluguntla, P., Yamano, T., Mohammed, I. 2022. Multiple agricultural cropland products of South Asia developed using Landsat-8 30 m and MODIS 250 m data using machine learning on the Google Earth Engine (GEE) cloud and spectral matching techniques (SMTs) in support of food and water security. Pp. 1048-1077. GIScience & Remote Sensing, 59:1, 1048-1077, DOI: 10.1080/15481603.2022.2088651. https://doi.org/10.1080/15481603.2022.2088651 IP-135578.Hanasaki, N., Inuzuka, T., Kanae, S., and Oki, T. 2010. An estimation of global virtual water flow and sources of water withdrawal for major crops and livestock products using a global hydrological model. Journal of Hydrology, 384(3): 232-244.

Gumma, M. K., Thenkabail, P. S., Teluguntla, P. G., Oliphant, A., Xiong, J., Giri, C., & Whitbread, A. M. (2019). Agricultural cropland extent and areas of South Asia derived using Landsat satellite 30-m time-series big-data using random forest machine learning algorithms on the Google Earth Engine cloud. GIScience & Remote Sensing, 1-21. https://doi.org/10.1080/15481603.2019.1690780

Gumma, M. K., Thenkabail, P. S., Teluguntla, P., Rao, M. N., Mohammed, I. A. and Whitbread, A. M. 2016. Mapping rice-fallow cropland areas for short-season grain legumes intensification in South Asia using MODIS 250 m time-series data. International Journal of Digital Earth, 9: 981-1003.

Hansen, M.C., DeFries, R.S., Townshend, J.R.G., Sohlberg, R., Dimiceli, C. and Carroll, M., 2002. Towards an operational MODIS continuous field of percent tree cover algorithm: examples using AVHRR and MODIS data. *Remote Sensing of Environment*, *83*(1-2), pp.303-319.

He, G., Liu, X., and Cui, Z. 2021. Achieving global food security by focusing on nitrogen efficiency potentials and local production. Global Food Security, 29: 100536, ISSN 2211-9124, https://doi.org/10.1016/j.gfs.2021.100536

Hefferon, K.L. 2016. Politics for Global Food Security. Reference Module in Food Science, Elsevier. https://doi.org/10.1016/B978-0-08-100596-5.03059-6.

Hu, Q., Xiang, M., Chen, D., Zhou, J., Wu, W., and Song, Q. 2020. Global cropland intensification surpassed expansion between 2000 and 2010: A spatio-temporal analysis based on GlobeLand30. Science of the Total Environment, 746: 141035, ISSN 0048-9697, https://doi.org/10.1016/j.scitotenv.2020.141035.

IME 2013. Global food. Waste not, Want not. Institute of Mechanical Engineering, January 2013, p 32

Karra, K., Kontgis, C., Statman-Weil, Z., Mazzariello, J.C., Mathis, M. and Brumby, S.P., 2021, July. Global land use/land cover with Sentinel 2 and deep learning. In *2021 IEEE international geoscience and remote sensing symposium IGARSS* (pp. 4704-4707). IEEE. https://www.arcgis.com/home/item.html?id=d3da5dd386d140cf93fc9ecbf8da5e31

Lawrence, R.L., Wood, S.D., & Sheley, R.L. (2006). Mapping invasive plants using hyperspectral imagery and Breiman Cutler classifications (RandomForest). *Remote Sensing of Environment, 100*, 356-362

Lenaerts, B., Collard, B.C.Y., and Demont, M. 2019. Review: Improving global food security through accelerated plant breeding, Plant Science, 287: 110207, ISSN 0168-9452, https://doi.org/10.1016/j.plantsci.2019.110207.

Lin, L., Di, L., Zhang, C, Guo, L., Di, Y., Li, H., and Yang, A. 2022. Validation and refinement of cropland data layer using a spatial-temporal decision tree algorithm. Scientific Data, 9(63). https://doi.org/10.1038/s41597-022-01169-w.

Lu, Y., Song, W., Lü, J., Chen, M., Su, Z., Zhang, X., and Li, H. 2021. A pixel-based spectral matching method for mapping high-resolution irrigated areas using EVI time series. Remote Sensing Letters, 12(2): 169-178. DOI: 10.1080/2150704X.2020.1837987

Lillesand, T., Kiefer, R.W. and Chipman, J., 2014. Remote sensing and image interpretation. John Wiley & Sons.

Loveland, T.R., Reed, B.C., Brown, J.F., Ohlen, D.O., Zhu, Z., Yang, L.W.M.J. and Merchant, J.W., 2000. Development of a global land cover characteristics database and IGBP DISCover from 1 km AVHRR data. *International journal of remote sensing*, *21*(6-7), pp.1303-1330.

Masek, J.G., Ju, J., Claverie, M., Skakun, S., Roger, J.C., Vermote, E., Franch, B., Yin, Z., Dungan. J.L. 2022. Harmonized Landsat Sentinel-2 (HLS) Product User Guide Product Version 2.0

Masek, J., Ju, J., Roger, J., Skakun, S., Vermote, E., Claverie, M., Dungan, J., Yin, Z., Freitag, B. and Justice, C. 2021. HLS Sentinel-2 MSI surface reflectance daily global 30m v2.0., distributed by NASA EOSDIS Land Processes DAAC, https://doi.org/10.5067/HLS/HLSS30.002.

Massey, R., Sankey, T.T., Congalton, R.G., Yadav, K., Thenkabail, P.S., Ozdogan, M. and Meador, A.J.S., 2017. MODIS phenology-derived, multi-year distribution of conterminous US crop types. *Remote Sensing of Environment*, *198*, pp.490-503.

Massey, R., Sankey, T.T., Yadav, K., Congalton, R.G. and Tilton, J.C., 2018. Integrating cloud-based workflows in continental-scale cropland extent classification. *Remote Sensing of Environment*, *219*, pp.162-179.

Mekonnen, A., Tessema, A., Ganewo, Z., and Haile, A. 2021. Climate change impacts on household food security and farmers adaptation strategies. Journal of Agriculture and Food Research, 6: 100197. ISSN 2666-1543, https://doi.org/10.1016/j.jafr.2021.100197. (https://www.sciencedirect.com/science/article/pii/S2666154321000995).

Mountrakis, G., Im, J., & Ogole, C. (2011). Support vector machines in remote sensing: A review. *ISPRS Journal of Photogrammetry and Remote Sensing, 66*, 247-259

Muhammad Zohaib, Hyunglok Kim, Minha Choi. Detecting global irrigated areas by using satellite and reanalysis products, Science of The Total Environment, Volume 677, 2019, Pages 679-691, ISSN 0048-9697, https://doi.org/10.1016/j.scitotenv.2019.04.365. (https://www.sciencedirect.com/science/article/pii/S0048969719319084)

Na, X., Zhang, S., Li, X., Yu, H., & Liu, C. (2010). Improved land cover mapping using random forests combined with landsat thematic mapper imagery and ancillary geographic data. *Photogrammetric Engineering & Remote Sensing, 76*, 833-840

Nagaraj, D., Proust, E., Todeschini, A., Rulli, M.C. and D'Odorico, P., 2021. A new dataset of global irrigation areas from 2001 to 2015. *Advances in Water Resources*, *152*, p.103910. https://doi.org/10.1016/j.advwatres.2021.103910.

Niedertscheider, M., Kastner, T., Fetzel, T., Haberl, H., Kroisleitner, C., Plutzar, C., and Erb, K.H. 2016. Mapping and analysing cropland use intensity from a NPP perspective. Environmental Research Letters, 11(1): 014008

Odegard, I., and Van der Voet, E. 2014. The future of food—scenarios and the effect on natural resource use in agriculture in 2050. Ecological Economics, 97: 51-59.

Oliphant, A. J., Thenkabail, P. S., Teluguntla, P., Xiong, J., Gumma, M. K., Congalton, R. G., & Yadav, K. (2019). Mapping cropland extent of Southeast and Northeast Asia using multi-year time-series Landsat 30-m data using a random forest classifier on the Google Earth Engine Cloud. International Journal of Applied Earth Observation and Geoinformation, 81, 110-124. https://doi.org/10.1016/j.jag.2018.11.014

Ozdogan, M. and Woodcock, C.E., 2006. Resolution dependent errors in remote sensing of cultivated areas. *Remote Sensing of Environment*, *103*(2), pp.203-217.

Puy, A., Piano, S. L., and Daltelli, A. 2020. Current models underestimate future irrigated areas. Geophysical Research Letters, 47 (8): https://doi.org/10.1029/2020GL087360.

Pelletier, C., Valero, S., Inglada, J., Champion, N., Dedieu, G., 2016. Assessing the robustness of Random Forests to map land cover with high resolution satellite image time series over large areas. Remote Sensing of Environment 187, 156–168.

Phalke, A.R., Özdoğan, M., Thenkabail, P.S., Erickson, T., Gorelick, N., Yadav, K. and Congalton, R.G., 2020. Mapping croplands of Europe, middle east, russia, and central asia using landsat, random forest, and google earth engine. *ISPRS Journal of Photogrammetry and Remote Sensing*, *167*, pp.104-122.

Pittman, K., Hansen, M.C., Becker-Reshef, I., Potapov, P.V. and Justice, C.O. 2010. Estimating global cropland extent with multi-year MODIS data. Remote Sensing, 2(7): 1844-1863.

Portmann, F.T., Siebert, S., & Döll, P. 2010. MIRCA2000—Global monthly irrigated and rainfed crop areas around the year 2000: A new high-resolution data set for agricultural and hydrological modeling. Global biogeochemical cycles, 24

Platonov, A., Thenkabail, P.S., Biradar, C.M., Cai, X., Gumma, M., Dheeravath, V., Cohen, Y., Alchanatis, V., Goldshlager, N., and Ben-Dor, E. 2008. Water productivity mapping (WPM) using Landsat ETM+ data for the irrigated croplands of the Syrdarya River basin in Central Asia. Sensors, 8(12): 8156-8180.

Potapov, P., Turubanova, S., Hansen, M.C., … and Cortez, J. 2022. Global maps of cropland extent and change show accelerated cropland expansion in the twenty-first century. Nature Food, 3: 19–28. https://doi.org/10.1038/s43016-021-00429-z.

Puigdueta, I., Aguilera, E., Cruz, J.L., Iglesias, A., and Sanz-Cobena, A. 2021. Urban agriculture may change food consumption towards low carbon diets. Global Food Security, 28: 100507, ISSN 2211-9124, https://doi.org/10.1016/j.gfs.2021.100507. (https://www.sciencedirect.com/science/article/pii/S2211912421000171).

Rijsberman, F. 2014. Why dry areas should invest massively in innovation to ensure food security. Keynote speech delivered by Frank Rijsberman, CEO, CGIAR Consortium at the Opening Ceremony of the Global Forum for Innovations in Agriculture, Abu Dhabi, February 3, 2014

Rosa, L., Chiarelli, D.D., Sangiorgio, M., Fung, I., 2020. Potential for sustainable irrigation expansion in a 3˚ C warmer climate. PNAS. 117 (47) 29526-29534.

Salmon, J.M., Friedl, M.A., Frolking, S., Wisser, D., & Douglas, E.M. 2015. Global rain-fed, irrigated, and paddy croplands: A new high resolution map derived from remote sensing, crop inventories and climate data. International Journal of Applied Earth Observation and Geoinformation, 38, 321-334

Siebert, S., Kummu, M., Porkka, M., Döll, P., Ramankutty, N., and Scanlon, B. R. 2015. A global data set of the extent of irrigated land from 1900 to 2005. Hydrology and Earth System Sciences, 19: 1521–1545, https://doi.org/10.5194/hess-19-1521-2015, 2015.

Siebert, S., Henrich, V., Frenken, K., and Burke, J. 2013. Update of the Digital Global Map of Irrigation, Areas to Version 5. Documentation. Institute of Crop Science and Resource Conservation, Rheinische Friedrich-Wilhelms-Universität Bonn, Germany. Pl. 161. https://www.fao.org/3/I9261EN/i9261en.pdf

Siebert S., and Döll P. 2010. Quantifying blue and green virtual water contents in global crop production as well as potential production losses without irrigation. Journal of Hydrology, 2384(3): 198-217.

Siebert, S., Döll, P. 2001. A Digital Global Map of Irrigated Areas - An Update for Latin America and Europe. Report A0102, Center for Environmental Systems Research, University of Kassel, Kurt Wolters Strasse 3, 34109 Kassel, Germany.

Siebert, S., Döll, P., Hoogeveen, J., Faures, J.M., Frenken, K. and Feick, S., 2005. Development and validation of the global map of irrigation areas. *Hydrology and Earth System Sciences*, *9*(5), pp.535-547.

Sukara, E. 2014. Tropical forest biodiversity to provide food, health and energy solution of the rapid growth of modern society. Procedia Environmental Sciences, 20: 803-808.

Sun, Y., Kamel, M.S., Wong, A.K., & Wang, Y. (2007). Cost-sensitive boosting for classification of imbalanced data. *Pattern Recognition, 40,* 3358-3378

Teluguntla, P., Thenkabail, P.S., Oliphant, A., Gumma, M., Aneece, I., Foley, D., and McCormick, R. 2023a. Landsat-derived Global Rainfed and Irrigated-Cropland Product @ 30-m (LGRIP30) of the World (GFSADLGRIP30WORLD). The Land Processes Distributed Active Archive Center (LP DAAC) of NASA and USGS. Pp. 103.
DOI: https://doi.org/10.5067/Community/LGRIP/LGRIP30.00

Teluguntla, P., Thenkabail, P.S., Oliphant, A., Gumma, M., Aneece, I., Foley, D., and McCormick, R. 2023b. Landsat-derived global rainfed and irrigated area product @ 30m (LGRIP30). Photogrammetric Engineering and Remote Sensing. In Preparation.

Teluguntla, P., Thenkabail, P.S., Oliphant, A., Xiong, J., Gumma, M.K., Congalton, R.G., Yadav, K. and Huete, A., 2018. A 30-m andsat-derived cropland extent product of Australia and China using random forest machine learning algorithm on Google Earth Engine cloud computing platform. *ISPRS Journal of Photogrammetry and Remote Sensing*, *144*, pp.325-340.

Teluguntla, P., Thenkabail, P.S., Xiong, J., Gumma, M.K., Congalton, R.G., Oliphant, A., Poehnelt, J., Yadav, K., Rao, M., and Massey, R. 2017. Spectral matching techniques (SMTs) and automated cropland classification algorithms (ACCAs) for mapping croplands of Australia using MODIS 250-m time-series (2000–2015) data, International Journal of Digital Earth. http://dx.doi.org/10.1080/17538947.2016.1267269.

Teluguntla, P., Thenkabail, P., Xiong, J., Gumma, M., Giri, C., Milesi, C., Ozdogan, M., Congalton, R., Tilton, J., Sankey, T., Massey, R., Phalke, A., and Yadav, K. 2016. NASA Making Earth System Data Records for Use in Research Environments (MEaSUREs) Global Food

Security Support Analysis Data (GFSAD) Crop Mask 2010 Global 1 km V001 [Data set]. NASA EOSDIS Land Processes DAAC. Accessed 2022-03-24 from https://doi.org/10.5067/MEaSUREs/GFSAD/GFSAD1KCM.001

Teluguntla, P., Thenkabail, P.S., Xiong, J., Gumma, M.K., Giri, C., Milesi, C., Ozdogan, M., Congalton, R., Tilton, J., Sankey, T.R., Massey, R., Phalke, A., and Yadav, K. 2015. Global Food Security Support Analysis Data at Nominal 1 km (GFSAD1km) Derived from Remote Sensing in Support of Food Security in the Twenty-First Century: Current Achievements and Future Possibilities, Chapter 6. In Thenkabail, P.S., (Editor-in-Chief), 2015. "Remote Sensing Handbook" (Volume II): Land Resources Monitoring, Modeling, and Mapping with Remote Sensing. Taylor and Francis Inc.\CRC Press, Boca Raton, London, New York. ISBN 9781482217957 - CAT# K22130. Pp. 131-160. IP-054785.

Thebo, A.L., Drechsel, P., and Lambin, E.F. 2014. Global assessment of urban and peri-urban agriculture: irrigated and rainfed croplands. Environmental Research Letters, 9: 114002.

Thenkabail, P.S., Teluguntla, P.G., Xiong, J., Oliphant, A., Congalton, R.G., Ozdogan, M., Gumma, M.K., Tilton, J.C., Giri, C., Milesi, C., Phalke, A., Massey, R., Yadav, K., Sankey, T., Zhong, Y., Aneece, I., and Foley, D. 2021. Global cropland-extent product at 30m resolution (GCEP30) derived from Landsat satellite time-series data for the year 2015 using multiple machine-learning algorithms on Google Earth Engine cloud: U.S. Geological Survey Professional Paper 1868, 63 p., https://doi.org/10.3133/pp1868.
https://lpdaac.usgs.gov/news/release-of-gfsad-30meter-cropland-extent-products/ IP-119164.

Thenkabail, P., Knox, J., Ozdogan, M., Gumma, M., Congalton, R., Wu, Z., Milesi, C., Finkral, A., Marshall, M., Mariotto, I., You, S., Giri, C., and Nagler, P. 2016. NASA Making Earth System Data Records for Use in Research Environments (MEaSUREs) Global Food Security Support Analysis Data (GFSAD) Crop Dominance 2010 Global 1 km V001 [Data set]. NASA EOSDIS Land Processes DAAC.
Accessed 2022-03-24 from https://doi.org/10.5067/MEaSUREs/GFSAD/GFSAD1KCD.001

Thenkabail, P.S., Knox, J.W., Ozdogan, M., Gumma, M.K., Congalton, R.G., Wu, Z., Milesi, C., Finkral, A., Marshall, M., and Mariotto, I. 2012. Assessing future risks to agricultural productivity, water resources and food security: how can remote sensing help? Photogrammetric Engineering and Remote Sensing, 78(8): 773-782.

Thenkabail, P.S., Hanjra, M.A., Dheeravath, V., Gumma, M. 2011. Book Chapter # 16: Global Croplands and Their Water Use Remote Sensing and Non-Remote Sensing Perspectives. In the Book entitled: "Advances in Environmental Remote Sensing: Sensors, Algorithms, and Applications". Taylor and Francis Edited by Dr. Qihao Weng. Pp. 383-419.

Thenkabail, P.S., Hanjra, M. a, Dheeravath, V., Gumma, M., 2010. A Holistic View of Global Croplands and Their Water Use for Ensuring Global Food Security in the 21st Century through Advanced Remote Sensing and Non-remote Sensing Approaches. Remote Sensing 2, 211.

Thenkabail, P.S., Biradar C.M., Noojipady, P., Dheeravath, V., Li, Y.J., Velpuri, M., Gumma, M., Reddy, G.P.O., Turral, H., Cai, X. L., Vithanage, J., Schull, M., and Dutta, R. 2009a. Global

irrigated area map (GIAM), derived from remote sensing, for the end of the last millennium. International Journal of Remote Sensing, 30(14): 3679-3733. July 20, 2009.

Thenkabail, P. S.; Dheeravath, V.; Biradar, C. M.; Gangalakunta, O. P.; Noojipady, P.; Gurappa, C.; Velpuri, M.; Gumma, M.; Li, Y. 2009b. Irrigated Area Maps and Statistics of India Using Remote Sensing and National Statistics. Journal Remote Sensing. 1:50-67. http://www.mdpi.com/2072-4292/1/2/50.

Thenkabail, P.S., GangadharaRao, P., Biggs, T., Krishna, M., and Turral, H. 2007. Spectral Matching Techniques to Determine Historical Land use/Land cover (LULC) and Irrigated Areas using Time-series AVHRR Pathfinder Datasets in the Krishna River Basin, India. Photogrammetric Engineering and Remote Sensing, 73(9): 1029-1040.

Thenkabail, P.S., Schull, M., and Turral, H. 2005. Ganges and Indus River Basin Land Use/Land Cover (LULC) and Irrigated Area Mapping using Continuous Streams of MODIS Data. Remote Sensing of Environment, 95(3): 317-341.

Thenkabail, P.S., and Wu, Z. 2012. An automated cropland classification algorithm (ACCA) for Tajikistan by combining Landsat, MODIS, and secondary data. Remote Sensing, 4(10): 2890-2918.

Tripathi, A., Tripathi, D.K., Chauhan, D., Kumar, N., and Singh, G. 2016. Paradigms of climate change impacts on some major food sources of the world: A review on current knowledge and future prospects. Agriculture, Ecosystems & Environment, 216: 356-373.

Tubiello, F.N., Karl, K., Flammini, A., Gütschow, J., Obli-Layrea, G., Conchedda, G., Pan, X., Qi, S.Y., Heiðarsdóttir, H.H., Wanner, N. and Quadrelli, R., 2021. Pre-and post-production processes along supply chains increasingly dominate GHG emissions from agri-food systems globally and in most countries. *Earth System Science Data Discussions*, pp.1-24.

UN DESA. 2021. United Nations Department of Economic and Social Affairs, Population Division (2021). Global Population Growth and Sustainable Development. UN DESA/POP/2021/TR/NO. 2. Download.

UNEP. 2021. United Nations Environment Programme (2021). Food Waste Index Report 2021. Nairobi. Download.

van Vliet, J., Eitelberg, D.A., and Verburg, P.H. 2017. A global analysis of land take in cropland areas and production displacement from urbanization. Global Environmental Change, 43: 107-115, ISSN 0959-3780, https://doi.org/10.1016/j.gloenvcha.2017.02.001.

Vermeulen, S.J., Campbell, B.M., and Ingram, J.S.I. 2012. Climate change and food systems. Annual Review of Environment and Resources, 37: 195-222.

Viana, C.M., Freire, D., Abrantes, P., Rocha, J., and Pereira, P. 2022. Agricultural land systems importance for supporting food security and sustainable development goals: A systematic review.

Science of the Total Environment, 806(3): 150718, ISSN 0048-9697, https://doi.org/10.1016/j.scitotenv.2021.150718.

Wardlow, B.D. and Egbert, S.L., 2008. Large-area crop mapping using time-series MODIS 250 m NDVI data: An assessment for the US Central Great Plains. *Remote sensing of environment*, *112*(3), pp.1096-1116.

Wardlow, B.D., Egbert, S.L. and Kastens, J.H., 2007. Analysis of time-series MODIS 250 m vegetation index data for crop classification in the US Central Great Plains. *Remote sensing of environment*, *108*(3), pp.290-310.

Wardlow, B.D., Kastens, J.H. and Egbert, S.L., 2006. Using USDA crop progress data for the evaluation of greenup onset date calculated from MODIS 250-meter data. *Photogrammetric Engineering & Remote Sensing*, *72*(11), pp.1225-1234.

Wheeler, R., and Lobley, M. 2021. Managing extreme weather and climate change in UK agriculture: Impacts, attitudes and action among farmers and stakeholders. Climate Risk Management, 32: 100313, ISSN 2212-0963, https://doi.org/10.1016/j.crm.2021.100313
Wilkinson, J. 2015. Food security and the global agrifood system: Ethical issues in historical and sociological perpspective. Global Food Security, 2211-9124.

World Bank, 2022. GovData360. https://govdata360.worldbank.org/indicators/h76e4f437.

World Bank, 2020. World Bank Signs Agreement to Improve Groundwater Management in Select States of India. The World Bank, Press Release, December 17, 2020.

Würtenberger, L., Koellner, T. and Binder, C.R., 2006. Virtual land use and agricultural trade: Estimating environmental and socio-economic impacts. Ecological Economics, 57(4), 679-697.
WorldBank, 2022. GovData360. Download.

Wu, Z., Thenkabail, P.S., Zakzeski, A., Mueller, R., Melton, F., Rosevelt, C., Dwyer, J., Johnson, J., and Verdin, J. P. 2014. Seasonal cultivated and fallow cropland mapping using MODIS-based automated cropland classification algorithm. Journal of Applied Remote Sensing, 8(1): 083685. doi: 10.1117/1.JRS.8.083685. IP-044862.

Wu, W., Yu, Q., You, L., Chen, K., Tang, H., and Liu, J. 2018. Global cropping intensity gaps: Increasing food production without cropland expansion. Land Use Policy, 76: 515-525, ISSN 0264-8377, https://doi.org/10.1016/j.landusepol.2018.02.032.

Xie, Y. and Lark, T.J., 2021. Mapping annual irrigation from Landsat imagery and environmental variables across the conterminous United States. Remote Sensing of Environment, 260, p.112445.

Xie, Y., Gibbs, H.K., and Lark, T.J. 2021. Landsat-based Irrigation Dataset (LANID): 30-m resolution maps of irrigation distribution, frequency, and change for the U.S., 1997-2017. Earth Syst. Sci. Data, 13, 5689–5710. https://doi.org/10.5194/essd-13-5689-202.

Xing, H., Chen, B., Feng, Y., Ni, Y., Hou, D., Wang, X. and Kong, Y., 2022. Mapping Irrigated, Rainfed and Paddy Croplands from Time-Series Sentinel-2 Images by Integrating Pixel-based Classification and Image Segmentation on Google Earth Engine. Geocarto International, , pp.1-20.

Xiong, J., Thenkabail, P., Tilton, J., Gumma, M., Teluguntla, P., Oliphant, A., Congalton, R., Yadav, K., & Gorelick, N. 2017a. Nominal 30-m Cropland Extent Map of Continental Africa by Integrating Pixel-Based and Object-Based Algorithms Using Sentinel-2 and Landsat-8 Data on Google Earth Engine. *Remote Sensing*, *9*, 1065

Xiong, J., Thenkabail, P.S., Gumma, M.K., Teluguntla, P., Poehnelt, J., Congalton, R.G., Yadav, K., Thau, D. 2017b. Automated cropland mapping of continental Africa using Google Earth Engine cloud computing, ISPRS Journal of Photogrammetry and Remote Sensing, Volume 126, April 2017, Pages 225-244, ISSN 0924-2716, https://doi.org/10.1016/j.isprsjprs.2017.01.019.

Yadav, K. and Congalton, R.G., 2018. Accuracy assessment of global food security-support analysis data (GFSAD) cropland extent maps produced at three different spatial resolutions. *Remote Sensing*, *10*(11), p.1800.

You, L., and Sun, Z. 2022. Mapping global cropping system: Challenges, opportunities, and future perspectives. Crop and Environment, 1(1): 68-73, ISSN 2773-126X, https://doi.org/10.1016/j.crope.2022.03.006

Yu, L., Wang, J., Clinton, N., Xin, Q., Zhong, L., Chen, Y., and Gong, P. 2013. FROM-GC: 30m global cropland extent derived through multisource data integration. International Journal of Digital Earth, 6(6): 521-533.

Zanaga, D., Van De Kerchove, R., De Keersmaecker, W., Souverijns, N., Brockmann, C., Quast, R., Wevers, J., Grosu, A., Paccini, A., Vergnaud, S., Cartus, O., Santoro, M., Fritz, S., Georgieva, I., Lesiv, M., Carter, S., Herold, M., Li, Linlin, Tsendbazar, N.E., Ramoino, F., Arino, O., 2021. ESA WorldCover 10 m 2020 v100. https://doi.org/10.5281/zenodo.5571936
https://developers.google.com/earth-engine/datasets/catalog/ESA_WorldCover_v100

Zanaga, D., Van De Kerchove, R., Daems, D., De Keersmaecker, W., Brockmann, C., Kirches, G., Wevers, J., Cartus, O., Santoro, M., Fritz, S., Lesiv, M., Herold, M., Tsendbazar, N.E., Xu, P., Ramoino, F., Arino, O., 2022. ESA WorldCover 10 m 2021 v200. *https://doi.org/10.5281/zenodo.7254221*
https://developers.google.com/earth-engine/datasets/catalog/ESA_WorldCover_v200

Zhang, C., Dong, J. and Ge, Q., 2022. Mapping 20 years of irrigated croplands in China using MODIS and statistics and existing irrigation products. *Scientific data*, *9*(1), pp.1-12.

Zohaib, M., Kim, H. and Choi, M., 2019. Detecting global irrigated areas by using satellite and reanalysis products. *Science of the Total Environment*, *677*, pp.679-691.